Illuminating the Dark Side of the Higgs: Yukawa Couplings, Exotic Decays and Baryogenesis

Memoria de Tesis Doctoral realizada por

José Manuel Cano Molina

y dirigida por

José Miguel No Redondo

Universidad Autónoma de Madrid
&
Instituto de Física Teórica UAM/CSIC

Presentada ante el Departamento de Física Teórica para la obtención del título

Doctor en Física Teórica

Madrid
Noviembre de 2023

Abstract

This doctoral thesis explores some of the remaining unknowns surrounding the Standard Model (SM) Higgs discovered at the Large Hadron Collider (LHC), including its potential role as a bridge and sensitive probe to new physics beyond.

We first focus on Higgs production in association with a photon, a rare process not yet observed at the LHC. We show that it is sensitive to significant deviations of Higgs couplings to first and second generation SM quarks (particularly the up-type) from their SM values, and use a multivariate neural network analysis to derive the prospects of the High-Luminosity LHC to probe deviations in the up and charm Higgs Yukawa couplings through $h + \gamma$ production. We then compare the sensitivity of this channel to existing experimental searches and other methods proposed in the literature.

Secondly, we study exotic Higgs decays $h \to ZX$, with X an invisible beyond the SM particle, resulting in a semi-dark final state. Such exotic Higgs decays may occur in theories of axion-like-particles (ALPs), dark photons or pseudoscalar mediators between the SM and dark matter. The SM process $h \to Z\nu\bar{\nu}$ represents an irreducible "neutrino floor" background to these new physics searches, but also provides a target experimental sensitivity for them. We analyze $h \to Z + \textit{invisible}$ searches at the LHC and a future ILC, showing that these exotic Higgs decays can yield sensitivity to unexplored regions of parameter space for ALPs and dark matter models.

Lastly, we explore the possibility that the CP violation (CPV) required for baryogenesis is active in the early Universe but is now suppressed. A scenario well motivated by the strong constraints placed by electric dipole moments on the existence of beyond the SM sources of CPV that could catalyze the latter. By considering CP-violating interactions between a dark and the Higgs sectors, the multi-scalar dynamics in the early Universe is able to yield a transient period of CPV enhancement. This CPV then leaks to the visible sector, enabling a first-order EW phase transition to generate the observed baryon asymmetry. We argue that the requirement to generate a net baryon asymmetry avoiding cosmic domains naturally leads to a viable DM candidate. Through this two-step phase transition, the latter becomes the catalyzer for baryogenesis via its CP-violating interactions. We study an explicit realization

through a non-minimal Higgs sector consisting of two Higgs doublets and a singlet scalar odd under a $\mathbb{Z}_2$ symmetry, which has CP-violating interactions with the Higgs doublets. We analyze the regions of parameter space where such an early Universe period of CPV enhancement occurs, showing that the required thermal history leads to a predictive scenario, and discuss ongoing efforts to test it through a combination of LHC and dark matter searches.

Resumen

Esta tesis doctoral explora algunas de las incógnitas restantes dentro del Modelo Estándar (SM, por sus siglas en inglés) en torno al bosón de Higgs descubierto en el Gran Colisionador de Hadrones (LHC, por sus siglas en inglés), incluyendo su potencial papel como puente y sonda sensible a nueva física más allá del mismo.

En primer lugar, nos centramos en la producción del Higgs en asociación con un fotón en colisionadores hadrónicos, un proceso poco probable que todavía no ha sido observado en el LHC. Mostramos que es sensible a desviaciones significativas de los acoplamientos del Higgs a los quarks del SM de primera y segunda generación (particularmente los de tipo *up*) con respecto a sus valores en el SM, y utilizamos un análisis multivariable de redes neuronales para determinar las perspectivas de la fase de Alta-Luminosidad del LHC de probar desviaciones en los acoplamientos Yukawa del Higgs a los quarks *up* y *charm* a través de la producción de $h + \gamma$. Por último, comparamos la sensibilidad de este canal con las búsquedas experimentales existentes y otros métodos propuestos en la literatura.

En segundo lugar, estudiamos decaimientos exóticos del bosón de Higgs $h \to ZX$, donde X es una partícula más allá del SM invisible, lo que da como resultado un estado final semi-oscuro. Estos decaimientos exóticos del Higgs pueden ocurrir en teorías de partículas tipo axión (ALPs, por sus siglas en inglés), fotones oscuros o mediadores pseudoescalares entre el SM y la materia oscura. El proceso del SM $h \to Z\nu\bar{\nu}$ representa un fondo irreducible, un "suelo de neutrinos" para estas nuevas búsquedas de física, pero también representa un objetivo para la sensibilidad experimental del análisis. Analizamos las búsquedas de $h \to Z + \textit{invisible}$ en el LHC y en un futuro ILC, demostrando que estos decaimientos exóticos del Higgs pueden proporcionar sensibilidad a regiones inexploradas del espacio de parámetros para modelos de ALPs y materia oscura.

Por último, exploramos la posibilidad de que la violación de CP (CPV) requerida para la bariogénesis se encontrase activa en el Universo primitivo pero esté suprimida ahora. Este escenario estaría motivado por las fuertes restricciones impuestas por la ausencia de momentos dipolares eléctricos a la existencia de fuentes más allá del SM de CPV, que podrían ser las encargadas de catalizar dicha bariogénesis. Mediante interacciones entre un sector oscuro y el sector del Higgs que violan CP,

la dinámica multi-escalar es capaz, en el Universo primitivo, de producir un período transitorio de aumento de la violación de CP. Esta violación de CP se filtraría luego hacia el sector visible, permitiendo que una transición de fase electrodébil de primer orden generase la asimetría bariónica observada. La necesidad de generar una asimetría bariónica neta evitando dominios cósmicos conduce naturalmente a un candidato viable de materia oscura. A través de esta transición de fase de dos etapas, esta última se convierte en el catalizador de la bariogénesis mediante sus interacciones que violan CP. Estudiaremos una realización explícita a través de un sector de Higgs no minimal que consta de dos dobletes de Higgs y un singlete escalar impar bajo una simetría $\mathbb{Z}_2$, que tendría dichas interacciones que violan CP con los dobletes de Higgs. Analizamos la región del espacio de parámetros en la que ocurre dicho período transitorio de CPV aumentada, mostrando que la historia térmica necesaria conduce a un escenario predictivo, y discutimos los esfuerzos en curso para probarlo a través de una combinación de búsquedas en el LHC y experimentos de materia oscura.

Contents

List of Publications

This thesis is based on research that led to the following scientific publications:

[1] *More light on Higgs flavor at the LHC: Higgs boson couplings to light quarks through $h + \gamma$ production*
J. A. Aguilar-Saavedra, J. M. Cano, J. M. No
Phys. Rev. D **103** (2021) 095023 [2008.12538]

[2] *Semidark Higgs boson decays: Sweeping the Higgs neutrino floor*
J. A. Aguilar-Saavedra, J. M. Cano, J. M. No, D. G. Cerdeño
Phys. Rev. D **106** (2022) 115023 [2206.01214]

- *A Higgs CP-violating portal: Assisting baryogenesis from the dark*
J. M. Cano, S. Gori, K. Mimasu, J. M. No
In preparation

also published during the development of this thesis:

- *Data Driven Flavour Model*
F. Arias-Aragón, C. Bouthelier-Madre, J. M. Cano, L. Merlo
Eur. Phys. J. C **80** (2020) 854 [2003.05941]

List of Figures

List of Tables

Purpose and Motivation

Modern theoretical physics is built upon the pillars of General Relativity and the Standard Model (SM) of particle physics. Both theories have been thoroughly tested and found to describe a subset of reality up to an extraordinary degree of precision. And yet, neither can be said to be completely satisfactory, whether from an observational standpoint or from theoretical considerations. Notwithstanding the quantum nature of gravity, two of the most pressing issues involve the evolution and current state of our Universe. On the one hand, an increasing amount of cosmological and astrophysical evidence points to large quantities of non-baryonic matter, its presence inferred only through its gravitational effects. Dubbed as dark matter (DM), for its apparent lack of interaction with the visible sector, many viable candidates beyond the SM (BSM) have been identified, but we have yet to find conclusive evidence regarding its nature. On the other, the visible Universe seems to be comprised almost entirely out of regular matter (in opposition to antimatter, which is found only sparsely), in what is referred to as the baryon asymmetry. However, and given their similarities, it remains highly unclear how this asymmetry was generated in the first place. While in principle the SM does in fact present all the theoretical ingredients necessary to generate this asymmetry, they have been found to be insufficient, leaving open the possibility for alternative explanations involving new physics. Perhaps a more theoretically oriented question, the why of the very particular flavor structure that we observe for the SM fermion spectrum (*i.e.* the structure of their couplings to the Higgs), also remains a mystery. The parameters of the SM appear to need a significant degree of *fine-tuning* to fit observations (also beyond the flavor sector), historically the hallmark of an incomplete theory.

Furthermore and beyond these and other open questions, many properties of the SM itself have yet to be tested, most notably involving the neutrino and Higgs sectors. Within the first, and despite the efforts of a successful and now mature program of neutrino detection experiments, we have yet to conclusively establish important properties of the neutrino spectrum. Most prominently the neutrino mass ordering and absolute scale, but also the size of charge-parity (CP) violation in the lepton sector and more fundamentally, the intriguing possibility that they may be Majorana fermions. The situation is analogous to that of the Higgs sector, where an also successful LHC program has yet to measure properties such as its couplings to itself and the lighter fermions of the SM, the extent of its CP properties or its lifetime. Hints to the solutions to the above problems could very well be hidden

within outstanding measurements, and if nothing else, it is our duty to test the extent to which the SM is a good description of reality. It is thus critical to devise and implement new strategies to probe the remaining unknowns.

The above arguments have ultimately constituted the driving force behind this dissertation. One tantalizing possibility is that the Higgs boson could, in one way or another, be at the forefront of a significant fraction of the aforementioned issues. It is for this reason that a large portion of this thesis has been devoted to it in some shape or form. From the development of new ideas at colliders to test its couplings (see Chapter 2) or the consideration of novel decay signatures into the dark sector (see Chapter 3), to exploring the rich possibilities of extended scalar sectors in relation to CP violation, dark matter and baryogenesis (see Chapter 4). The preceding Chapter 1 will serve as an introduction and provide a brief review of the current phenomenological status of the Higgs boson. Finally, a summary of our conclusions is presented at the end of the thesis.

1

The Higgs Boson and its Phenomenology

1 The Standard Model

1.1 Gauge Symmetry

Symmetry and the gauge principle can be singled out as the main drivers of success in building our understanding of high-energy particle physics. Their implementation within the framework of quantum field theory allows for the prediction of experimentally observable magnitudes such as cross sections or decay rates, among many others. The SM [3–6] embodies these principles, being, at its core, a quantum field theory based on the gauge symmetry group

$$\mathcal{G} = SU(3)_C \times SU(2)_L \times U(1)_Y. \tag{1.1}$$

This gauge group encodes the behavior of the strong and electroweak (EW) interactions, along with the description of the spin-1 bosons which form part of the elementary SM particle content and are said to mediate them. The strong interactions manifest between those particles which transform under the gauge symmetry group $SU(3)_C$ (C stands for color), and are thus charged under it. On the other hand, the EW interaction $SU(2)_L \times U(1)_Y$, comprises the weak isospin symmetry group $SU(2)_L$ and the weak hypercharge group $U(1)_Y$. Given the group and the coupling constants of each subgroup, hereby defined as g_s for $SU(3)_C$, g for $SU(2)_L$ and g' for $U(1)_Y$ at a certain energy scale μ, this part of the theory is completely determined. A number of spin-1 bosons arise as a consequence, one for each of the generators belonging to each subgroup, that are said to mediate the interaction. Thus we have eight gluons for the strong interaction, three W bosons as the mediators of the weak isospin interaction, and the B boson mediating the hypercharge interaction.

We can now write the Lagrangian density for the gauge sector of the SM

$$-\mathscr{L}_g = \frac{1}{2}\mathrm{Tr}\left(G^{\mu\nu}G_{\mu\nu}\right) + \frac{1}{2}\mathrm{Tr}\left(W^{\mu\nu}W_{\mu\nu}\right) + \frac{1}{4}B^{\mu\nu}B_{\mu\nu}, \tag{1.2}$$

where μ and ν are contracted Lorentz indexes following Einstein's summation convention, and $G_{\mu\nu}$, $W_{\mu\nu}$ and $B_{\mu\nu}$ are defined as the field strengths of $SU(3)_C$, $SU(2)_L$ and $U(1)_Y$ respectively in the following way

$$\begin{aligned} G_{\mu\nu} &= \partial_\mu \boldsymbol{G}_\nu - \partial_\nu \boldsymbol{G}_\mu + ig_s\left[\boldsymbol{G}_\mu, \boldsymbol{G}_\nu\right], \\ W_{\mu\nu} &= \partial_\mu \boldsymbol{W}_\nu - \partial_\nu \boldsymbol{W}_\mu + ig\left[\boldsymbol{W}_\mu, \boldsymbol{W}_\nu\right], \\ B_{\mu\nu} &= \partial_\mu B_\nu - \partial_\nu B_\mu, \end{aligned} \tag{1.3}$$

with $\boldsymbol{G}_\mu$ and $\boldsymbol{W}_\mu$ subsequently defined as

$$\boldsymbol{G}_\mu \equiv \frac{\lambda_i}{2}G^i_\mu, \quad \boldsymbol{W}_\mu \equiv \frac{\sigma_i}{2}W^i_\mu. \tag{1.4}$$

G^i_μ denote the eight gluon vector-boson fields, W^i_μ, the three weak-isospin mediators, and B_μ, the hypercharge boson, whereas λ_i, the Gell-Mann matrices, are the generators of $SU(3)$, and σ_i, the Pauli matrices, the equivalent of $SU(2)$. The above Lagrangian describes the propagation and self-interaction of these fields. We shall introduce as well for later convenience the covariant derivative, which will allow for their interaction with the rest of the particle content of the SM, defined as follows

$$D_\mu \equiv \partial_\mu + ig_s\boldsymbol{G}_\mu + ig\boldsymbol{W}_\mu + ig'Q_Y B_\mu, \tag{1.5}$$

where Q_Y will be the hypercharge of the field the covariant derivative is acting upon, while $\boldsymbol{G}_\mu$ and $\boldsymbol{W}_\mu$ will only be present if the latter belongs to the fundamental representation of the corresponding gauge subgroup.

1.2 Electroweak Symmetry Breaking

The complete description of the SM relies yet on another key element. Canonical bare mass terms cannot be added directly to the Lagrangian, as they are not invariant under $\mathcal{G}$. The SM circumvents this issue through the celebrated Higgs[1] mechanism [7–9], which requires the addition of a $SU(2)_L$ doublet spinless boson (scalar under Lorentz transformations) with two complex components, denoted H, with the following transformation properties under $\mathcal{G}$

$$H \in (1, 2, 1/2)_{\mathcal{G}}\,. \tag{1.6}$$

[1] Throughout this work we will refer to both particle and mechanism as "Higgs" for conciseness. However, as it usually happens, the full extent of its development was due to the work of many individuals. A more complete (but still probably non-exhaustive) list would include Anderson, Brout, Englert, Guralnik, Hagen, Higgs, Kibble and 't Hooft.

Its implementation within the SM Lagrangian relies on the addition of two new parameters

$$\mathscr{L}_H = (D_\mu H)^\dagger D^\mu H - \lambda \left(H^\dagger H - \frac{v^2}{2} \right)^2 , \tag{1.7}$$

one with dimensions of energy, v, which implicitly defines the EW scale $v \approx 246$ GeV, and the dimensionless self-Higgs-coupling constant, $\lambda \approx 0.13$ [10]. Both parameters are experimentally determined by the measurement of the Fermi constant $v = (\sqrt{2} G_F)^{-1/2}$ from muon decay measurements and Higgs boson mass $m_h = \sqrt{2\lambda} v$. The second term in Eq. (1.7), the Higgs potential, is minimized for $H^\dagger H = v^2/2$, consequently inducing a non-zero vacuum expectation value (VEV) for the Higgs field. When expanding around this vacuum, its interaction with the rest of the fields will give rise to the mass terms needed to properly accommodate the physical particle spectrum. This interaction is in turn determined by the Higgs charges (or equivalently, transformation properties) under $\mathcal{G}$, which were shown in Eq. (1.6).

The Higgs non-zero VEV induces the spontaneous symmetry breaking of three out of the four generators (often referred to as "directions") of the gauge group $SU(2)_L \times U(1)_Y$ of the EW interactions, a phenomenon commonly referred to as Electroweak Symmetry Breaking (EWSB). Three out of the four degrees of freedom in the Higgs field would then ordinarily resolve as massless Goldstone bosons under the Goldstone theorem. However, being coupled to the EW gauge fields through the covariant derivatives of the above Lagrangian, they end mixing with the combinations of W and B bosons matching the broken generators, and become, in the unitary gauge, the longitudinal components of the physical W^+, W^- and Z bosons, made massive as a result of their inclusion. The single remaining degree of freedom in the doublet becomes a new massive scalar particle, the Higgs boson.

The combination of generators of $SU(2)_L \times U(1)_Y$ that still preserves the vacuum, and thus, defines the gauge group that remains unbroken after EW symmetry breaking, is the one corresponding to the electromagnetic group $U(1)_{em}$. The combination of gauge fields pointing in this direction stays massless, and amounts to the physical photon γ. All in all, after the rotation from the weak interaction eigenstates to the mass eigenstates, we are left with the physical spectrum of gauge boson fields

$$\begin{aligned} \begin{pmatrix} W_\mu^+ \\ W_\mu^- \end{pmatrix} &= \frac{1}{\sqrt{2}} \begin{pmatrix} 1 & -i \\ 1 & +i \end{pmatrix} \begin{pmatrix} W_\mu^1 \\ W_\mu^2 \end{pmatrix} , \\ \begin{pmatrix} \gamma_\mu \\ Z_\mu \end{pmatrix} &= \begin{pmatrix} \cos\theta_W & \sin\theta_W \\ -\sin\theta_W & \cos\theta_W \end{pmatrix} \begin{pmatrix} B_\mu \\ W_\mu^3 \end{pmatrix} , \end{aligned} \tag{1.8}$$

where the weak mixing angle $\theta_W \equiv \tan^{-1}(g'/g)$ has been introduced. Expanding the covariant derivatives in Eq. (1.7), the masses of the W and Z bosons read

	$SU(3)_C$	$SU(2)_L$	$U(1)_Y$
Q_L	3	2	1/6
U_R	3	1	2/3
D_R	3	1	-1/3
ℓ_L	1	2	-1/2
E_R	1	1	-1

Table 1.1: Fermion transformation properties under $\mathcal{G}$.

$$m_W^2 = \frac{g^2 v^2}{4}, \qquad m_Z^2 = \frac{(g^2 + g'^2) v^2}{4}. \tag{1.9}$$

1.3 Fermion Fields

Next in order, completing the sequence of intrinsic angular momentum between the spin-1 vector and spin-0 scalar bosons, come the spin-1/2 fermions. They can be classified according to their transformation properties under $\mathcal{G}$, which in turn determine the way they interact with the rest of the fields of the SM. We can draw the first distinction on whether they are able or not to interact strongly under the gauge group $SU(3)_C$. Those who can, are referred to as quarks, those who cannot, we call leptons. We can split them even further according to the way they behave under the weak isospin group $SU(2)_L$. Among the quarks, we can distinguish between the doublets, Q_L, and the singlets, U_R, and D_R; whereas leptons divide into doublets, ℓ_L, and singlets, E_R. Lastly, each of these is charged differently under the hypercharge $U(1)_Y$ group. The transformation properties of the fermions in the SM are summarized in Table 1.1.

The representations of the non-abelian groups ($SU(3)_C$ and $SU(2)_L$) form a discrete set, *e.g.* the fundamental representation, the adjoint representation, etc. Every fermion in the SM either transforms in the simplest non-trivial of them, the fundamental, denoted in the above table as N for $SU(N)$, or does not transform at all, acting as a singlet, denoted by 1 in the first two columns (we already used this notation for the Higgs field in Eq. (1.6)). As for the abelian gauge group $U(1)_Y$, the seemingly random choice of representations (charges) for the different fermions comes as a predictive success of the gauge principle (modulo a normalization factor). The cancellation of anomalies, or equivalently, the conservation of the symmetry at a quantum loop level, imposes hard constraints on the assignment of hypercharges. The subscripts L and R have been used to denote the left and right handed chirality components of fermions.

The interaction between fermions and gauge fields is implemented in the Lagrangian through the covariant derivative in the kinetic terms

$$\mathscr{L}_{kin} = i \sum_{\Psi} \overline{\Psi} \not{D} \Psi , \tag{1.10}$$

where $\not{D} \equiv \gamma^\mu D_\mu$ with γ^μ denoting the Dirac matrices, and the sum over Ψ extends over the fermions in Table 1.1.

1.4 Fermion Flavor

There is yet another layer to the fermion structure of the SM, namely, the flavor. Three copies of the fermion fields described in Table 1.1 are observed in nature, with the exact same charges but disorderly masses. These are commonly referred to as families or generations, and can be arranged in the following way

$$\begin{aligned} Q_L^i &= \left(\begin{pmatrix} u_L \\ d_L \end{pmatrix}, \begin{pmatrix} c_L \\ s_L \end{pmatrix}, \begin{pmatrix} t_L \\ b_L \end{pmatrix} \right) \\ \ell_L^i &= \left(\begin{pmatrix} \nu_L^e \\ e_L \end{pmatrix}, \begin{pmatrix} \nu_L^\mu \\ \mu_L \end{pmatrix}, \begin{pmatrix} \nu_L^\tau \\ \tau_L \end{pmatrix} \right) \end{aligned} \qquad \begin{cases} U_R^i = (u_R, c_R, t_R) \\ D_R^i = (d_R, s_R, b_R) \\ E_R^i = (e_R, \mu_R, \tau_R) \end{cases} , \tag{1.11}$$

where we have used i as the index running in flavor space, denoting the up, down, charm, strange, top and bottom quarks as u, d, c, s, t and b respectively; and in the lepton sector, the electron, the muon, the tau and their corresponding neutrinos as e, μ, τ and ν; finally displaying the whole fermion spectrum of the SM.

In the simplest realization of the SM, neutrinos are massless, and the mass terms for the rest of the fermions arise through Yukawa interactions between these and the Higgs field once the latter is expanded around its VEV. The piece of the SM Lagrangian containing this mass generating terms reads as follows

$$-\mathscr{L}_{Yuk} = \overline{Q}_L \tilde{H} Y_U U_R + \overline{Q}_L H Y_D D_R + \overline{\ell}_L H Y_E E_R + H.c. , \tag{1.12}$$

where $\tilde{H} \equiv i\sigma_2 H^*$, with the second Pauli matrix σ_2 acting over the weak isospin space, and Y_U, Y_D and Y_E denote 3×3 matrices acting over flavor space, each of their entries giving rise to the different Yukawa couplings between quarks and leptons and the Higgs. As we shall see, these matrices encode the entire flavor structure of the SM, from masses to mixings, and will constitute one of the main objects of our study throughout this thesis.

Without loss of generality, the Yukawa matrices in Eq. (1.12) can be written as the product of a unitary matrix, a diagonal matrix of eigenvalues, and a different unitary matrix on the right end, explicitly

$$Y_U = \mathcal{U}_L^U y_U \mathcal{U}_R^U , \quad Y_D = \mathcal{U}_L^D y_D \mathcal{U}_R^D , \tag{1.13}$$

where $\mathcal{U}_{L.R}^{U,D}$ are the unitary matrices and $y_{U,D}$ the diagonal matrices composed

by the eigenvalues of the original Yukawa matrices. The following redefinition of the quark fields in flavor space

$$Q_L \to \mathcal{U}_L^U Q_L, \quad U_R \to \mathcal{U}_R^{U\dagger} U_R, \quad D_R \to \mathcal{U}_R^{D\dagger} D_R, \tag{1.14}$$

simplifies, while leaving the rest of the Lagrangian invariant, the Yukawa matrices in Eq. (1.12) to the form

$$Y_U = y_U, \quad Y_D = \mathcal{U}_L^{U\dagger} \mathcal{U}_L^D y_D, \tag{1.15}$$

where the Cabibbo-Kobayashi-Maskawa (CKM) quark mixing matrix $V_{CKM} \equiv \mathcal{U}_L^{U\dagger} \mathcal{U}_L^D$ [11, 12] has been made apparent. Its appearance is ultimately a consequence of the mismatch between the weak interaction eigenstates and the mass eigenstates, those which propagate freely.

After the Higgs takes a non-zero VEV breaking the EW symmetry, the independent rotation of the lower component of the quark isospin doublet: $D_L \to V_{CKM} D_L$, brings us to the mass basis, rendering the Yukawa terms diagonal in flavor space

$$-\mathscr{L}_{Yuk}^q = y_i \frac{v+h}{\sqrt{2}} \overline{U}_L^i U_R^i + y_j \frac{v+h}{\sqrt{2}} \overline{D}_L^j D_R^j + H.c.\,, \tag{1.16}$$

where h is the physical Higgs boson. Quark masses are then read straightforwardly as

$$m_q = y_q \frac{v}{\sqrt{2}} \approx y_q \, 174 \text{ GeV}. \tag{1.17}$$

It is then a SM prediction that their couplings to the Higgs are proportional to their masses, making light quark Yukawa couplings extremely hard to access experimentally. The development of new ideas to probe these couplings is one of the main goals driving the research on this thesis (see Chapter 2).

This rotation to the mass basis goes unnoticed in all but one of the rest of the terms in the Lagrangian, the one coupling the two components of the quark doublet through the EW interaction, which now reads

$$\mathscr{L}_{CC} = i \frac{g}{\sqrt{2}} \overline{U}_L V_{CKM} \not{W}^+ D_L + H.c. \tag{1.18}$$

The end result is that the flavor violating source has been effectively shifted from the mass terms to the coupling of the quarks to the $W^\pm$ gauge bosons. It is important to note why this mixing matrix emerges in the SM. We cannot diagonalize both Yukawa matrices at the same time because the two terms involving the up and down quarks contain the same weak isospin doublet Q_L, causing the appearance of an irreducible mixing matrix. Moreover, this mixing matrix only has an effect in the first place because U_L and D_L interact weakly, since its unitarity makes it drop form the rest of the terms in the Lagrangian. Both mass terms and $SU(2)_L$ interactions

are needed in conjunction for flavor violation phenomena to manifest in the SM. The role of the unitary matrix entering the Yukawa couplings has been made apparent now, the mixing matrix parametrizes the change of basis from the interaction to the mass basis. As a 3 × 3 unitary matrix, the CKM can be parametrized by three mixing angles and a CP-violating phase. Conventionally, it is often written as

$$V_{CKM} = \begin{pmatrix} c_{12}c_{13} & s_{12}c_{13} & s_{13}e^{-i\delta} \\ -s_{12}c_{23} - c_{12}s_{23}s_{13}e^{i\delta} & c_{12}c_{23} - s_{12}s_{23}s_{13}e^{i\delta} & s_{23}c_{13} \\ s_{12}s_{23} - c_{12}c_{23}s_{13}e^{i\delta} & -c_{12}s_{23} - s_{12}c_{23}s_{13}e^{i\delta} & c_{23}c_{13} \end{pmatrix}, \tag{1.19}$$

where $s_{ij} = \sin\theta_{ij}$, $c_{ij} = \cos\theta_{ij}$ and δ is the phase responsible for all CP-violating (CPV) phenomena in the SM. Experimentally, the CKM matrix is found to be close to the identity [10], with a very hierarchical structure characterized by

$$\sin\theta_{13} \ll \sin\theta_{23} \ll \sin\theta_{12} \ll 1. \tag{1.20}$$

Due to the uncertain nature of neutrinos, specifically whether they are Dirac or Majorana fermions, providing a comprehensive overview of the lepton sector is beyond the scope of this introduction. However, the diagonalization of the Yukawa matrices can proceed in analogous fashion to what we have shown for the quark sector, with the Pontecorvo–Maki–Nakagawa–Sakata (PMNS) matrix [13, 14] taking the place of the CKM.

2 Higgs Phenomenology: Into the Era of Precision

With the long-sought discovery of the Higgs boson in 2012 by the ATLAS [15] and CMS [16] collaborations at the Large Hadron Collider (LHC) came the first conclusive piece of experimental evidence supporting the EWSB mechanism depicted in the previous Section. In a relatively short span of time, following LHC Run 1 and 2 of data collection, we have gained remarkable insights into this new fundamental particle, which so far appears to conform to SM expectations. Despite this considerable success, there is still much to be established concerning the Higgs sector. The problem is two-fold, on the one hand, there exist interactions that have yet to be observed, some of which pose significant experimental challenges. On the other, while the SM is indeed consistent with present observations, the same can be said for other theoretically motivated alternatives, demanding higher levels of precision in existing measurements to conclusively distinguish between them. The aim of this section is to provide a concise overview of this progress, serving as valuable context for the work presented in this thesis.

Starting with what we know, the LHC has made substantial progress in determining the properties of the Higgs boson by investigating its production and decay through various channels. The primary production mechanisms for a Higgs boson in

a proton-proton collider at the center of mass energies of the LHC are, in descending order of cross-section: gluon fusion (ggF), weak-boson fusion (VBF), associated production with a gauge boson (Vh), associated production with a pair of top and anti-top quarks ($t\bar{t}h$), and associated production with a single top quark (thq). Notably, the LHC is also capable of producing pairs of Higgs bosons (hh). All of these Higgs bosons decay promptly inside the detector after they are created, with the dominant decay channels being $h \to b\bar{b}$ and $h \to WW^*$, followed by $h \to gg$, $h \to \tau^+\tau^-$, $h \to c\bar{c}$ and $h \to ZZ^*$. With smaller branching ratios yet aided by cleaner experimental signatures come the decays $h \to \gamma\gamma$, $h \to Z\gamma$, and $h \to \mu^+\mu^-$.

While it is impossible to disentangle the Higgs couplings involved in production and decay from each of these channels individually at the LHC, observable combinations can be grouped together and compared to SM predictions to gather information on each of these couplings separately. These comparisons, often referred to as signal strengths, along with other approaches like off-shell probes or the comprehensive use of kinematic distributions, enable the extraction of the properties that characterize the Higgs boson. These include its couplings to itself and the rest of the SM particles (and potentially to other BSM particles), the branching ratios of its decay modes (that could include exotic BSM decays), its mass, lifetime, spin and CP quantum numbers. Each of these measurements presents its own experimental challenges, making them difficult to varying degrees.

Overall, assembling the information obtained from the methods just described, a picture of agreement with the SM predictions has emerged [17, 18]. Today we are fairly certain that we are dealing with an approximately CP-even scalar, with a precisely measured mass of $m_h = 125.25 \pm 0.17$ GeV [10]. We have also been able to measure Higgs couplings to vector bosons and third generation fermions, the heaviest particles in the SM spectrum besides the Higgs, and thus the ones that couple more strongly to it, with accuracies that range from just a few percent to $\mathcal{O}(10\%)$, having found them to be in agreement with SM expectations. However, and despite this significant progress, to claim that we have established the SM picture would be highly premature at this stage. While experimentally remarkable, percent-level precision is simply not enough to rule out well-motivated alternatives to the SM that address, for instance, some of the open problems that will be outlined in the section below.

Moreover, our exploration of the interactions of the Higgs boson is far from complete. Only recently have the ATLAS and CMS collaborations reported data suggestive of the observation of the Higgs decay $h \to \mu^+\mu^-$ [19, 20], which would provide sensitivity to this coupling. Beyond the muon, there still remains the challenge of measuring the Higgs coupling to the charm quark, potentially accessible at the LHC as well, but also its couplings to the strange quark and the charged fermions of the first generation (not to mention neutrinos).[1] The latter are fundamental to our understanding of the Universe, as they ultimately shape nuclear and atomic phenomena. In addition, we have yet to measure the couplings of the Higgs to itself, which determine the scalar potential of the theory and thus constitute a key element

[1] For a more complete review of the status of these measurements, refer to Chapter 2.

in the description of the EWSB mechanism. Owing to Higgs pair production, the Higgs tri-linear coupling might become accessible within the lifetime of the LHC.

To conclude this brief (and non-exhaustive) summary of the open challenges in the Higgs sector, we too have yet to test the SM prediction for the width (or equivalently, the lifetime) of the Higgs boson. Nevertheless, both the width and the decays that contribute to it constitute a particularly well-motivated avenue to search for new physics. Since the Higgs can only decay into particles to which it couples weakly in the SM, any BSM coupling opening new decay channels could provide a sizable contribution to its width, and consequently, lead to observable branching ratios. While the width would provide sensitivity to these decays indirectly, this also opens the tantalizing possibility to search for these exotic BSM decay modes directly in various final states, extending the reach of the LHC (and future colliders). The investigation of one such possibility, further motivated by some of the theoretical issues we will review in the next Section, will be the primary focus of Chapter 3.

The path forward is relatively clear, the LHC will need to collect more data (beyond the currently running Run-3, a High-Luminosity phase is also planned) and eventually, we might require the construction of different or more powerful colliders (such as the ILC or the FCC). In the meantime, however, it is critical that we continue devising novel ways to optimally exploit the full extent of the data. The latter has been one of the main goals of this dissertation and the motivation for the work in Chapters 2 and 3.

3 Open Problems in the Standard Model: the Central Role of the Higgs

The SM has proven a remarkably robust framework to describe physics up to the energies probed by the LHC. It not only stands in agreement with the Higgs measurements outlined in the previous section, but also with a myriad other observations spanning numerous experiments and different scales, from quantum chromodynamics to electroweak physics, including varied and complex flavor phenomena. While it would appear natural to become complacent with its description of nature, there are still several fundamental questions for which the SM offers no compelling explanation. Intriguingly, the Higgs boson plays a central role in many of these open problems, which raises the tantalizing possibility of an unified explanation. The aim of this Section is to briefly review three of these issues, namely: the flavor puzzle, observed DM abundance and the baryon asymmetry of the Universe, as well as their connection to the Higgs boson, which has ultimately served as the unifying thread for the work on this thesis.

The flavor sector of the SM has long been regarded as problematic. On the one hand, we face a naturalness issue commonly referred to as the flavor puzzle: there is no explanation for the heterogeneity of fermion masses and mixings, which in the SM, is merely displayed parametrically. On the other, attempts at more natural dynamical explanations are often met by phenomenologically dangerous predictions

of flavor violating processes.

Naturalness is, however, a subtle theoretical issue, with implications that are not yet clearly understood. In this context, we employ the term "naturalness" to refer to 't Hooft's naturalness criteria [21, 22], which states that any dimensionless parameter in the theory is generally expected to be of order one, and all dimensionful ones should be of the order of the scale(s) of the theory. Stronger than $\mathcal{O}(10\%)$ adjustments (typical Clebsch-Gordan coefficients) are usually considered to be fine-tuned, and regarded as undesirable. While the free parameters of the gauge sector, g_s, g, g' and λ, are small but $\mathcal{O}(1)$ at the typical scale of the theory (namely, the EWSB scale $v \approx 246$ GeV), the Yukawa couplings of the quark sector span over five orders of magnitude. Moreover, while the down quark happens to be heavier than the up quark (a fact which is crucial for the stability of the proton), the opposite holds true for the other two families. The situation is even worse in the leptonic sector, where neutrinos are extremely light and thus demand exceedingly small Yukawa couplings. On the other hand, the mixing patterns of the CKM and PMNS matrices stand as a mystery of their own, with no known explanation for their particular shape. For comparison, in the gauge sector, hypercharges turn out to be heavily constrained by the consistency of the theory. Furthermore, gauge invariance forces particles into representations of the group, so that the dimension of the representation dictates the number of particles, *e.g.* there are up and down quarks in each generation to fit the fundamental representation of $SU(2)_L$. It is this degree of fine-tuning and apparent arbitrariness characterizing the parameters in the flavor sector what causes us to refer to their enigmatic origin within the theory as the flavor puzzle.

At its heart, the flavor puzzle is an issue revolving around the Higgs, as it is ultimately its couplings that generate this non-trivial structure. In order to shed light at this matter, it is thus critical to devise new methods to probe the Yukawa couplings of the Higgs to the SM fermions, particularly those which, as discussed in the previous section, remain difficult to measure at the LHC. In Chapter 2, we will introduce one such method to probe light quark Yukawa couplings.

On the other hand, the remaining of this thesis will deal with two major issues that involve the cosmological evolution and state of our Universe. The first is the existence of dark matter, designated this way in reference to its apparent lack of interaction with visible matter beyond the gravitational effects it is inferred for. By now, a plethora of astrophysical and cosmological evidence has mounted towards its existence, from the formation, evolution and morphology of galactic structures, stellar streams, gravitational lensing effects (and more), to vast galaxy surveys charting baryon acoustic oscillations or its effects on the cosmic microwave background, that ultimately lead to the most precise determination of its abundance. However, the reality is that despite accounting for approximately 26% of the energy budget of our Universe and 84% of its matter [23], the microscopic nature of DM has so far eluded our experimental efforts. Although the SM does in fact predict the existence of a DM component, the weakly interacting neutrinos, their abundance is predicted to be far below that required to match observations. It is thus clear that the enigmatic

origin of DM requires new yet undiscovered phenomena.

A very plausible resolution to this conundrum is that the DM is composed by yet unknown BSM particles that interact with the visible sector. Accordingly, an ambitious experimental program has been deployed to detect these and identify their nature. This program operates mainly in two fronts, that are commonly referred to as direct or indirect detection. Experiments on the first look closely at targets placed on isolated environments, with the hope of eventually observing any disturbances caused by the interaction with the DM passing through them. Whereas experiments of the second kind are hoping to observe the annihilation of DM into visible particles instead, looking at the regions where the largest abundances of the first are expected. Importantly there is yet another complementary avenue for discovery, that relies instead on producing the DM ourselves in collider experiments. Generally, this DM will escape the detectors unnoticed, so that the aim of these experiments is to either detect its presence through missing momentum searches triggered by the visible particles in the event, or to search for the particles mediating the interaction between the DM and the SM. The latter could manifest either as new resonances or through their effect on the kinematic distributions of the final state.

These searches are theoretically motivated by the three well-known possibilities to build a "portal" from the SM to the dark sector, the hypercharge [24], neutrino [25], and Higgs [26–28] portals. Building on the SM success, portals encompass the idea of bridging the visible and dark sectors in a gauge-invariant renormalizable way. Given its apparent lack of interaction, it is only natural to consider scenarios where the DM is a singlet of $SU(3)\times SU(2)\times U(1)$. If this is the case, the Higgs portal emerges as the only feasible renormalizable realization of its interaction with the visible sector, highlighting the uniquely central role of the Higgs in addressing this issue. This connection will be further explored in both Chapters 3 and 4.

The second, but no less important issue, is that we have yet to understand how our Universe came to be matter-dominated. If assuming the widely accepted inflationary scenario, any initial baryon asymmetry would have been washed out into a symmetric, hot and dense plasma, where particle-antiparticle pairs would have been copiously produced and annihilated. Under such conditions, a balanced universe with equal amounts of matter and antimatter would be expected. The observation of a predominantly matter-based universe challenges this expectation, and suggests a dynamical explanation for this asymmetry, a *baryogenesis* mechanism. There are three necessary conditions for successful baryogenesis, known as the Sakharov conditions [29]. These are the requirement of baryon number violation, both the violation of particle-antiparticle (charge or C) symmetry and its combination with left-right (parity or P) symmetry, and a departure from thermal equilibrium. Together, they ensure the presence of net baryon number generating interactions that cannot be counterbalanced by other processes connected to them through these symmetries, or acting in both directions.

Remarkably, the SM does in fact present all the necessary ingredients to fulfill Sakharov conditions. Within it, the combination of baryon (B) and lepton (L) numbers $B+L$, is found to be anomalous, *i.e.* broken at the quantum level. This

breaking happens through transitions between inequivalent vacua of the $SU(2)_L$ gauge group. These transitions conserve the difference $B - L$ and can thus generate net baryon number differences $\Delta B \neq 0$. If active at temperatures above the EW phase transition, these non-perturbative processes could induce a baryon asymmetry during the latter [30]. If first-order, this transition could provide sufficient departure from thermal equilibrium in the form of bubbles of the EW vacuum expanding in the unbroken phase. Moreover, the SM violates parity maximally, with right-handed fermions that do not engage in electroweak interactions. Since the SM is CP symmetric in the limit of vanishing Yukawa couplings, this P breaking signals C violation as well. It is nevertheless the fact that these couplings do not vanish, that leads to an observably small amount of CPV in the form of the CP phase of the CKM (and potentially PMNS).

As it turns out, however, we have long known this CP violation is insufficient to generate the observed baryon asymmetry [31–34]. Furthermore, and after the discovery of the Higgs, we now believe the SM presents a second order EW phase transition, which would be characterized by a soft *rollover* between the two phases. It is thus clear the SM cannot account for the observed baryon asymmetry of the Universe by itself, and instead, the latter constitutes further evidence for the existence of new physics.

While there are various proposals for baryogenesis, one well-motivated possibility involves addressing both of these limitations. These scenarios, known as theories of EW baryogenesis [35, 36], require both the presence of new sources of CP violation and a sufficiently strong first-order EW phase transition. They generally incorporate extended scalar sectors beyond the SM (for instance, an extra singlet, or a second Higgs doublet) and thus lead to relevant phenomenological predictions for the observed Higgs boson. Typically, it is difficult to achieve both while satisfying current experimental constraints. To accomplish such has been one of the goals of the work in Chapter 4.

2

Probing Higgs Yukawa Couplings to Light Quarks

1 State of the Art

As discussed in Chapter 1, Higgs boson couplings can be measured at the LHC through combinations of the different production and decay channels, measured together and compared to SM predictions in the form of signal strengths. In general, different couplings contribute to production and decay, so that the combination of all measurements is necessary to constrain each individually. In the SM, there is a one-to-one correspondence between these and particle masses. Any deviation could thus become the first signal of BSM physics.

So far these tests reveal that the Higgs boson discovered more than ten years ago is remarkably consistent with the SM expectation. Nevertheless, it is crucial to measure its couplings without relying on the SM assumption. This requires a framework that can treat deviations coherently within quantum field theory and provide predictions for the observables to be confronted with experimental data. One such approach that has become standard in the field, largely because of its simplicity, is the so-called κ-formalism [37]. Within it, Higgs couplings are rescaled by free factors, κ's, retaining their Lorentz structure, and thus, allowing to efficiently reuse SM computations. These κ's can then be fitted to experimental observations and compared to the SM hypothesis, *i.e.* $\kappa_q = 1$, where q labels each of the couplings of the Higgs. Figure 2.1 (extracted from Ref. [17]) depicts the agreement between the 125 GeV boson discovered at the LHC and the expectations for the SM Higgs boson within this formalism.

It is important to note the κ-formalism comes with important limitations, as it certainly cannot capture the whole extent of the effects of a departure from the SM in the framework of quantum field theory, even under the assumption of heavy decoupling degrees of freedom. Effective field theories (EFT) have become a popular alternative within the field to address some of these limitations [38–42]. However, they come with problems of their own, most notably, they either have to assume the absence or account for any possible new physics at a lighter scale.

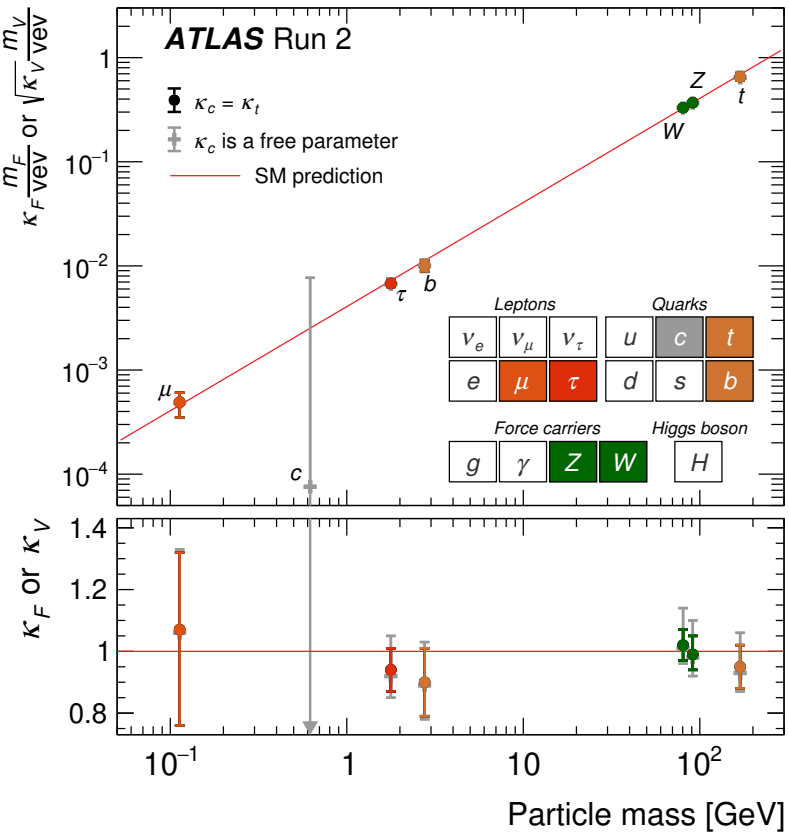

Figure 2.1: Measured Higgs boson coupling strengths and their uncertainties (68% CL) versus particle masses. Red line shows expected SM behavior, *i.e.* couplings that are linearly proportional to the corresponding particle mass (or quadratically for the W and Z bosons). Two fit scenarios with $\kappa_c = \kappa_t$ (colored circle markers), or k_c left free-floating in the fit (gray cross markers) are shown. Loop-induced processes are assumed to have the SM structure, and Higgs boson decays to non-SM particles are not allowed. Individual κ's are shown on the lower panel. Plot extracted from Ref. [17] by the ATLAS collaboration, the CMS collaboration has presented similar results [18].

Figure 2.1 also showcases two of the salient features of Higgs couplings phenomenology. The first is straightforward, in the SM, the heavier the particle the larger its coupling to the Higgs. Thus, in general, couplings of the Higgs to the heavier particles of the SM spectrum are easier to observe and quantify in experiments. The second has to do with the technical characteristics of particle detectors at colliders. Generally, leptons and particles decaying into them provide cleaner experimental signatures than quarks, which undergo showering and hadronization under the strong interaction, leading to more complex final states and larger backgrounds. The combination of these factors explains the chronology of Higgs couplings measurements at the LHC: starting from its coupling to the W and Z bosons, progressing to the top, tau and bottom, completing the third generation, and lastly, the recent reports of the first evidence for the Higgs coupling to the muon [19, 20].

Following the path of discovery, we now turn our attention to the Higgs Yukawa coupling of the charm quark. The relatively broad constraints on its magnitude are the rationale behind Figure 2.1, which displays its results under two scenarios. In the first, the charm coupling modifier is set to that of the top quark, $\kappa_c = \kappa_t$, in an effort to address the limited sensitivity to this coupling. The second scenario allows κ_c to remain a free parameter within the fit. The latter approach yields an upper limit of $\kappa_c < 5.7$ at 95% CL [17]. Nevertheless, by leveraging novel charm jet identification and analysis methods using machine learning techniques applied to the $H \to c\bar{c}$ decay, the CMS collaboration has been able to establish one of the strongest direct bounds to date, $1.1 < |\kappa_c| < 5.5$ at 95% CL [43]. Furthermore, a combination of several channels recently enabled the ATLAS collaboration to report what is currently the most stringent constrain on this coupling, $\kappa_c \in [-4.46, 4.81]$ at 95% CL [44]. Given these and ongoing advances on detectors and experimental techniques, there are reasons to remain hopeful going into the High-Luminosity (HL) phase of the LHC. On the other hand, there is no clear route to conclusively establish Higgs couplings to the rest of the light SM fermions, which are believed to be out of the reach of the LHC. This includes the strange, up and down quarks, electron and neutrinos, with current bounds that lie orders of magnitude above SM predictions (see Section 4 for a more comprehensive review).

Motivated within this context, this Chapter introduces a novel approach to further constrain Higgs couplings to first and second generation quarks (particularly the up and charm Yukawa couplings). Following an study of its feasibility, it will be compared to other existing and proposed methods, including the experimental results that have resulted from its adoption [45].

2 Theoretical Motivation

Even if the couplings of the Higgs to the first two generations of quarks as predicted by the SM turn out to be beyond the reach of the LHC, it remains crucial to maximize its sensitivity to them. Doing so will enable exploration of well-motivated BSM scenarios, where significant enhancements in these Yukawa couplings are possible or even expected. This Section will present a concise review of some of these realiza-

tions, which provide motivation to search for these couplings even when resulting bounds lie far above SM expectations.

The first and perhaps simplest idea involves Higgs democracy in the Yukawa sector [46]. Such models propose the existence of a "private Higgs" and a dark scalar associated with each fermion, thus addressing the large hierarchy among fermion masses and decorrelating the corresponding Yukawa couplings.

Alternatively, Yukawa couplings could be dynamical instead, arising when a given combination of scalar fields (usually referred to as *flavons*) acquires a vacuum expectation value. An economical solution is to consider the Higgs doublet itself [47]. These Higgs-dependent Yukawa couplings would explain the fermion mass hierarchy through appropriate powers of the Higgs vacuum expectation value, leading to modified Higgs couplings and flavor phenomenology with respect to SM predictions.

A popular extension of the SM considers the addition of a second Higgs doublet, as there is no theoretical prior that would suggest there should exist only one. Known as two Higgs doublet models (2HDM, for a review see Ref. [48]), they feature rich and complex (flavor) phenomenology, and could realize scenarios with enhanced Yukawa couplings. For instance, the two doublets could jointly act as the flavon [49, 50], as an alternative to the previously discussed single-Higgs scenario.

In *flavorful* 2HDM with a non-standard Yukawa sector, one Higgs doublet could give masses to weak gauge bosons and third generation fermions, while the second provides mass to the lighter fermion generations [51, 52]. The collider signatures of such flavorful Higgs bosons differ significantly from well-studied 2HDM with natural flavor conservation, flavor alignment or minimal flavor violation, traditional hypotheses to avoid phenomenologically dangerous flavor changing neutral currents (FCNC). These models could also realize enhanced couplings to the first two generations of fermions, in which case new production mechanisms and decay modes involving the latter for the heavy scalar, pseudoscalar, and charged Higgs (characteristic of the 2HDM), could become dominant.

More generally, one could consider additional contributions to these couplings coming from higher dimensional operators within the EFT framework [53]. EFT capture the broad effects of integrating out physics at higher scales, while remaining agnostic with regards to any particular UV completion. They are usually employed along spurion[1] methods, most commonly through the well-known minimal flavor violating (MFV) ansatz [54], to address the flavor puzzle. But it was also noted they could be the source of non-standard Yukawa couplings through generalizations of this ansatz termed aligned flavor violation (AFV) and spontaneous flavor violation (SFV) [55, 56]. AFV allows for new physics couplings to quarks that align with the SM Yukawa couplings but do not necessarily share their hierarchies or family universality. SFV, a subset of AFV, naturally arises in UV completions where quark family number and CP groups are spontaneously broken. SFV extensions of the SM lead to suppressed FCNC and may provide a connection to TeV-scale new physics

[1] Spurions are auxiliary fields without mass-dimension used to parametrize the breaking of a symmetry (in this case, the SM flavor symmetry arising in the limit of vanishing Yukawa couplings) and determine the set of operators invariant under the latter.

with significant and preferential couplings to first or second generation quarks.

It is thus clear how exploring the couplings of the Higgs boson to the first two generations of quarks beyond the current reach of the LHC holds significant importance for the investigation of well-motivated BSM scenarios. By considering diverse realizations, such as those discussed above, we broaden the scope of new physics that can be tested through these measurements. These efforts ultimately pave the way for future advancements in our understanding of the fundamental nature of the Higgs boson and its role in the broader flavor structure of the SM.

3 Higgs Couplings to Light Quarks through $h + \gamma$ Production

This Section will explore the sensitivity of the LHC to the Yukawa couplings of the Higgs to light SM quarks through the production of a Higgs boson in association with a photon, $pp \to h\gamma$ (see [57–63] for other Higgs plus photon LHC studies).

Beyond its role as a probe of these couplings, this process is inherently interesting, as it is a rare, yet unobserved process within the SM. This is partially because the leading-order (LO) gluon-initiated contribution $gg \to h\gamma$ (see Fig. 2.2–left) vanishes as a consequence of Furry's theorem [64, 65]. This theorem states that any Feynman diagram with an odd number of photon insertions on a closed fermion loop leads to a vanishing amplitude. This is because the diagram can be related to its charge conjugate by reversing the direction of the fermion loop, which changes its sign. Therefore, the diagram and its charge conjugate cancel each other. In the case of $gg \to h\gamma$, the diagram involves a closed quark loop with one photon insertion and two gluon insertions. It thus vanishes because of the odd number of photon insertions. The gluons do not affect the application of Furry's theorem because they are in a color singlet state. That means they do not change the color charge of the quark in the loop, and thus, the diagram is still related to its charge conjugate by reversing the loop.

On the other hand, the largest contributions to the inclusive $h+\gamma$ production at the LHC include extra objects with high transverse momentum in their final states [60]. In the absence of such extra final-state particles besides the Higgs boson and photon, the contribution to Higgs plus photon production at the LHC from bottom-antibottom ($b\bar{b}$) and charm-anticharm ($c\bar{c}$) initial states (see Fig. 2.2–right) becomes important, making this process sensitive to the respective Higgs Yukawa couplings y_b and y_c. In addition, the presence of a large deviation from its SM value in the Yukawa couplings of the quarks $q = s, u, d$ (strange, up and down) would greatly enhance the corresponding $q\bar{q}$-initiated contribution from Fig. 2.2–right. These contributions are at the same time proportional to the square of the quark electric charge Q_q, which suppresses the cross-section for down-type quark-initiated $q\bar{q} \to h\gamma$ processes relative to up-type quark-initiated by a factor $(Q_u/Q_d)^2 = 4$.

In the following, we will discuss the features of Higgs plus photon production and study the sensitivity of this process to the Yukawa couplings y_q for $q = u, c$

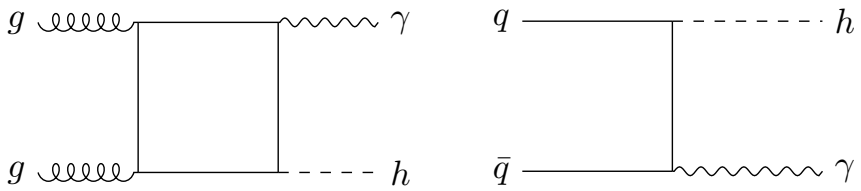

Figure 2.2: Left: Feynman diagram for $gg \to h\gamma$, whose amplitude vanishes due to Furry's theorem. Right: Example tree-level Feynman diagram for $q\bar{q} \to h\gamma$ (with $q = u, d, s, c, b$) in the SM. Diagrams were drawn using TikZ-Feynman [66].

at the HL-LHC, focusing on what is in our view, the most promising Higgs decay channel for this purpose, $h \to WW^* \to \ell\nu\ell\nu$ (with ℓ representing either electrons or muons).

3.1 $h + \gamma$ Production at LHC

As outlined in the previous section, the dominant $q\bar{q}$-initiated contributions to the exclusive production of a 125 GeV Higgs boson in association with a photon at hadron colliders (see Fig. 2.2–right) are proportional to the square of the corresponding light quark Yukawa coupling y_q^2. These couplings are evaluated at the scale of the Higgs mass m_h, the relevant mass scale for this process. The latter is crucial for precise results, as the renormalization group running for these couplings is significant between light-quark and Higgs mass scales, and is thus essential for a realistic comparison between theoretical computations and experimental cross sections. The running masses for the bottom, charm and up quarks, evaluated at the scale $m_h = 125$ GeV, are given in the tadpole-free pure $\overline{MS}$ scheme by $m_b(m_h) = 2.777$ GeV, $m_c(m_h) = 0.605$ GeV, $m_u(m_h) = 0.0013$ GeV [67], with the SM values of the Yukawa couplings at this scale given by $y_q^{\rm SM}(m_h) = \sqrt{2}m_q(m_h)/v$. We then parametrize the departure of the Higgs Yukawa couplings to light quarks from their SM values within the κ-framework as $\kappa_q = y_q(m_h)/y_q^{\rm SM}(m_h)$. Note this definition is scale (and thus, process) dependent, and is not consistent across the literature. This fact has to be taken into account for a realistic comparison between the different probes (see Section 4 below).

The respective $\sqrt{s} = 14$ TeV center of mass (c.o.m.) LHC cross sections at LO for $b\bar{b} \to h\gamma$, $c\bar{c} \to h\gamma$ and $u\bar{u} \to h\gamma$ evaluated with MG5_aMC@NLO v2.8.2 [68], for a photon with transverse momentum $p_T^\gamma > 20$ GeV and pseudorapidity $|\eta^\gamma| < 2.5$, using the NNPDF31_nnlo_as_0118_luxqed [69] parton distribution functions (PDF) set, are

$$\sigma_{b\bar{b}} = \kappa_b^2 \times 0.397 \text{ fb} \quad , \quad \sigma_{c\bar{c}} = \kappa_c^2 \times 0.160 \text{ fb}, \\ \sigma_{u\bar{u}} = \kappa_u^2 \times 5.16 \times 10^{-3} \text{ ab}. \tag{2.1}$$

For the SM, the $c\bar{c}$ contribution is found to be smaller but comparable to $\sigma_{b\bar{b}}$ (despite the large hierarchy between Yukawa couplings), owing to the relative $(Q_c/Q_b)^2 = 4$ factor and larger PDF of the charm quark with respect to the bottom.

At the same time, while $\sigma_{u\bar{u}}$ in the SM is negligible, an enhancement of the up-quark Yukawa making it comparable to the SM charm Yukawa $y_u(m_h) \sim y_c^{\rm SM}(m_h)$ (corresponding to $\kappa_u \sim 500$) would raise the $u\bar{u}$-initiated $h+\gamma$ cross section to ~ 1.3 fb.[1] This might allow for a test of first *vs* second generation Yukawa universality in the up quark sector via this process at HL-LHC with 3 ab^{-1} of integrated luminosity. We also note that subdominant contributions to the $q\bar{q} \to h\,\gamma$ exclusive production, such as $q\bar{q} \to \gamma^*/Z^* \to h\,\gamma$, quickly become negligible for sizable light Yukawa enhancements, *e.g.* for $\kappa_c \sim 3$ their size is $\sim 5\%$ of the $\sigma_{b\bar{b}} + \sigma_{c\bar{c}}$ cross section sum.

Before presenting our analysis in the next section, let us briefly discuss the production of a Higgs boson and a photon at the LHC in an inclusive manner, allowing for extra high-p_T objects to be produced in the process. The dominant contributions to the inclusive $h+\gamma$ production are [60, 61] vector boson fusion (VBF, $h\gamma jj$) and associated production with a W or Z boson (AP, $hV\gamma$). Slightly smaller than the latter but also important are the production together with a high-p_T jet ($h\gamma j$) and production in association with a top quark pair ($t\bar{t}h\gamma$). Cross sections for these processes are in the $\mathcal{O}(1-10)$-fb ballpark, and they do not depend on κ_q (except for small contributions to $h\gamma j$ and $h\gamma jj$, only important for large κ_c values). Thus, to gain sensitivity to the Higgs Yukawa couplings to light quarks, these processes need to be efficiently suppressed in favor of the $b\bar{b}$ and $c\bar{c}$-initiated ones. Fortunately, this may be easily achieved by vetoing extra hard activity in the $h\,\gamma$ event selection and exploiting the different kinematics of the Higgs boson and photon among these processes, as we will discuss below.

3.2 Sensitivity via $h \to WW^* \to \ell\nu\ell\nu$

In what follows we will focus on the $h \to WW^* \to \ell^+\nu\ell^-\bar{\nu}$ decay of the Higgs boson as the most sensitive channel for our purposes. Other Higgs decay choices like $h \to b\bar{b}$ and $h \to \tau^+\tau^-$ face very large SM backgrounds ($b\bar{b}\gamma$ and $Z(\to \tau\tau)\gamma$ respectively), or suffer from very small decay branching ratios, as is the case of $h \to \gamma\gamma$ and $h \to ZZ^* \to 4\ell$.

To search for the $h\,\gamma$ signature via the decay $h \to WW^* \to \ell^+\nu\ell^-\bar{\nu}$ at the LHC with $\sqrt{s} = 14$ TeV c.o.m. energy, we select events with exactly two oppositely charged leptons (electrons or muons) and a photon with pseudorapidities $|\eta^{\ell,\gamma}| < 4$. The transverse momentum of the photon is required to satisfy $p_T^\gamma > 25$ GeV, and the transverse momenta of the leading (ℓ_1) and sub-leading (ℓ_2) lepton need to satisfy $p_T^{\ell_1} > 18$ GeV, $p_T^{\ell_2} > 15$ GeV or $p_T^{\ell_1} > 23$ GeV, $p_T^{\ell_2} > 9$ GeV, following Run-2 ATLAS di-lepton triggers [70]. Di-lepton trigger thresholds are in fact expected to lower for HL-LHC [71], and a di-lepton plus photon trigger with lower thresholds could also be implemented. We also require the missing transverse energy in the event to be $\not{E}_T > 35$ GeV. In order to suppress events with extra high-p_T activity, we veto events having a jet with $p_T > 50$ GeV or two jets with $p_T > 20$ GeV and a pseudorapidity gap $\Delta\eta^{j_1 j_2} > 3$.

[1] This is a factor ~ 10 larger than the SM value for $\sigma_{c\bar{c}}$ from (2.1) due to the much larger PDF for the up-quark inside the proton.

2. PROBING HIGGS YUKAWA COUPLINGS TO LIGHT QUARKS

The dominant SM backgrounds are the irreducible processes $pp \to \ell^+\nu\ell^-\bar{\nu}\gamma$ and $pp \to Z\gamma$, $Z \to \tau^+\tau^-$ with both τ-leptons decaying leptonically, together with the reducible background $pp \to t\bar{t}\gamma$ (with $t \to b\ell^+\nu$, $\bar{t} \to \bar{b}\ell^-\bar{\nu}$). The latter can be further suppressed by imposing a b-tagged jet veto on the selected events. We note that the Z + jets and $Z(\to \ell\ell)\gamma$ SM backgrounds have very large cross sections (see *e.g.* [72–74]). However, the above selection, in particular the $\not{E}_T$ cut, combined with a Z-mass window veto on the invariant mass of the two leptons $|m_Z - m_{\ell\ell}| > 30$ GeV greatly suppresses these processes. Selecting the two leptons in the event to be of opposite flavor (OF) would provide an additional suppression for these backgrounds. In any case, we retain both OF and SF (same flavor) lepton events,[1] and disregard Z + jets and $Z(\to \ell\ell)\gamma$ backgrounds altogether.

We generate our signal and SM background event samples (both at LO) in MADGRAPH 5 [68] with subsequent parton showering and hadronization with PYTHIA 8 [75] and detector simulation via DELPHES v3.4.2 [76], using the anti-k_T algorithm [77] with $R = 0.4$ for jet reconstruction with FASTJET [78] and the DELPHES detector card designed for HL-LHC studies. For simplicity, our simulation does not include pile-up effects, as it has been shown that the contamination of experimental measurements can be efficiently mitigated through pile-up subtraction algorithms such as PUPPI [79], SOFTKILLER [80], or constituent level subtraction [81]. Moreover, further advancements can be anticipated towards the HL-LHC.

After event selection, SM background cross sections are 5.08 fb for $pp \to \ell^+\nu\ell^-\bar{\nu}\gamma$, 3.86 fb for $Z\gamma$, $Z \to \tau^+\tau^-$ and 1.07 fb for $t\bar{t}\gamma$, where the latter includes the effect of the various vetoes in the selection. Assuming SM branching fractions for the Higgs boson (we discuss variants of this assumption in the next section), the signal cross section after event selection is 27.6 ab for $\kappa_b = \kappa_u = 1$, $\kappa_c = 10$, and 41.2 ab for $\kappa_b = \kappa_c = 1$, $\kappa_u = 2000$. In the following, we consider independently the possible enhancement of the charm and up-quark Yukawa couplings with respect to their SM values, performing two separate sensitivity studies.

The rich event kinematics enable efficient signal discrimination following the initial event selection discussed above. An important role is played by the transverse mass M_T reconstructed out of the di-lepton system + missing energy:

$$M_T^2 = \left(\sqrt{M_{\ell\ell}^2 + |\vec{p}_T^{\,\ell\ell}|^2} + \not{E}_T\right)^2 - \left|\vec{p}_T^{\,\ell\ell} + \vec{\not{E}}_T\right|^2 , \tag{2.2}$$

with $\vec{p}_T^{\,\ell\ell}$ the vector sum of the lepton transverse momenta, $M_{\ell\ell}$ the invariant mass of the di-lepton system and $\vec{\not{E}}_T$ the missing transverse momentum of the event. Other key variables are the di-lepton invariant mass $M_{\ell\ell}$ itself, the transverse angular separation $\Delta\phi^{(\ell\ell,\not{E}_T)}$ between di-lepton momentum $\vec{p}_T^{\,\ell\ell}$ and missing momentum $\vec{\not{E}}_T$, or the distance $\Delta R \equiv \sqrt{\Delta\phi^2 + \Delta\eta^2}$ between each lepton and the photon $\Delta R^{\ell_1\gamma}$,

[1] Considering only OF events results in a $\sim \sqrt{2}$ reduction in our signal sensitivity. Yet, an experimental analysis splitting the events into OF and SF categories would recover part of this sensitivity. We also note that the SF signal events contain a minor contribution from $h \to ZZ^* \to \nu\bar{\nu}\,\ell^+\ell^-$.

$\Delta R^{\ell_2\gamma}$. In Fig. 2.3 we show the M_T (top) and $M_{\ell\ell}$ (middle) distributions for the signal (with $\kappa_b = \kappa_u = 1, \kappa_c = 30$) and the dominant SM backgrounds at the HL-LHC. We also show in Fig. 2.3 (bottom) the normalized $\Delta\phi^{(\ell\ell,\not{E}_T)}$ and $\Delta R^{\ell_2\gamma}$ distributions for the signal and SM backgrounds. Performing a cut-and-count signal selection $M_T \in [80, 150]$ GeV, $M_{\ell\ell} \in [5, 55]$ GeV, $\Delta R^{\ell_1\gamma} > 1$, $\Delta R^{\ell_2\gamma} > 0.8$ and $\Delta\phi^{(\ell\ell,\not{E}_T)} > 2$ allows to extract a HL-LHC projected sensitivity $|\kappa_c| < 13.9$ at 95% confidence level (C.L.), using a simple $S/\sqrt{B} \simeq 2$ estimate (with S and B the number of signal and background events) and assuming Higgs boson SM branching fractions.

Given the variety of relevant event kinematic variables and the significant correlations among several of them, it is possible to enhance the signal sensitivity with respect to the above "squared" cut-and-count analysis by accessing the full kinematic information of the events. To this end, we adopt a multivariate approach and employ the following set of variables (containing all the relevant kinematic information of each event):

$$\begin{aligned} &M_T\,, M_{\ell\ell}\,, M_{\ell\ell\gamma}\,, p_T^{\ell_1}\,, p_T^{\ell_2}\,, p_T^{\gamma}\,, \not{E}_T\,, \\ &\Delta\phi^{\ell\ell}\,, \Delta\phi^{\ell_1\gamma}\,, \Delta\phi^{\ell_2\gamma}\,, \Delta\phi^{(\ell\ell,\not{E}_T)}\,, \eta^{\ell_1}\,, \eta^{\ell_2}\,, \eta^{\gamma}\,, \end{aligned} \tag{2.3}$$

to train a neural network (NN) to discriminate the $h+\gamma$ signal from the various SM backgrounds. The NN architecture uses two hidden layers of 128 and 64 nodes, with Rectified Linear Unit (ReLU) activation for the hidden layers and a sigmoid function for the output layer. The NN is optimized using as loss function the binary cross-entropy, employing the Adam optimizer [82] (other generalized loss functions such as the one proposed in [83] do not lead to an appreciable improvement). Since the experimental dataset is unbalanced, that is, the SM background overwhelms the signal, it is useful to train the NN using more SM background than signal events, so that the NN learns optimally to identify (and reject) the former. Specifically, we use 1.5×10^4 events for the $\ell^+\nu\ell^-\bar{\nu}\gamma$ background, 10^4 events for the $t\bar{t}\gamma$ background and 5000 events for the $Z\gamma$ ($Z\to\tau^+\tau^-$) background (a total of 3×10^4 SM background events) in the NN training, together with 1.5×10^4 events of $h\,\gamma$ signal. The validation set contains the same number of events from each class.

The signal discrimination power achieved by our multivariate analysis is very high, with an area under the "receiver operating characteristic" (ROC) curve of 0.941 and 0.938 respectively for charm-quark and up-quark Yukawa sensitivity studies. The multivariate NN score variable $\theta_{\rm NN}$ (which may be regarded as a highly non-linear function of the kinematic variables in Eq. (2.3)) for the signal and dominant SM backgrounds in the charm-quark Yukawa study is shown in Fig. 2.4. In this case, a cut in the NN score variable $\theta_{\rm NN} > 0.78$ yields a signal efficiency ~ 0.57 together with SM background efficiencies 0.057, 0.034 and 0.003 respectively for $\ell^+\nu\ell^-\bar{\nu}\gamma$, $t\bar{t}\gamma$ and $Z(\to\tau^+\tau^-)\gamma$. For the up-quark Yukawa study, the optimal cut is also found to be $\theta_{\rm NN} > 0.78$, yielding a signal efficiency ~ 0.56 and respective SM background efficiencies 0.056, 0.031 and 0.003.

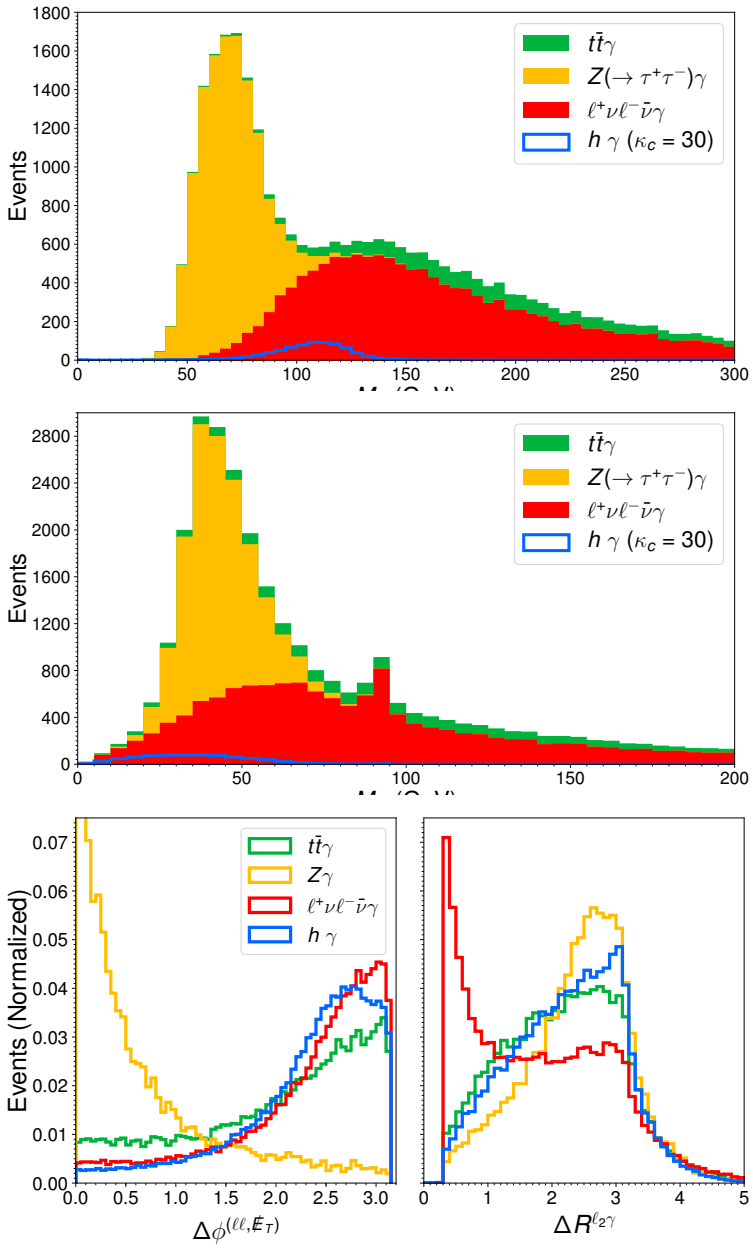

Figure 2.3: Top: M_T distribution of events for the dominant SM backgrounds $\ell^+\nu\ell^-\bar{\nu}\gamma$ (red), $t\bar{t}\gamma$ (green), and $Z(\to \tau^+\tau^-)\gamma$ (yellow), all stacked, at the HL-LHC ($\sqrt{s} = 14$ TeV, 3 ab^{-1}). In blue the corresponding M_T distribution for the $h+\gamma$ signal with $\kappa_b = \kappa_u = 1, \kappa_c = 30$. Middle: same as above, but for $M_{\ell\ell}$. Bottom: Normalized $\Delta\phi^{(\ell\ell,\not{E}_T)}$ and $\Delta R^{\ell_2\gamma}$ distributions for signal and SM backgrounds.

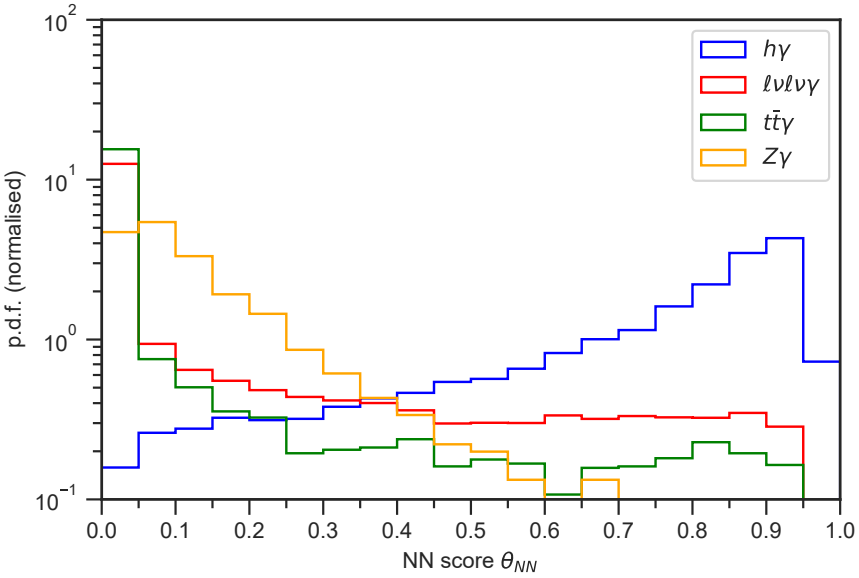

Figure 2.4: Multivariate-NN-score-variable $\theta_{\rm NN}$ for-the $h+\gamma$ signal-(blue)-and-dominant-SM-backgrounds-$\ell^+\nu\ell^-\bar{\nu}\gamma$ (red),-$t\bar{t}\gamma$ (green),-and-$Z(\to\tau^+\tau^-)\gamma$ (yellow)-in-the-charm-quark-Yukawa-sensitivity-study.-

In-addition-to-the-dominant-SM-backgrounds,-we-also-consider-the-VBF-and-AP-$h+\gamma$ production-processes-as-potential,-yet-minor-backgrounds-for-our-charm-and-up-quark-Yukawa-sensitivity-analysis,-as-discussed-in-Section-3.1.-The-extra-high-p_T activity-vetoes-imposed-in-our-initial-event-selection-suppress-these-processes-down-to-a-$h(\to\ \ell^+\nu\ell^-\bar{\nu})\gamma$ cross-section-(assuming-SM-branching-fractions-for-the-Higgs-boson)-of-32.6-ab-for-VBF,-2.24-ab-for-$h\gamma W$ (with-$W\to jj$ or-$W\to\ell\nu$)-and-1.84-ab-for-$h\gamma Z$ (with-$Z\to jj$ or-$Z\to\nu\bar{\nu}$),-with-other-backgrounds-like-$h\gamma j$ and-$tth\gamma$ negligible-after-the-event-selection.-Due-to-such-small-cross-sections,-these-backgrounds-are-not-included-in-the-NN-training.-The-NN-selection-efficiencies-for-them-are-the-following:-in-the-charm-quark-Yukawa-study,-the-cut-$\theta_{\rm NN}>0.78$-yields-the-efficiencies-0.42,-0.25-and-0.27-for-the-VBF,-$h\gamma W$ and-$h\gamma Z$ backgrounds,-respectively;-for-the-up-quark-Yukawa-case,-the-cut-$\theta_{\rm NN}>0.78$-yields-the-corresponding-efficiencies-0.42,-0.26-and-0.28.-Altogether,-these-backgrounds-do-not-appreciably-reduce-the-sensitivity-to-κ_c and-κ_u from-our-multivariate-analysis,-which-is-driven-by-the-NN-ability-to-reject-the-main-irreducible-SM-background,-$pp\to\ell^+\nu\ell^-\bar{\nu}\gamma$.-

3.3 Constraints on κ_c & κ_u.

For-SM-branching-fractions-of-the-Higgs-boson,-the-sensitivity-to-κ_c and-κ_u at-HL-LHC-from-the-NN-analysis-of-the-previous-section-is-$|\kappa_c|<11.8$-and-$|\kappa_u|<1920$-at-95%-C.L.-(improving-on-the-cut-and-count-analysis-from-Section-3.2,-as-expected).-This-assumes-that-the-statistical-uncertainty-of-the-SM-background-will-largely-

dominate over its systematic uncertainty at the HL-LHC, which is justified in the present scenario, particularly since the main backgrounds are electroweak processes. The above projected bounds also assume that only one Yukawa coupling of the Higgs boson departs from its SM value.

Enhancing y_c or y_u by an amount that makes them comparable to the SM bottom quark Yukawa coupling would modify significantly the total width of the Higgs boson and therefore its branching ratios. Nevertheless, it has long been realized that light quark Yukawa couplings remain essentially unconstrained by global fits to Higgs production and decay rates at the LHC [84–86] (see also [87]), unless further assumptions are made. The effect of an enhanced Higgs Yukawa coupling y_q to a light quark $q = u, d, c, s$ on the Higgs branching ratios may be compensated by a related increase of the Higgs couplings to gauge bosons and third-generation fermions, leading to a "flat direction" in the fit along which the Higgs signal strengths remain unchanged. From the present agreement between SM predictions and LHC Higgs measurements [88–90], this flat direction may be approximately described by a single generic κ_h enhancement factor for all Higgs couplings other than the light quark Yukawa y_q of interest [87]

$$\kappa_h^2 \simeq \frac{1 - Br_{q\bar{q}}^{\mathrm{SM}}}{2} + \frac{\sqrt{(1 - Br_{q\bar{q}}^{\mathrm{SM}})^2 + 4\, Br_{q\bar{q}}^{\mathrm{SM}}\, \kappa_q^2}}{2}\,, \tag{2.4}$$

with $Br_{q\bar{q}}^{\mathrm{SM}}$ the branching fraction for $h \to q\bar{q}$ in the SM. While the combination of Higgs signal strengths with other measurements, *e.g.* with electroweak precision observables or an indirect measurement of the Higgs total width (model dependent, see [91]) can help lifting the flat direction (2.4), this discussion highlights the importance of complementary probes of Higgs couplings to light quarks.

Considering κ_c and κ_u along the flat direction defined by (2.4) weakens our analysis' sensitivity with respect to the assumption of SM branching ratios, as the quadratic growth of the $h + \gamma$ cross section is partially compensated by the decrease in the branching ratio of the $h \to WW^*$ decay. While negligible for small κ_q, the latter becomes significant as $y_q / y_b^{\mathrm{SM}} \gtrsim 1$ and the $h \to q\bar{q}$ decay grows into the dominant contribution to the total width. Beyond this point, the scaling of the total cross section becomes linear instead. The projected 95% C.L. sensitivities to κ_c and κ_u along the flat direction are $|\kappa_c| < 26.3$ and $|\kappa_u| < 2280$.

4 Comparison with Existing Methods

The aim of this section is to offer a concise review and comparison of the methods that have been proposed and are currently employed by experiments to constrain light quark Yukawa couplings. This review will contextualize the results presented in the previous section and provide some insight into the complementarity and limitations of the various probes.

When comparing bounds obtained from different methods, particularly within the κ-framework, several aspects must be considered. First, it is important to clar-

ify the reference value used for normalizing κ_q to the SM prediction, as Yukawa couplings run significantly from the scale of the lighter quark masses to the relevant energy scale of the process (in many cases, the Higgs mass m_h). Secondly, the various methods generally require distinct sets of assumptions to extrapolate experimental results into bounds on the targeted coupling. Often, a certain degree of similarity to the SM is assumed, constraining the degrees of freedom in the analysis and enabling the extraction of information on particular couplings. As discussed in the previous section, consistency with current Higgs signal strength measurements requires to modify Higgs couplings along the flat direction when light quark Yukawa couplings are enhanced. Nevertheless, this is not always taken into account when quoting bounds for each coupling individually. Lastly, comparing different probes in the literature frequently involves rescaling to account for the varying luminosities at which each bound was reported. Depending on the method, this rescaling might not always be trivial. We will highlight these differences at the end of this Section, where the results of the various probes for the charm and up quarks will be summarized in Tables 2.1 and 2.2 respectively.

Light quark Yukawa couplings have garnered substantial theoretical and experimental attention in recent years. This is especially notable for the charm quark, as it remains the largest coupling we have yet to gather evidence for among those potentially accessible to present experiments. As a result, a large number of methods have been proposed to probe these couplings: some are quark-flavor specific, relying on tagging or identifying a particular quark in the event; while others are flavor-blind, meaning they could be sensitive to deviations in any of the Higgs couplings to first and second generation quarks. Overall, a strong interplay exists among the different probes, which, in the event of a detection, could be harnessed to pinpoint the responsible couplings.

As was the case for $h+\gamma$ production, some methods seek to gain sensitivity on these couplings through their role in Higgs production mechanisms. One example is Higgs production in association with a charm-tagged or light jet $pp \to h(c/j)$, which has been proposed as a probe of the Yukawa couplings to charm and first generation quarks [92, 93]. In general, Higgs p_T distributions have been pointed out as a powerful probe of light quark Yukawa couplings, as enhanced quark mediated contributions would lead to a softer distribution for the Higgs, either through their interference with top loops or directly through quark fusion for second and first generation quarks respectively [94–96]. Higgs pair production has been similarly shown to be sensitive to the couplings of the latter, and further, to that of the charm if the $h \to c\bar{c}$ decay is considered [97, 98].

Alternatively, the charge asymmetry in $W^{\pm}h$ production, stemming from the variation of the LHC pp PDFs under charge conjugation, has been shown to be dependent on both, first and second generation Yukawa couplings. Enhancements of their values could wash it out or even flip it with respect to SM predictions [87, 99].

On the other hand, modifications of Higgs couplings can also manifest through *off-shell* Higgs channels, following the idea of "measuring Higgs couplings without the Higgs" [100]. The key observation behind this approach is that these modifica-

tions can influence the delicate cancellations that prevent the violation of perturbative unitarity in high-energy scatterings involving electroweak gauge bosons, and could lead to observable energy-growing effects. The recently observed triple heavy vector boson production $pp \to VVV$ ($V = W, Z$) has been shown to be sensitive to the up, down and strange Yukawa couplings [101]. While the charm Yukawa could be probed through the production of two gauge bosons plus a charm tagged and light jets $pp \to VVcj$ [102]. Off-shell Higgs production has also been shown to be sensitive to first generation couplings through kinematic discriminants similar to those employed in Higgs width measurements [103].

Beyond production channels, there are other methods which rely instead on the growth of otherwise rare Higgs decays that would follow an enhancement of these couplings. Some of them involve measuring rare Higgs decays of the form $h \to MV$, where M denotes a vector meson and V represents an electroweak gauge boson (such as a photon, W or Z boson) [87, 104–109]. These decays can be sensitive to Higgs flavor-diagonal couplings to first and second generation quarks when they happen into vector quarkonia (*i.e.*, the J/ψ, ϕ, ρ or η mesons). However, these searches pose significant experimental challenges, as branching ratios are typically very small.

As discussed in Section 1, currently leading constraints on the charm Yukawa originate from direct searches of the $h \to c\bar{c}$ decay, assisted by significant advancements in jet substructure and flavor tagging techniques. This avenue has been explored for several production channels, including associated Higgs production with W and Z bosons and vector boson fusion [87, 106, 107, 110], which offer the best prospects for this measurement in light of the substantial QCD backgrounds involved. This possibility has also been considered for vector boson fusion along a photon, which both suppresses the latter and provides an effective handle to trigger the event [111].

Furthermore, there are other low-energy probes which have been proposed to test light quark Yukawa couplings. Isotope shift spectroscopy in atomic clock transitions could be sensitive to the Higgs couplings to atomic matter, including the up, down and even electron Yukawa couplings [112]. Additionally, flavor processes could provide an indirect handle on up and particularly down quark Yukawa couplings, as modifications of the SM Yukawa matrices that affect them generically also induce modifications in off-diagonal entries in the mass basis, leading to potentially observable FCNCs [113]. Lastly, it should be noted modifications of the up, down or strange quark Yukawa couplings could also affect DM direct detection prospects [114].

Searches conducted with present experimental data include those for the exotic $h \to MV$ decays into vector quarkonia [115–121] and the direct $h \to c\bar{c}$ decay. The latter have predominantly focused on Z/W associated production [43, 122–124], but recently, this decay channel has also been investigated for high p_T Higgs bosons produced via ggF [125], wherein the boosted $c\bar{c}$ pair is reconstructed as a single large-radius jet and identified through neural network techniques. Additionally, Higgs p_T distributions have also been exploited to derive constraints on the charm Yukawa coupling [44, 90, 126]. Lastly, preliminary results for the $h + \gamma$ search proposed in

this work have recently been reported by CMS [45], constraining Higgs couplings to first and second generation quarks.

While direct searches are potentially more sensitive and generally rely on less theoretical assumptions, global combinations of Higgs data could also provide bounds on light quark Yukawa couplings. However, as previously noted, global fits to Higgs production and decay rates at the LHC leave light quark Yukawa couplings essentially unconstrained along a flat direction. Since the LHC cannot measure the Higgs width directly, limited by an experimental resolution of approximately 1 GeV on the invariant-mass distributions of the $h \to 4\ell$ and $h \to \gamma\gamma$ channels, it becomes imperative to combine this data with either additional measurements or theoretical assumptions to derive meaningful bounds on these couplings [87, 106, 127].

A well-motivated assumption is to consider $|\kappa_V| < 1$ ($V = W, Z$), as these couplings are generically diluted with respect to the SM in a wide class of BSM models.[1] In particular, this assumption is valid in models featuring any number of Higgs doublets, with or without additional Higgs singlets (such as 2HDMs). Alternatively, the global fit to signal strengths could be combined with an indirect measurement of the Higgs total width [130, 131]. However, it is important to highlight that the latter relies on further theoretical assumptions. Its measurement leverages the ratio between the on-shell and off-shell ZZ production cross sections. To achieve this, it assumes that the relationship between the Higgs couplings involved in both regimes is as predicted by the SM, and furthermore, that no new particles enter the ggF process. Yet another possibility is to combine LHC data with EW precision observables. Assuming a 3 TeV cutoff scale for the new physics, the latter lead to $\kappa_V = 1.08 \pm 0.07$ [132]. Note, however, that resulting bounds will depend on the chosen scale.

To summarize, we present some of the leading bounds stemming from both proposed methods and experimental results for the charm and up quark Yukawa couplings in Tables 2.1 and 2.2 respectively. The results of this work have been reported in a variety of formats for comparison with existing probes, illustrating the impact of these choices on the resulting bounds. These tables showcase the sensitivity of the different approaches, highlighting some of their assumptions and limitations. Given the particularities of each method, a more comprehensive review of these features would merit a separate analysis and is thus beyond the scope of this thesis.

5 Conclusion

In this Chapter we have studied $h + \gamma$ production at the LHC. While interesting in its own right, as this process remains yet to be observed, we have demonstrated its role as a sensitive probe of the Higgs boson couplings to the light quarks of the first two generations of matter, still largely unconstrained by present measurements. The associated production with a photon is quadratically sensitive to a combination of

[1] Although there are some exceptions, see [128, 129].

	Probe	Refs.	Normalization $y_c/\kappa_c \equiv$	$\mathcal{L}$ [fb^{-1}]	95%CL Bound $\lvert\kappa_c\rvert <$ / $\kappa_c \in$	Observations
Projections	This work	[1]	$y_c^{SM}(m_h)$	138	167	Flat direction, OF leptons ($h\gamma \to e\mu\gamma$)
				3000	11.8	SM couplings + κ_c
					26.3	Flat direction
				6000	9.86	SM couplings + κ_c
					19.2	Flat direction
			$y_c^{SM}(m_c)$	3000	5.6	SM couplings + κ_c
					12.5	Flat direction
	$pp \to hc$	[92] [87]	$y_c^{SM}(m_c)$	3000	2.6 – 3.9 2.1 – 4.0	SM couplings + κ_c Flat direction
	Higgs p_T dist.	[94]	$y_c^{SM}(m_h/2)$	3000	$[-(1.3 - 0.6), 3.0 - 3.7]$	SM couplings + $\kappa_{c,b}$ $\sqrt{s}$ = 13 TeV
	$pp \to hh \to b\bar{b}\gamma\gamma$	[97]	$y_c^{SM}(m_c)$	3000	$[-(9.2 - 4.8), 4.6 - 9.0]$	SMEFT + $\kappa_{c,s}$
	$W^{\pm}h$ asym.	[87, 99]	$y_c^{SM}(m_c)$	3000	$\lesssim 30$	Flat direction
	Zh ($h \to c\bar{c}$)	[87, 133]	$y_c^{SM}(m_c)$	3000	$\lesssim 2.7$	Flat direction
	Z/Wh + VBF ($h \to c\bar{c}$)	[110]	$y_c^{SM}(m_c)$	3000	$\kappa_c \leq 1.47^{+0.21}_{-0.16}$	2D κ_c (best) fit
	VBFγ ($h \to c\bar{c}$)	[111]	$y_c^{SM}(m_c)$	3000	13	SM couplings + κ_c
	Global fit	[127]	$y_c^{SM}(m_c)$	6000	1.2	$\lvert\kappa_V\rvert < 1$
Exp. Results	$pp \to h\gamma \to e\mu\gamma$	[45]	$y_c^{SM}(m_h)$	138	200 (110)	Flat direction
	$h \to J/\psi\gamma$	[120]	$y_c^{SM}(m_c)$	139	$[-136\,(123), 178\,(164)]$	SM couplings + κ_c/κ_γ
	Z/Wh ($h \to c\bar{c}$)	[43]	$y_c^{SM}(m_c)$	138	$1.1 < \lvert\kappa_c\rvert < 5.5\,(3.4)$	SM couplings + κ_c
	Higgs p_T dist.	[126]	$y_c^{SM}(m_c)$	138	$[-5.3\,(5.7), 5.2\,(5.7)]$	SM, no BSM + $\kappa_{c,b}$
	Higgs p_T + Vh ($h \to q\bar{q}$) $q = c, b$	[44]	$y_c^{SM}(m_c)$	139	$[-4.46, 4.81]$	SM couplings + $\kappa_{c,b}$

Table 2.1: Summary of projected and experimental observed (expected) 95% CL upper limits on the ***charm quark*** Yukawa coupling resulting from LHC searches (at $\sqrt{s}$ = 14, 13 TeV respectively, unless otherwise specified).

	Probe	Refs.	Normalization $y_u/\kappa_u \equiv$	$\mathcal{L}$ [fb^{-1}]	95%CL Bound $\lvert\kappa_u\rvert <$ / $\kappa_u \in$	Observations
Projections	This work	[1]	$y_u^{SM}(m_h)$	138	9780	Flat direction, OF leptons ($h\gamma \to e\mu\gamma$)
				3000	1920	SM couplings + κ_u
					2280	Flat direction
				6000	1600	SM couplings + κ_u
					1820	Flat direction
			y_u^{SM}(2 GeV)	3000	1070	SM couplings + κ_u
					1270	Flat direction
	Higgs p_T dist.	[95]	$y_b^{SM}(m_h)$	300	$\kappa_u < 0.27 - 0.36$	SM couplings + $\kappa_{u,d}$ $\sqrt{s}$ = 13 TeV
		[96]	$m_b(m_h)/v$	3000	$[-0.73, 0.33]$	SM couplings + $\kappa_{g,u,d}$ $\sqrt{s}$ = 13 TeV
	$pp \to hh \to b\bar{b}\gamma\gamma$	[97]	y_u^{SM}(2 GeV)	3000	$[-1771, 1750]$	SMEFT + $\kappa_{u,d}$
		[98]		6000	530	SMEFT + κ_u
	$pp \to VVV$	[101]	$y_u^{SM}(m_h)$	6000	830	SMEFT + κ_u
	Off-shell $h \to 4\ell$	[103]	y_u^{SM}(2 GeV)	6000	194	SMEFT + κ_u
	Global fit	[127]	y_u^{SM}(2 GeV)	6000	560	$\lvert\kappa_V\rvert < 1$
Exp.	$pp \to h\gamma \to e\mu\gamma$	[45]	y_u^{SM}(2 GeV)	138	16000 (13000)	Flat direction

Table 2.2: Summary of projected and experimental observed (expected) 95% CL upper limits on the ***up quark*** Yukawa coupling resulting from LHC searches (at $\sqrt{s}$ = 14, 13 TeV respectively, unless otherwise specified).

these couplings weighted by their respective electric charges. The contribution of up-type quarks is thus enhanced with respect to that of their down-type counterparts, providing an unique way to disentangle deviations between them. This makes $h + \gamma$ highly complementary to other existing light-quark Yukawa probes, which are often flavor-blind or sensitive to their masses instead.

Focusing on the $h \to \ell^+ \nu \ell^- \bar{\nu}$ decay channel of the Higgs boson, we have performed a multivariate neural network analysis to fully exploit the rich kinematics of this final state, and derived HL-LHC projected sensitivities to the Higgs Yukawa couplings to charm and up quarks. These have been summarized along with other representative probes in Tables 2.1 and 2.2. While the projected bounds on κ_c which we obtain are complementary to existing methods in the literature, they may not be competitive with the most sensitive direct probes of the Yukawa coupling of the charm, which benefits the most from flavor-specific approaches as it is the heaviest of the remaining quarks. In contrast, the achievable $h + \gamma$ sensitivity to κ_u does lie in the same ballpark of other currently proposed probes. Particularly in the latter case, $h + \gamma$ may help to gain further insight on Higgs flavor at the LHC.

3

Searching for Exotic Semi-Dark Higgs Decays

1 Introduction

In this Chapter we turn our attention to the search for exotic decay modes of the Higgs boson. Exotic Higgs decays, *i.e.* decays of the Higgs boson not present in the SM, constitute a primary avenue to probe the existence of new physics [134]. This is because, as previously discussed, new physics with light degrees of freedom coupling to the Higgs generically opens new decay channels with sizable branching ratios. Additionally, as a scalar field, the Higgs is uniquely positioned within the SM to interact with these new particles. It is therefore no surprise that these decays have been the target of an intense experimental program at the LHC [135–146] (see also [147] and references therein). However, these searches have mainly targeted either fully visible final states, *e.g.* $h \to 2f\,2f'$ (with f, f' SM fermions) or the fully invisible Higgs decay (so-called *invisible Higgs width*).

Considering all/part of the Higgs boson decay products in these exotic decays to be invisible at colliders is well-motivated theoretically, *e.g.* if the Higgs boson directly interacts with a dark (*i.e.* not feeling the SM gauge interactions) sector of nature, possibly containing the DM particle(s), or if the Higgs decay products are very long-lived and decay outside the LHC detectors. Yet, partially invisible (*semi-dark*) Higgs boson decays constitute a much less explored avenue to search for new BSM physics coupled to the Higgs boson, both theoretically and experimentally. Studies of these semi-dark Higgs decays exist in the literature for very few BSM scenarios [148–150]. And existing experimental searches have focused on two final states: one or two photons plus missing energy, $h \to (2)\gamma + \not{E}_T$ [151–155], or a bottom quark pair, $h \to b\bar{b} + \not{E}_T$ [156]. Nevertheless, semi-dark searches are fully complementary to searches for invisible Higgs decays, and generally probe different regions of parameter space of the same BSM theories. Furthermore, semi-invisible Higgs decays can also provide key information on the nature of the coupling between the Higgs and the invisible state(s), by reconstructing the visible part of the exotic Higgs decay.

This Chapter will introduce a promising yet largely unexplored semi-invisible Higgs decay topology. Section 2 will investigate the prospects for this search at both the LHC and a future ILC, whereas Section 3 will provide a brief review of some well-motivated BSM realizations that can be probed through this search. Lastly, our conclusions are presented in Section 4.

2 Sweeping the Higgs Neutrino Floor: $h \to Z + \not{E}_T$

In this Section we target the hitherto unexplored semi-dark Higgs decay $h \to ZX$, with X a BSM particle invisible at the LHC (manifesting as missing transverse energy $\not{E}_T$),[1] and we show it is a promising avenue to probe various well-motivated BSM scenarios: X could be an axion-like particle (ALP) or dark photon that decays invisibly or is long-lived, escaping the detector. It could also be a pseudoscalar mediator particle between the SM and a dark sector of nature containing the DM particle(s). These realizations will be further explored in Section 3, where we will also present the resulting constraints on their parameter space.

To search for this channel at colliders, we focus our study on the leptonic decay of the Z boson, $Z \to \ell\ell$ (with $\ell = e, \mu$), leading to the Higgs final state $h \to ZX \to \ell\ell + \not{E}_T$. Incidentally, the SM decays $h \to ZZ^* \to \ell\ell\nu\bar{\nu}$ and $h \to WW^* \to \ell\nu\ell\bar{\nu}$ yield the same final state. Although for the latter, the di-lepton mass distribution will not reconstruct the Z boson mass pole $m_Z \simeq 91$ GeV, which can be exploited to differentiate $h \to ZX$ from this SM decay process. On the other hand, $h \to ZZ^* \to \ell\ell\nu\bar{\nu}$ completely mimics a possible BSM signal. The SM decay $h \to Z\nu\bar{\nu}$ then constitutes a "*neutrino floor*" to experimental searches for new physics in the semi-dark $h \to ZX$ ($X \to \not{E}_T$) channel,[2] below which a possible BSM signal would be buried. However, it also provides a target sensitivity for the $h \to ZX$ ($X \to \not{E}_T$) search at the LHC and future colliders which would guarantee a detection (albeit in that case not of BSM physics!), given by the SM branching fraction $\text{BR}(h \to Z\nu\bar{\nu})_{\text{SM}} = 5.4 \cdot 10^{-3}$ [158].

2.1 LHC Searches for $h \to ZX \to \ell\ell + \not{E}_T$

Our analysis reveals the convenience of focusing on the production of the Higgs boson at the LHC in association with a Z boson, $pp \to Zh$: for gluon-fusion (ggF) and vector-boson-fusion (VBF) Higgs production channels, the Higgs is either produced on its own (ggF) or recoiling against jets (ggF, VBF). Since the phase space for the Higgs decay $h \to ZX$ is fairly small (as $(m_h - m_Z)/m_h \ll 1$), an accurate $\not{E}_T$ reconstruction may be limited by the transverse momentum (p_T) resolution of the jets. In addition, the $\ell\ell + \not{E}_T +$jets final state has very large SM backgrounds, in particular reducible ones if the $\not{E}_T$ reconstruction is not perfect. Higgs production in association with an electroweak gauge boson, $pp \to W^\pm h$ and $pp \to Zh$, is thus

[1] Ref. [148] briefly discussed this possibility in the context of dark photons.

[2] In analogy to DM direct detection experiments, where coherent elastic neutrino-nucleus scattering can pose an irreducible background to DM searches, known as the "neutrino floor" [157].

better suited for the $h \to ZX$ ($X \to \not{E}_T$) exotic Higgs decay search at the LHC. Yet, the leptonic decay of the W boson in $pp \to Wh$ adds $\not{E}_T$ to the final state, making it challenging to disentangle this contribution from the Higgs boson decay products. In addition, the LHC cross section for the dominant SM background in this case, $pp \to W^\pm Z$, is very large, $\mathcal{O}(50)$ pb. In contrast, for $pp \to Zh$ ($h \to Z + \not{E}_T$) the leptonic decay of both Z bosons offers a sharp reconstruction of the two di-lepton resonances together with an accurate $\not{E}_T$ measurement, combined with SM backgrounds that can be efficiently suppressed or are very small to begin with, as we discuss in detail below.

For our analysis, we generate the BSM signal specifically using a `FeynRules` [159] implementation of the two-Higgs-doublet-model plus pseudoscalar singlet (2HDM+a) extension of the SM (see *e.g.* [160–162], *c.f.* Section 3), through the decay $h \to Za$ (with a invisible). Nevertheless, our results apply to any two-body Higgs decay $h \to ZX$, $X \to \not{E}_T$. Both Z bosons from the signal are considered to decay leptonically, $Z \to \ell\ell$. The relevant SM backgrounds are $pp \to ZZ \to 4\ell$ (with $\not{E}_T$ appearing via mismeasurements and detector effects), $pp \to ZZZ, WWZ \to 4\ell + 2\nu$, $pp \to t\bar{t}Z, tWZ \to 4\ell + 2\nu +$ jets, and $pp \to Zh$ ($h \to WW^* \to 2\ell + 2\nu$). We generate signal and SM background event samples with MG5_aMC@NLO v2.8.2 [68] (using the NNPDF31_nnlo [69] parton distribution functions) at a center-of-mass energy $\sqrt{s} =$ 14 TeV, with subsequent parton showering and hadronization via Pythia 8 [75] and detector simulation via Delphes v3.4.2 [76], using the detector card designed for High-Luminosity (HL)-LHC studies. We normalize the respective cross sections to their next-to-leading-order (NLO) in QCD values, obtained from the literature [163, 164] (for the $pp \to Zh$ and $pp \to ZZ$ processes the normalization is however performed to the NNLO cross section [158, 165]; to avoid known issues at NLO in QCD related to real b-quark emission [166, 167], tWZ is kept at LO with a negligible impact on our analysis). For the sake of simplicity, we do not include pile-up in our simulation: in the experimental measurements, it has been shown that the pile-up contamination can be very efficiently removed by using pile-up subtraction algorithms such as Puppi [79], Softkiller [80] or constituent level subtraction [81]. Selected events are required to contain exactly four reconstructed leptons after detector simulation, comprising two pairs of opposite-sign, same-flavor leptons. Events must pass the single, two or three-lepton trigger requirements from the ATLAS-2018 Trigger menu [168]. When multiple di-lepton combinations satisfying the selection requirements exist, the one minimizing $\Delta^2 = m_Z^{-2}[(m_{\ell\ell_1} - m_Z)^2 + (m_{\ell\ell_2} - m_Z)^2]$ (with $m_{\ell\ell_i}$ the di-lepton invariant masses) is chosen. Extra hadronic activity is vetoed by rejecting events with either b-tagged jets or hard jets with $p_T > 50$ GeV.

Since the Higgs decay is partially invisible, its invariant mass cannot be fully reconstructed, nor can the di-lepton pair from its decay be straightforwardly identified. The latter, however, is key to better exploit the kinematic properties of the BSM signal in the analysis. We may identify the di-lepton pair corresponding to the Z boson from the Higgs decay using the transverse mass M_T, given by

$$M_T^2 = \left(\sqrt{m_{\ell\ell}^2 + |\vec{p}_T^{\,\ell\ell}|^2} + \not{E}_T \right)^2 - \left| \vec{p}_T^{\,\ell\ell} + \vec{\not{E}}_T \right|^2 , \tag{3.1}$$

with $\vec{\not{E}}_T$ and $\vec{p}_T^{\,\ell\ell}$ the missing transverse 3-momentum and Z boson transverse 3-momentum, respectively; a complementary approach would be to select the Z boson closest to $\vec{\not{E}}_T$ in the azimuthal plane as the one from the Higgs decay. Figure 3.1 shows the M_T (top) and $\Delta\phi(Z, \vec{\not{E}}_T)$ (azimuthal angle between $\vec{\not{E}}_T$ and the 3-momentum of the di-lepton pair, bottom) distributions for the leptonically-decaying Z boson from the Higgs decay (labeled as Z_1) and the Z boson produced in association with the Higgs (labeled as Z_2). To optimally exploit the event kinematic information in identifying Z_1 and Z_2 for the BSM signal, we build a neural network (NN) (two hidden layers, 32 nodes each, using rectified linear unit activation for the hidden layers and a sigmoid function for the output) which takes as input M_T and $\Delta\phi(Z, \vec{\not{E}}_T)$ for both di-lepton pairs. The correct and wrong Z_i assignments for the NN training are labeled using generator-level information. The NN is trained with a Monte Carlo sample of 20000 signal events (not used in our subsequent analysis) with $m_X = 1$ GeV, using the Adam algorithm for the optimization. The efficiency obtained for a correct $Z_{1,2}$ choice for the signal is 73%, and the NN is then applied in our sensitivity analysis to both the BSM signal (for $m_X \in [1, 32.5]$ GeV) and the SM backgrounds.

The signal cross section (for BR($h \to ZX$) = 1, BR($X \to \not{E}_T$) = 1 and $m_X = 1$ GeV) after the initial event selection is 1.420 fb. The respective SM background cross sections after event selection are 25.6 fb for $ZZ \to 4\ell$, 0.76 fb for $ZZ \to 2\ell + 2\tau$, 0.169 fb for $WW^{(*)}Z \to 4\ell + 2\nu$ (including the $pp \to Zh$, $h \to WW^*$ contribution), 0.012 fb for $ZZZ \to 4\ell + 2\nu$, and 0.044 fb for $t\bar{t}Z$, $tWZ \to 4\ell + 2\nu +$ jets. Our $h \to ZX$ LHC signal region must target relatively high-p_T Zh associated production, with reconstructed Z-boson resonances for the two di-lepton pairs and the Higgs transverse mass M_T from the Z_1 di-lepton candidate. Requiring a moderately large amount of $\not{E}_T$, demanding Z_1 to be well-aligned with $\vec{\not{E}}_T$ in the azimuthal plane and rejecting events with a large rapidity gap between di-lepton pairs also improves the sensitivity of the analysis.

The rich event kinematics (four visible objects in the final state plus the missing transverse energy) indicates that a multivariate approach which accesses the full kinematic information of the events could enhance our BSM signal sensitivity. We use another NN (two hidden layers of 256 nodes, same activation functions and optimization as before) for the discrimination between signal and SM background, with input variables: $\not{E}_T$, $m_{4\ell}$ (four-lepton invariant mass), $m_{\ell\ell_1}$ and $m_{\ell\ell_2}$, $\Delta\phi(Z_1, \vec{\not{E}}_T)$ and $\Delta\phi(Z_2, \vec{\not{E}}_T)$, M_T (built from Z_1), $p_T^{\ell\ell_1}$ and $p_T^{\ell\ell_2}$ (di-lepton transverse momenta), $p_T^{\ell_1}$, $p_T^{\ell_2}$, $p_T^{\ell_3}$, $p_T^{\ell_4}$ (transverse momenta of the four leptons, ordered from higher to lower) and $(p_T^{\ell\ell_2} + \not{E}_T)/p_T^{\ell\ell_1}$.

The NN is trained with an unbalanced Monte Carlo set dominated by $ZZ \to 4\ell$ events, precisely to optimize the rejection of this SM background (as it has by far

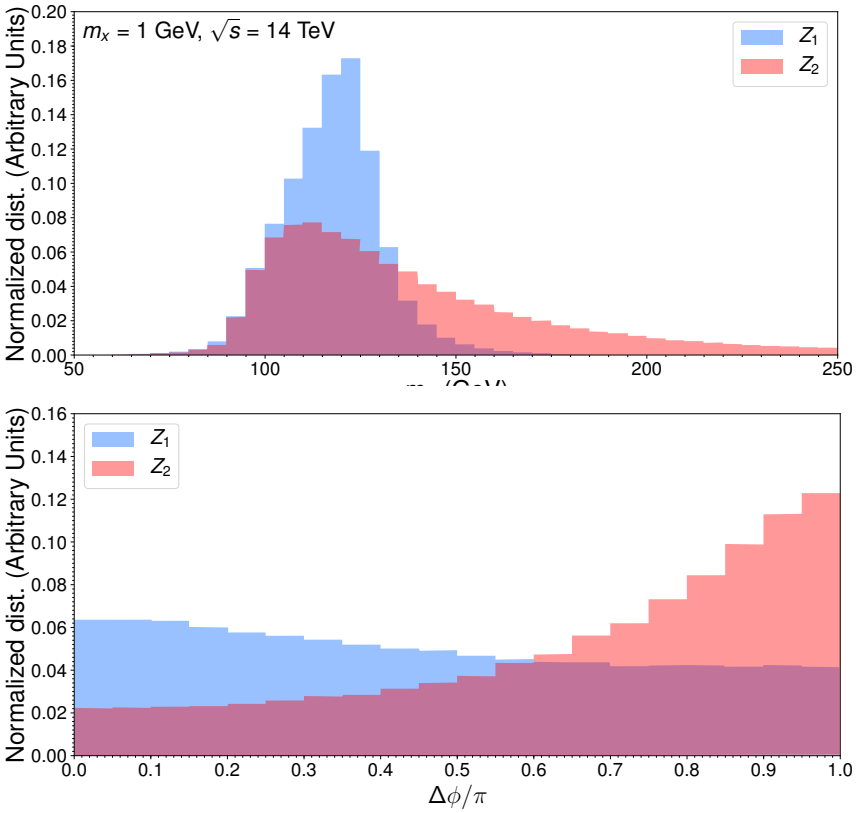

Figure 3.1: M_T (top) and $\Delta\phi(Z, \vec{\not{E}}_T)/\pi$ (bottom) for Z_1 (blue) and Z_2 (red), see text for details.

the largest LHC cross section among SM backgrounds). For the training set we use 25000 ZH events, 20000 ZZ events and 5000 WWZ events. The ZZ background with $Z \to \tau\tau$ is not used in the training. The validation sets have similar size as the training ones. The test sets have respectively 82000 events (ZH), 412000 (ZZ), 57000 (WWZ) and 36000 (ZZ, $Z \to \tau\tau$). For other signal masses, the test sets have around 150000 events. The NN achieves a very high discrimination power, with an area under the curve (ROC) of 0.927. The NN score θ_{NN} for the $m_X = 1$ GeV signal and relevant SM backgrounds is shown in Figure 3.2 (for X of spin-1, angular correlations in the Z_1 di-lepton pair mildly differ from the spin-0 X case analyzed here, yet our signal sensitivity results would be nearly unchanged).

Our signal region is defined for the HL-LHC as $\theta_{NN} \geq 0.997$. The resulting signal and SM background efficiencies (evaluated on the NN test sets) are 0.12, $1.5 \cdot 10^{-4}$, $2.8 \cdot 10^{-5}$, 0.0013, 0.012, 0.0016 and $< 9.4 \cdot 10^{-4}$, respectively for the signal (with $m_X = 1$ GeV), $ZZ \to 4\ell$, WWZ, $ZZ \to 2\ell + 2\tau$, ZZZ, tWZ and $t\bar{t}Z$. Since $\mathcal{O}(s/b)$ corrections are not negligible, we employ the "Asimov estimate" [169] to derive the 2σ exclusion regions on BR($h \to ZX$) $\times$ BR(X $\to \not{E}_{\rm T}$) with 3 ab^{-1} of integrated luminosity. Bounds cover the range $m_X \in [1, 32.5]$ GeV, but they may also be directly extrapolated to the $m_X \to 0$ limit. We find our NN results to improve by

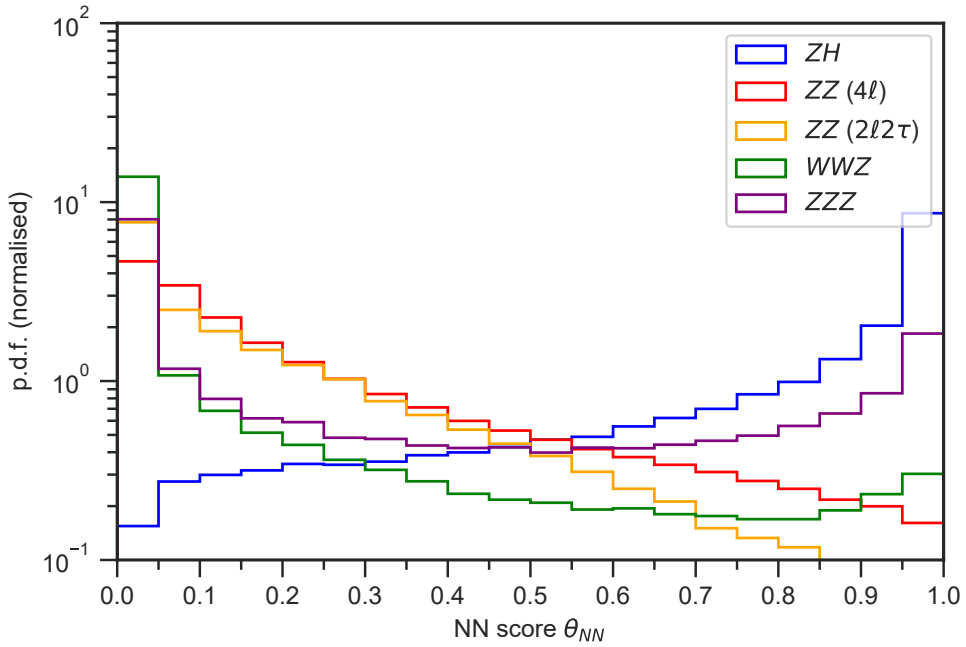

Figure 3.2: Score θ_{NN} of the neural-network-discriminating-BSM-signal-vs-SM-background in our analysis, for the BSM-signal-with $m_X = 1$ GeV (labeled ZH, blue), and the relevant SM backgrounds: $ZZ \to 4\ell$ (red), $ZZ \to 2\ell 2\tau$ (yellow), $WWZ \to 4\ell + 2\nu$ (green), $ZZZ \to 4\ell + 2\nu$ (purple).

$\sim$ 30% the sensitivity of a cut-and-count analysis, and come close to probing the *Higgs neutrino floor* (for $m_X = 1$ GeV, it probes $\mathrm{BR}(h \to ZX) \times \mathrm{BR}(\mathrm{X} \to \not{E}_{\mathrm{T}}) = 2.8 \times \mathrm{BR}(\mathrm{h} \to \mathrm{Z}\nu\bar{\nu})_{\mathrm{SM}}$ at 2σ). We repeat our analysis for an integrated luminosity of 300 fb^{-1}, with a less stringent signal region cut $\theta_{NN} \geq 0.985$ to increase the fraction of signal events surviving the selection. The sensitivity results for 300 fb^{-1} and 3 ab^{-1} (HL-LHC) are shown in Figure 3.3.

Lastly, we note that while mono-Z searches could, in principle, be sensitive to the 125 GeV Higgs $h \to Z\not{E}_T$ decay, neither ATLAS [170] nor CMS [171] searches can constrain its branching ratio effectively. This is mainly due to the stringent cuts applied in both analyses on the missing energy $\not{E}_T$ and transverse mass m_T of the events. The first requires a hard jet on ggF, while the former ($m_T > 200$ GeV in both searches) virtually excludes the entirety of the signal, since the transverse mass is expected to be upper bounded by the resonance mass (m_h) barring detector effects. While suitable for the production of heavy scalars within the 2HDM+a, these cuts limit severely the sensitivity to the exotic decays of the 125 GeV Higgs boson, stressing the importance of direct searches.

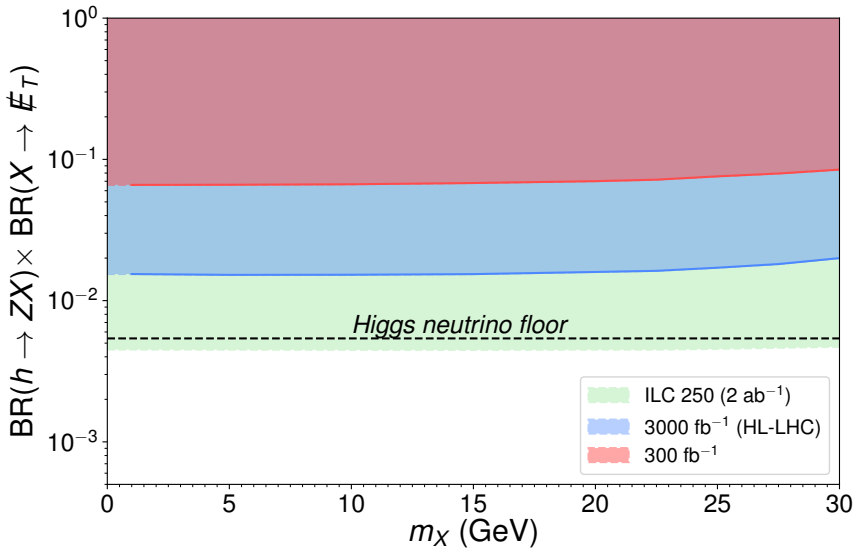

Figure 3.3: 2σ exclusion sensitivity for BR($h \to ZX$)× BR(X$\to \not{E}_{\rm T}$) as a function of m_X for an LHC integrated luminosity of 300 fb^{-1} (red) and 3000 fb^{-1} (HL-LHC, blue). The *Higgs neutrino floor* is shown as a dashed-black line. The ILC $\sqrt{s}$ = 250 GeV (2 ab^{-1}) would-be sensitivity is shown in green.

2.2 ILC Searches for $h \to ZX \to \ell\ell + \not{E}$

A future International Linear Collider (ILC) [172, 173] operating at $\sqrt{s}$ = 250 GeV would be able to probe BR($h \to ZX$) down to the *Higgs neutrino floor* by exploiting several advantages over the LHC search discussed in the previous section:

(i) Higgstrahlung $e^+e^- \to Zh$ is now the dominant Higgs production mode.

(ii) The e^+e^- collisions at ILC offer a much cleaner environment (largely void of hadronic activity) and the 3-momenta of the incoming particles is known up to radiative and smearing effects, allowing for full missing momentum reconstruction.

(iii) The Higgs recoil mass, constructed from the Z-boson recoiling against the Higgs boson (Z_2) as $M^2_{\rm reco} = s + m^2_{Z_2} - 2E_{Z_2}\sqrt{s}$, provides a straightforward way to correctly identify $Z_{1,2}$ for the BSM signal ($M_{\rm reco}$ built out of the Z-boson from the Higgs decay, Z_1, will not present any resonant structure).

For our analysis, we specifically consider $\sqrt{s}$ = 250 GeV with 2 ab^{-1} of integrated luminosity (90% of it evenly split between the two opposite beam helicities) and beam polarizations of 80% for the electrons and 30% for the positrons respectively [173]. Again, we consider the SM Higgs produced in association with a Z-boson, $e^+e^- \to Zh$ for our BSM signal. The relevant SM backgrounds are now $e^+e^- \to ZZ$ ($\to 4\ell$, $2\ell + 2\tau$), $e^+e^- \to WWZ$ and $e^+e^- \to ZZ\nu\bar{\nu}$ (including VBF initiated contributions; Higgs mediated contributions correspond to the SM *Higgs neutrino floor*,

and are not included). Our signal and background event generation is performed as in the previous section, using in this case the DELPHES detector card designed for ILC studies [76, 174] (a study of lepton collider capabilities including the effects of initial state radiation or beamstrahlung is left for future work).

Our initial event selection mimics that of the previous LHC analysis. The cross sections for the signal (for BR($h \to ZX$) = 1 and m_X = 1 GeV) and SM backgrounds after event selection are respectively 1.421 fb, 5.64 fb (for $ZZ \to 4\ell$), 0.13 fb (for $ZZ \to 2\ell\, 2\tau$), 0.073 fb (for $WW^{(*)}Z \to 4\ell + 2\nu$, dominated by the $e^-e^+ \to Zh, h \to WW^*$ contribution), and 0.011 ab (for $ZZ\nu\bar{\nu} \to 4\ell + 2\nu$). For the ILC environment, the use of a NN does not offer such a strong advantage over a simpler (cut-and-count) analysis. We thus define our kinematic region for signal extraction in the latter way: we demand reconstructed Z-boson resonances for the two di-lepton pairs, $m_{Z_1} \in [55, 100]$ GeV, $m_{Z_2} \in [80, 105]$ GeV; we require the recoil mass constructed out of Z_2 in the range $M_{\rm reco} \in [120, 135]$ GeV, together with $p_{Z_2} > 50$ GeV and $\not{E} \in [5, 60]$ GeV (p_{Z_2}, $\not{E}$ respectively the modulus of the Z_2 di-lepton candidate's 3-momentum and the modulus of the missing 3-momentum); the invariant mass $m^{\rm miss}_{Z_1}$ built from Z_1 and $\vec{\not{E}}$, given by $(m^{\rm miss}_{Z_1})^2 = \left(\sqrt{m^2_{Z_1} + p^2_{Z_1}} + \not{E}\right)^2 - \left|\vec{p}_{Z_1} + \vec{\not{E}}\right|^2$, is required to reconstruct the 125 GeV Higgs mass, $m^{\rm miss}_{Z_1} \in [95, 130]$ GeV; we further require $m_{4\ell} > 160$ GeV, $(p_{Z_1} + \not{E})/p_{Z_2} < 1.8$ and $(m^{\rm miss}_{Z_2})^2 = \left(\sqrt{m^2_{Z_2} + p^2_{Z_2}} + \not{E}\right)^2 - \left|\vec{p}_{Z_2} + \vec{\not{E}}\right|^2 > (95\ \text{GeV})^2$. These signal region cuts have an efficiency of 0.89 for the BSM signal (for m_X = 1 GeV), and $1.7 \cdot 10^{-5}$, 0.013, 0.085, 0.24 for the $ZZ \to 4\ell$, $ZZ \to 2\ell\, 2\tau$, WWZ and $ZZ\nu\bar{\nu}$ SM backgrounds, respectively. Using the "Asimov-estimate", we derive a 2σ sensitivity BR($h \to ZX$) $\times$ BR(X $\to \not{E}$) = 0.0045. We show the corresponding ILC sensitivity as a function of m_X in Figure 3.3. We note that this sensitivity lies below the SM *Higgs neutrino floor*, not included in our analysis. This means that we should now instead consider the ILC discovery potential of BR($h \to Z\nu\bar{\nu}$)$_{\rm SM}$; the expected significance over the background-only hypothesis reaches 2.4σ (the significance may be enhanced to $\sim 4\sigma$, at the expense of our BSM analysis not yielding a uniform sensitivity in m_X). The ILC can thus sweep the entire new physics parameter space of semi-dark Higgs decays down to the *Higgs neutrino floor*.

3 Constraints on Dark Matter Scenarios

We now turn our attention to some of the BSM realizations that are constrained by our projections for the sensitivity to BR($h \to ZX$) $\times$ BR(X $\to \not{E}_{\rm T}$) (see Figure 3.3) and could thus be probed through the semi-invisible $h \to ZX \to \ell\ell + \not{E}_T$ decay. In particular, we will consider three different scenarios where X is taken to be: an axion-like particle (ALP) that couples to the Higgs and decays invisibly; a pseudoscalar mediator (a) to the dark sector within a two-Higgs-doublet model plus pseudoscalar (2HDM+a); or a dark photon. These realizations are well-motivated theoretically, as they can provide DM in quantities sufficient to explain its observed

abundance. They also suggest that the dark sector may be accessible through the Higgs boson at colliders, highlighting the complementarity of these searches with traditional direct or indirect DM detection experiments. In the following we provide a concise overview of these realizations, casting our results into their respective parameter spaces and offering context to their significance.

3.1 Axion-like Particles

Axion-like particles (ALPs) are generally defined as CP-odd (pseudo)Nambu-Goldstone bosons which are singlets under the SM gauge group. They take their name from the eponymous axion, a particle first formulated as a solution to the strong CP problem [175–177]. The strong CP problem can be succinctly summarized as the puzzling experimental observations that seem to suggest the absence of a CP-violating term in the strong sector of the SM which is nonetheless perfectly consistent with its symmetries. The paradigmatic axion solution relies on an anomalous (*i.e.* broken at the quantum level) global $U(1)$ symmetry which is spontaneously broken. Since the symmetry is anomalous, the latter resolves with the appearance of a pseudo-Nambu-Goldstone boson which needs not be massless, the axion, leading to the dynamical vanishing of the CPV term. While the original axion is disfavored by present data, there are other popular constructions which remain viable such as the DFSZ [178, 179] and KSVZ [180, 181] models. The requirement that they solve the strong CP problem imposes stringent constraints on their couplings to SM particles.

ALPs on the other hand need not abide by this requirement. They are ubiquitous in many well-motivated BSM extensions, arising as a result of the spontaneous breaking of one or several global $U(1)$ symmetries. If not exact or broken by non-perturbative effects, the resulting ALPs can have small masses naturally below the EW or even the QCD scale, making them good DM candidates as well. As Nambu-Goldstone bosons, their signature characteristic is that they can only couple derivatively due to the underlying shift symmetry (which is only softly broken by mass-dependent terms). Their interaction with the rest of the SM fields is most generally implemented in terms of an effective Lagrangian, for which there exist two distinct phenomenologically relevant possibilities [182, 183]: a $SU(2)_L \times U(1)_Y$-symmetric expansion in terms of operators invariant under the SM gauge group and ordered by their mass dimension (referred to as SMEFT when only SM fields are considered), or a $U(1)_{em}$-symmetric expansion which does not assume the Higgs boson necessarily belongs to an EW doublet at the level of the effective Lagrangian (similarly referred to as Higgs EFT or HEFT). With the key distinction between them being whether the spontaneous breaking of the EW symmetry is "linearly" or "non-linearly" realized respectively. While the second expansion is more general and covers a wider spectra of possible new physics phenomena (it also contains the first), it needs to deal with the phenomenological disadvantage of having a significantly larger number of degrees of freedom.

Crucially, both realizations feature scenarios where light ALPs interact with the SM Higgs, for which exotic Higgs decays represent a key experimental signature. In

what follows, we will focus on the Higgs $h \to Za$ decay relevant to our search, into a SM Z boson and an ALP a. We can parametrize the partial decay width of this decay as

$$\Gamma(h \to Za) = \frac{m_h^3}{16\pi f_a^2} c_{aZh}^2 \lambda^{3/2} \left(\frac{m_Z}{m_h}, \frac{m_Z}{m_h} \right) \Bigg(\tag{3.2}$$

with f_a the ALP decay constant, $\lambda(x,y) \equiv \left(1 - x^2 - y^2\right)^2 - 4x^2y^2$ and c_{aZh} an effective tri-linear coupling between the ALP and the SM Higgs and Z boson fields. In the non-linear expansion, the leading contribution comes from dimension-5 operators and this effective coupling can be shown to be a particular combination of their Wilson coefficients. In contrast, the dimension-5 contribution vanishes in the linear expansion, where the leading contribution comes from dimension-7 operators and is thus suppressed by two extra powers of the axion scale. Lastly, both expansions can also include an additional contribution coming from fermion loop graphs at dimension-5. The latter is dominated by the top contribution, as both the Higgs and the ALP couple to fermions proportionally to their masses.[1]

If a also couples to some hidden sector particle(s) (see *e.g.* [184, 185]), its dominant decay mode(s) may be into the dark sector, thus invisible at colliders. This encompasses the intriguing possibility that the ALP may be a mediator between the SM and the DM candidate [184]. Alternatively, the ALP may be long-lived and leave the LHC detectors without decaying, due to its suppressed couplings to photons (*i.e.* a photo-phobic ALP [186]) and/or leptons (in this case, even if a coupling to gluons exists, the ALP will be invisible for masses below the last-available hadronic decay threshold, $m_a \lesssim 3m_\pi$ [187]). Higgs decays $h \to Za, a \to \not{E}_T$ can then probe such ALP scenarios.

To translate the model-independent LHC and ILC projected sensitivities from the previous Sections into a probe of the parameter space of ALPs, we specifically consider, together with the coupling between the ALP and the SM Higgs, an ALP coupling to a hidden fermion χ, given by $y_\chi\, \bar{\chi}\gamma^\mu\gamma^5\chi\, \partial_\mu a/f_a$ as well as an ALP coupling to photons $c_{a\gamma\gamma}/f_a\, a\, F^{\mu\nu}\tilde{F}_{\mu\nu}$ (we do not include an ALP coupling to gluons or SM fermions for simplicity). y_χ does not have a preferred value, while the expectation for the bosonic Wilson coefficient is $c_{a\gamma\gamma} \sim \alpha_{\rm EM}$ [188] (the electromagnetic coupling constant). We then set $c_{a\gamma\gamma} = \alpha_{\rm EM}(Q)$ (Q being the energy scale of the process considered), and $y_\chi = 1, c_{aZh} = 1, m_\chi = 0.45 m_a$ (to allow for the invisible ALP decay $a \to \chi\bar{\chi}$), and show in Figure 3.4 the LHC projected 2σ sensitivity on $\text{BR}(h \to Za) \times \text{BR}(\text{a} \to \chi\bar{\chi})$ in the $(m_a,\, f_a)$ plane. We also depict the *Higgs neutrino floor*, within reach of the $\sqrt{s} = 250$ GeV ILC. Figure 3.4 also shows, under the assumption that χ is the DM particle, the $(m_a,\, f_a)$ relation yielding (for the choice of parameters described above) the observed DM relic abundance $\Omega_{\rm DM}h^2 = 0.12$ [189] generated via thermal freeze-out in the early Universe (taken from [184]), as well as the existing and projected constraints on this ALP scenario from searches at LEP, LHC and flavor factories (Babar, Belle-II), and astrophysics (supernova 1987A).

[1] See Refs. [182, 183] for more details on the EFT contributions to this decay.

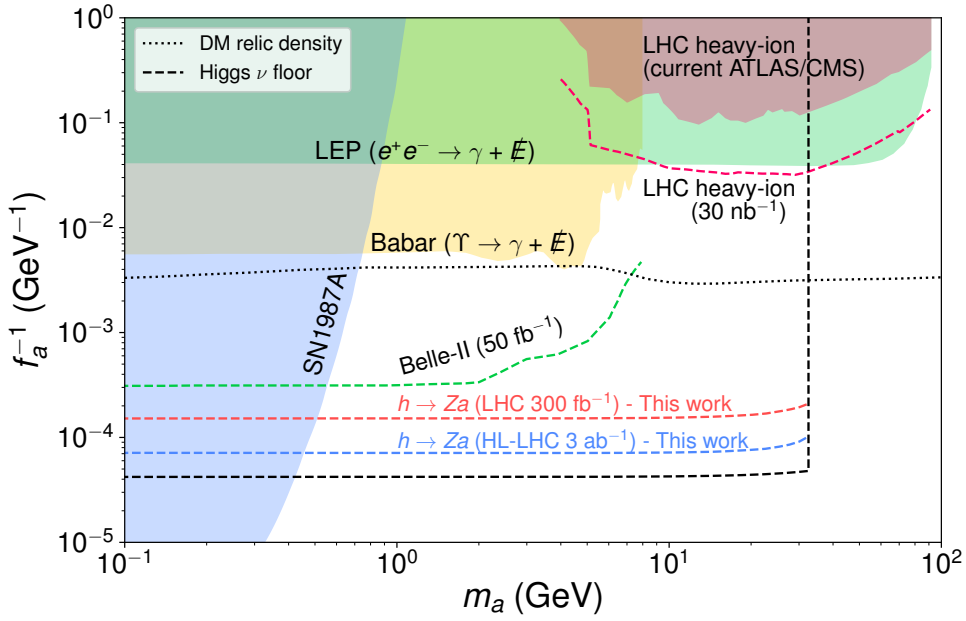

Figure 3.4: Present (solid) and projected (dashed) constraints on the $(m_a,\ f_a)$ plane for an ALP with coupling to photons, a hidden (DM) fermion χ and the SM Higgs (via a c_{aZh} coupling), see text for details.

From [184], we obtain the 95% C.L. LEP limits from mono-photon searches [190, 191], which constrain an ALP produced via its coupling to photons and decaying invisibly, as well as the 90% C.L. limits from $e^+e^- \to \gamma + \not{E}$ (with $\not{E}$ the missing energy of the event) and rare upsilon decays into $\gamma + \not{E}$ from Babar [192, 193] (see also [194]) and the projected 90% C.L. sensitivity of Belle-II in the $\gamma + \not{E}$ final state. Also shown in Figure 3.4 are the current 95% C.L. limits from heavy-ion (Pb-Pb) collisions at the LHC, from ALP searches in light-by-light scattering (as proposed in [195]) performed by ATLAS [196] and CMS [197] (see also [198]). We also include a projection drawn from rescaling the current ATLAS expected sensitivity to an (optimistic) integrated luminosity of 30 nb^{-1}. Finally, we show the bound from the energy loss of supernova 1987A from ALP emission, as taken from [184]. The supernova 1987A limit is stronger than usually quoted for an ALP coupling only to photons since the invisible decay of the ALP allows its corresponding energy to escape the supernova core even for parameter regions with a sizable coupling to photons (contrary to the usual case, where a large enough coupling to photons will result in the ALP being trapped in the core [199]).

We note that the existence of the invisible decay mode of the ALP leads (under the assumptions discussed above) to a strongly suppressed ALP branching fraction to two photons, BR$(a \to \gamma\gamma) \sim 3 \times 10^{-4}$. Limits from ALP searches in visible final states, like tri-photon searches at LEP 1 and LEP 2 via the process $e^+e^- \to \gamma^* \to$

$\gamma\, a$, $a \to \gamma\gamma$ (as studied in [187, 200]), and searches for $Z \to \gamma\gamma$ decays[1] at LEP 1 have to be rescaled by BR($a \to \gamma\gamma$) (assumed to be 100% in [187, 200]), and are too weak to appear in Figure 3.4. Similarly, the dominant invisible decay of the ALP significantly weakens the limits from beam-dump experiments as compared to the case of visible ALP scenarios (see *e.g.* Ref. [201]) roughly by a factor BR($a \to \gamma\gamma$) $\sim 10^{-4}$. A naive re-scaling of beam-dump limits results in no meaningful constraints (beyond what is currently excluded by other experiments/observations) from these, and we choose not to include them in Figure 3.4. A precise re-derivation of these limits requires to additionally take into account the geometry of each experiment to obtain the expected number of $a \to \gamma\gamma$ events in the detector decay volume, which is beyond the scope of this work.

Finally, we also show in Figure 3.5 the corresponding limits on the $(m_a,\ f_a)$ plane if a hypercharge coupling $c_{aBB}/f_a\, a\, B^{\mu\nu}\tilde{B}_{\mu\nu}$ (rather than a coupling only to photons) is assumed. The latter introduces a coupling of the ALP to ZZ and $Z\gamma$ (besides the already considered coupling to photons), given respectively by $c_{aZZ}/f_a\, a\, Z^{\mu\nu}\tilde{Z}_{\mu\nu}$ and $c_{aZ\gamma}/f_a\, a\, F^{\mu\nu}\tilde{Z}_{\mu\nu}$, with $c_{aZZ} = \sin^2\theta_W\, c_{aBB}$ and $c_{aZ\gamma} = -2\sin\theta_W \cos\theta_W\, c_{aBB}$ (with θ_W the weak mixing angle). Fixing $c_{aBB} = \alpha_{\rm EM}/\cos^2\theta_W$ to match the ALP coupling to photons $c_{a\gamma\gamma}$ we assumed before, the above limits do not change, yet from $c_{aZ\gamma} \neq 0$ there is another constraint from LEP searches for rare $Z \to \gamma + a$ decays, with a invisible. The L3 collaboration at LEP has set a limit BR($Z \to \gamma + a$) $< 1.1 \times 10^{-6}$ at 90% C.L. [202], shown in Figure 3.5 (in purple) together with the already considered constraints on our scenario (Figure 3.4). Other potential bounds from rare Z decays at LEP and LHC, *e.g.* from $Z \to 3\gamma$ or $Z \to \gamma\ell\ell$ (see [183]), do not lead to meaningful constraints in Figure 3.5.

Lastly, we comment on the possibility of probing the ALP a via exotic Higgs decays $h \to Za$ with $a \to \gamma\gamma$, as discussed in [183]. We note that, while the corresponding final state allows to consider Higgs production in gluon-fusion (resulting in an $\mathcal{O}(50)$ enhancement of the Higgs production cross section w.r.t. our scenario, which must rely on Higgs associated production), this is counteracted by the large suppression from BR($a \to \gamma\gamma$). A preliminary study of the LHC sensitivity to ALPs in exotic Higgs decays via $pp \to h \to Za$, $Z \to \ell\ell$, $a \to \gamma\gamma$ including the leading SM backgrounds has been performed in [203], indicating that such decay channel is much less sensitive than the one discussed in this work (given our assumptions for the ALP branching fractions).

3.2 2HDM+a

Two-Higgs-doublet models extended by a singlet pseudoscalar mediator (2HDM+a) and a fermionic singlet DM particle constitute the minimal renormalizable realization of a pseudoscalar portal to DM [160–162, 204, 205]. A pseudoscalar mediator would nicely explain the absence of a signal in current DM direct detection exper-

[1] For light ALPs, with masses $\lesssim 10$ GeV, the two photons from the ALP decay would appear merged in the detector, and $e^+e^- \to \gamma\gamma$ searches would be sensitive to the presence of the ALP [200].

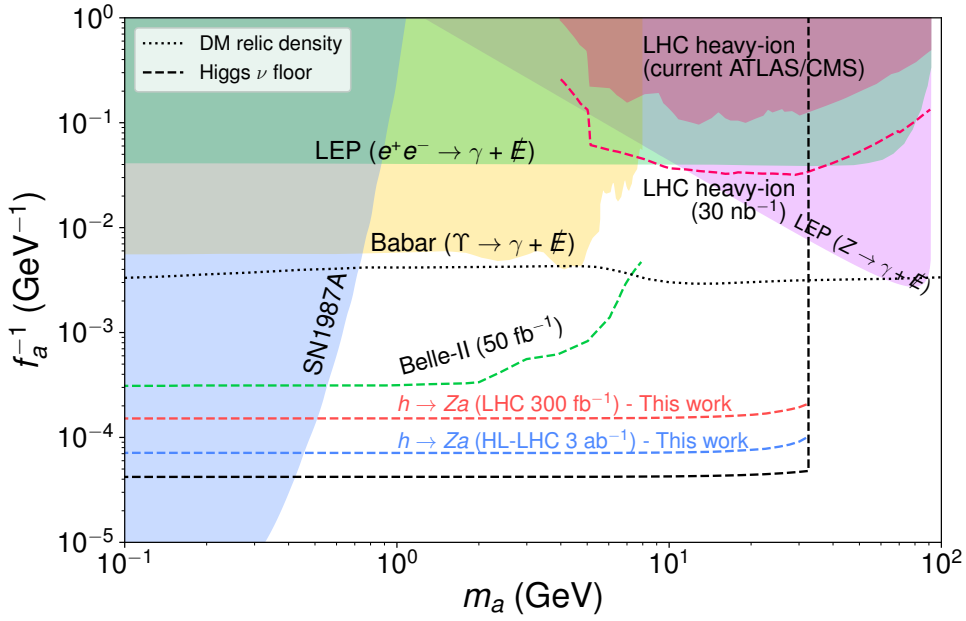

Figure 3.5: Present (solid) and projected (dashed) constraints on the $(m_a,\ f_a)$ plane for an ALP with coupling to the hypercharge field strength, a hidden (DM) fermion χ and the SM Higgs (via a c_{aZh} coupling), see text for details.

iments [206], yielding a spin-independent DM-nucleon scattering cross section only at the loop level [207, 208]. Pseudoscalar portal to DM scenarios (and in particular the 2HDM+a) have also been proposed to explain [204, 209–211] the γ-ray excess [212–214] in the Fermi-LAT observations of the Milky Way Galactic Center [215]. Furthermore, the 2HDM+a has become a leading benchmark scenario for the DM interpretation of LHC searches [216]. The base tree-level 2HDM scalar potential reads [48, 217]

$$\begin{aligned} V_{\text{2HDM}} = & \mu_1^2 |H_1|^2 + \mu_2^2 |H_2|^2 - \left[\mu_3^2 H_1^\dagger H_2 + \text{H.c.}\right] + \frac{\lambda_1}{2} |H_1|^4 + \frac{\lambda_2}{2} |H_2|^4 \\ & + \lambda_3 |H_1|^2 |H_2|^2 + \lambda_4 \left|H_1^\dagger H_2\right|^2 + \frac{1}{2}\left[\lambda_5 \left(H_1^\dagger H_2\right)^2 + \text{H.c.}\right] \end{aligned} \tag{3.3}$$

where both CP invariance and a $\mathbb{Z}_2$-symmetry between the doublets (under which $H_1 \to H_1$ and $H_2 \to -H_2$) have been assumed, while allowing for the former to be softly broken by the μ_3-dependent term (see *e.g.* Ref. [218]). Both choices are motivated by the phenomenology of these realizations: CP invariance naturally suppress electric dipole moments in accordance with experiments, whereas the $\mathbb{Z}_2$-symmetry is typically extended to the Yukawa sector so that each fermion type couples exclusively to one of the doublets $H_{1,2}$ and not the other, avoiding tree-level FCNCs (see Chapter 4 for an extended discussion on these topics). Conventionally,

and without the loss of generality, up-type quarks are always coupled to H_2, leading to four different possibilities (*Types*) to couple down-type quarks and leptons to each of the doublets: Type-I 2HDM couple both of them to H_2 as well, whereas Type-II assign them to H_1 instead, lastly, the *lepton-specific* and *flipped* types swap the leptons in each case respectively (*c.f.* Table 4.1 in Chapter 4).

The EW symmetry is spontaneously broken by the VEVs of the doublets $\langle H_i^\dagger H_i \rangle = v_i^2/2$, which can be expanded around them as $H_i = (\phi_i^+, (v_i + h_i + \eta_i)/\sqrt{2})^T$ $(i = 1, 2)$. Customarily, it is also useful to define $v \equiv \sqrt{v_1^2 + v_2^2} \simeq 246$ GeV and $\tan\beta \equiv v_2/v_1$. After EWSB, the scalar spectrum of the 2HDM contains a charged scalar $H^\pm$, a neutral CP-odd scalar A_0 and two neutral CP-even scalars h and H. These mass-eigenstates result from two different rotations of the fields in the doublets by mixing angles α and β:

$$\begin{aligned} H^\pm &= \cos\beta\, \phi_2^\pm - \sin\beta\, \phi_1^\pm, \qquad A_0 = \cos\beta\, \eta_2 - \sin\beta\, \eta_1, \\ h &= \cos\alpha\, h_2 - \sin\alpha\, h_1, \qquad H = -\sin\alpha\, h_2 - \cos\alpha\, h_1. \end{aligned} \tag{3.4}$$

The 125 GeV Higgs boson discovered at the LHC is typically identified with h, which becomes SM-like in the *alignment limit* $\beta - \alpha = \pi/2$ (see *e.g.* Refs. [48, 218]). The 2HDM+a builds on this picture to provide the most economical realization of a pseudoscalar portal between the SM and a fermionic DM candidate, by mixing an additional CP-odd mediator a_0 with the CP-odd boson A_0 that would ordinarily result from the two doublets. This can be achieved if the new field is implemented by an expansion of the scalar potential in Eq. (3.3) of the form [162]

$$V_a = \frac{\mu_{a_0}^2}{2} a_0^2 + \frac{\lambda_a}{4} a_0^4 + a_0 \left(i\kappa H_1^\dagger H_2 + \text{H.c.} \right) + a_0^2 \left(\lambda_{a1} |H_1|^2 + \lambda_{a2} |H_2|^2 \right). \tag{3.5}$$

The interaction between the real pseudoscalar mediator a_0 and a Dirac fermion DM candidate χ with mass m_χ (both singlets under the SM gauge group) can then be implemented as

$$\mathcal{L}_\chi = \bar{\chi} \left(\not{\partial} - m_\chi \right) \chi - y_\chi\, a_0\, \bar{\chi} i\gamma^5 \chi. \tag{3.6}$$

The κ-dependent term in (3.5) mixes a_0 and A_0, bridging the dark and visible sectors and leading to the appearance of two different mass eigenstates a and A (with $m_a < m_A$) parametrized in terms of the mixing angle θ as

$$a = \cos\theta\, a_0 - \sin\theta\, A_0, \qquad A = \cos\theta\, A_0 + \sin\theta\, a_0. \tag{3.7}$$

For a light a ($m_a \lesssim 30$ GeV), the main direct experimental probes of this scenario are the exotic Higgs decays $h \to Za$ and $h \to aa$. Given that a naturally decays to DM particles with a branching fraction $\text{BR}(a \to \chi\bar{\chi}) \simeq 1$ unless the relevant coupling is greatly suppressed $y_\chi \ll 1$, the first leads to the semi-invisible Higgs

decay topology targeted in this work, while the former contributes to the Higgs invisible width. The tree-level hZa coupling $g_{hZa} = \sin\theta\cos(\beta-\alpha)m_Z/v\,(p_h^\mu - p_a^\mu)$ [160, 162] results in a partial width

$$\Gamma(h\to Za) = \frac{m_h^3}{16\pi v^2}s_\theta^2 c_{\beta-\alpha}^2\lambda^{3/2}\left(\frac{m_Z}{m_h},\frac{m_Z}{m_h}\right) \tag{3.8}$$

where $s_\theta \equiv \sin\theta$, and $c_{\beta-\alpha}\equiv\cos(\beta-\alpha)$ parametrizes the deviation away from the alignment limit. Whereas the partial width for the fully-invisible topology is

$$\Gamma(h\to aa) = \frac{v^2}{32\pi m_h}g_{haa}^2\sqrt{1-4m_a^2/m_h^2}, \tag{3.9}$$

with the Higgs-pseudoscalar coupling g_{haa} given by

$$g_{haa} = (\lambda_7 s_{\beta-\alpha}-\lambda_8 c_{\beta-\alpha})s_\theta^2 + 2\left(\frac{\lambda_{a1}+t_\beta^2\lambda_{a2}}{1+t_\beta^2}s_{\beta-\alpha} - \frac{(\lambda_{a2}-\lambda_{a1})t_\beta}{1+t_\beta^2}c_{\beta-\alpha}\right)c_\theta^2, \tag{3.10}$$

where $\lambda_{7,8}$ have been defined as

$$\begin{aligned}\lambda_7 v^2 &\equiv 2m_a^2 + 2(m_H^2-M^2) - m_h^2 + (m_H^2-m_h^2)[1+s_{\beta-\alpha}(s_{\beta-\alpha}-c_{\beta-\alpha}(t_\beta - t_\beta^{-1}))],\\ \lambda_8 v^2 &\equiv (M^2-m_H^2)(t_\beta - t_\beta^{-1}) - c_{\beta-\alpha}(m_H^2-m_h^2)(s_{\beta-\alpha}-c_{\beta-\alpha}(t_\beta-t_\beta^{-1})).\end{aligned} \tag{3.11}$$

For $|\cos(\beta-\alpha)|\ll 1$, as needed to satisfy the present LHC Higgs signal strength measurements [88, 219], we generally expect $\Gamma(h\to aa)\gg\Gamma(h\to Za)$, yet in certain (albeit small) regions of the 2HDM+a parameter space, the $h\to Za$ semi-dark Higgs decay can provide stronger sensitivity than the $h\to aa$ invisible Higgs decay. In particular, we will consider two benchmarks: for the first, we will restrict to the region of the parameter space where the invisible partial widh vanishes, by fixing $\lambda_{a1}=\lambda_{a2}$ and setting both to the value that yields $g_{haa}=0$; for the second, we will fix $\lambda_{a1}=\lambda_{a2}=0$ instead, such that $\Gamma(h\to aa)\neq 0$. Both scenarios involve a Type-I 2HDM (see Ref. [48]) with $c_{\beta-\alpha}=0.2$, $t_\beta\equiv\tan\beta=6$, $M\equiv\sqrt{\mu_3^2/s_\beta c_\beta}=600$ GeV, $m_H = m_{H^\pm}=m_{A_0}=700$ GeV. We further take $m_\chi = 0.45\,m_a$ and fix y_χ to yield the observed DM relic density via thermal freeze-out (see *e.g.* Refs. [161, 211] and discussion below), and show in Figures 3.6 and 3.7 the projected LHC sensitivity (with 300 fb^{-1} and at HL-LHC with 3 ab^{-1}) of the semi-dark Higgs decay $h\to Z(\ell\ell)+\not{E}_T$ in the $(m_a,\sin\theta)$ plane for both benchmarks respectively. We also depict in Figure 3.7 the constraint on the Higgs invisible width from $h\to aa$ decays, which at present is $\mathrm{BR}(h\to\not{E}_T)<0.11$ at 95% C.L. [220] under the assumption of SM Higgs production, and is expected to be $\mathrm{BR}(h\to\not{E}_T)<0.04$ at 95% C.L. [221] at the HL-LHC.

Furthermore, while our 2HDM $(c_{\beta-\alpha}, t_\beta)$ benchmark satisfies both present and HL-LHC projected limits from Higgs signal strengths on 2HDM parameters [222],

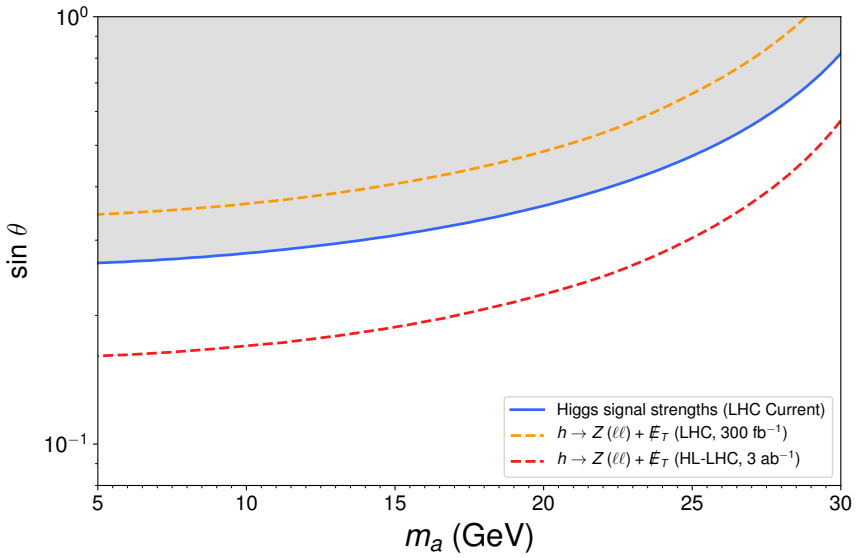

Figure 3.6: Present (solid, gray) and projected (dashed) constraints on the $(m_a, \sin\theta)$ plane for the ***first benchmark*** 2HDM+a scenario analyzed in this work (with $\Gamma(h \to aa) = 0$), see text for details.

the 2HDM+a is further constrained by additional contributions to the Higgs total width $\Gamma(h \to Za)$, $\Gamma(h \to aa) \neq 0$. For $c_{\beta-\alpha} = 0.2$, $t_\beta = 6$, we have performed a global χ^2 fit to present Higgs signal strength measurements via the HiggsSignals [223, 224] numerical code interfaced to Scanners [225], yielding a 95% C.L. upper bound $\mathrm{BR}(h \to Za) + \mathrm{BR}(h \to aa) < 0.042$, which is also shown in Figures 3.6 and 3.7. While this bound will certainly improve at the HL-LHC, the corresponding sensitivity improvement in $\sin\theta$ will only be mild since $\Gamma(h \to Za) \propto \sin^2\theta$ and $\Gamma(h \to aa) \propto \sin^4\theta$ (for our $\lambda_{a1} = \lambda_{a2} = 0$ benchmark), and we expect direct searches for a in exotic Higgs decays to remain competitive with indirect probes through Higgs signal strength measurements.

Other searches for the state a do not provide meaningful sensitivity in the scenario we consider: searches for $h \to aa$ in visible final states (see [147] for a review) like $b\bar{b}\tau\tau$ [143] and $\tau\tau\tau\tau$ [139] are found to be $\mathcal{O}(10^3)$ less sensitive than probes of the Higgs invisible width, and fall short of providing any limit on $\mathrm{BR}(h \to aa)$ by a factor $\sim 50 - 100$, with searches in other final states (*e.g.* $b\bar{b}\mu\mu$ [141], $\tau\tau\mu\mu$ [137, 138]) yielding even smaller sensitivity. Such visible decays of a are then generally not relevant in the 2HDM+a with $m_a > 2m_\chi$, since matching the observed DM relic density requires $y_\chi \sim 1$ (see below), leading to $\mathrm{BR}(a \to \chi\bar{\chi}) > 0.99$ in general. We also find that current LHC mono-jet searches [226] fall short of probing any region of the $(m_a, \sin\theta)$ plane of Figures 3.6 and 3.7 by a factor $\sim 1/(3t_\beta^2)$. Lastly, we note that, while the hZa coupling could be constrained via Higgs boson production in association with missing energy at LEP2 through the $e^+e^- \to Z^* \to ha$ process, these searches do not yield meaningful constraints on the 2HDM+a parameter space: the

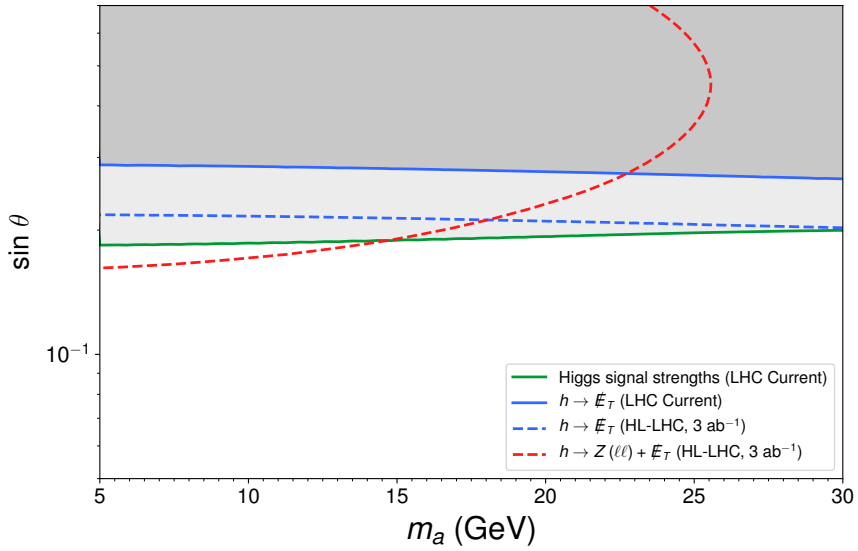

Figure 3.7: Present (solid, gray) and projected (dashed) constraints on the $(m_a, \sin\theta)$ plane for the ***second benchmark*** 2HDM+a scenario analyzed in this work (with $\Gamma(h \to aa) \neq 0$), see text for details.

analyses for $h + \bar{\nu}\nu$ signatures by the OPAL [227], L3 [228] and ALEPH [229, 230] experiments at LEP impose a constraint on the missing mass M_{miss} of the event (equal to m_a in our scenario) which is not fulfilled by our signal (*e.g.* the OPAL analysis [227] requires $50\,\text{GeV} < M_{\text{miss}} < 130\,\text{GeV}$, and it is thus not sensitive to $m_a < 30\,\text{GeV}$). The corresponding search by the DELPHI experiment [231], while not imposing such a cut on M_{miss}, does not consider Higgs boson masses above 120 GeV.

Moreover, we also consider possible constraints on the spin-0 states from the 2HDM, $H^\pm$, H and A (doublet-like). Electroweak precision observables (EWPO) constrain (dominantly via the oblique T-parameter) the mass splittings among the 2HDM scalars, since the 2HDM scalar potential of the 2HDM is custodially invariant for $m_{A_0} = m_{H^\pm}$ or $m_H = m_{H^\pm}$. The latter is chosen for our benchmark scenario, directly satisfying EWPO. Potential constraints from flavor physics, in particular from B-meson decays: $\bar{B} \to X_s\gamma$ decays (which constrain $m_{H^\pm}$ [232, 233]) and from $B_s \to \mu^+\mu^-$ (which constrain the presence of a light a coupling to SM fermions [234, 235]), are also directly satisfied for a Type-I 2HDM with moderately high t_β (we have chosen in particular $t_\beta = 6$ in our benchmark analysis). Finally, we also discuss direct searches for the 2HDM states as a probe of our scenario: away from the 2HDM alignment limit, $H \to W^+W^-$ and $H \to ZZ$ decays could yield sensitivity if the mass scale of the 2HDM scalars is not very high. At the same time, $H \to Za$ decays would lead to resonant mono-Z signatures [160, 162], which have been recently been searched for by both ATLAS and CMS [170, 171] (ATLAS also searches for this final state in $H \to ZZ \to \ell\ell\nu\bar{\nu}$ decays [236]). However, in all

these cases, we find that for $|s_{\beta-\alpha}t_\beta^{-1} - c_{\beta-\alpha}| \ll 1$ (as our scenario features) the production of H at the LHC is suppressed, and no meaningful limit is obtained.

To conclude, we discuss the need to reproduce the observed DM relic density $\Omega_{\rm DM}h^2 = 0.12$ [189] within the 2HDM+a, via DM thermal freeze-out in the early-Universe. For $m_\chi \gtrsim 2$ GeV, the DM annihilation cross section into SM particles (via $\chi\bar{\chi} \to q_{\rm SM}q_{\rm SM}$, with $q_{\rm SM}$ here being generic SM particles) in the non-relativistic limit is

$$\langle\sigma{\rm v}\rangle = \frac{y_\chi^2}{2\pi}\frac{m_\chi^2}{m_a^4\, t_\beta^2}s_\theta^2 c_\theta^2 \left[\left(1 - \frac{4m_\chi^2}{m_a^2}\right)^2 + \frac{\Gamma_a^2}{m_a^2}\right]^{-1} \times \sum_f N_C \frac{m_f^2}{v^2}\sqrt{1 - \frac{m_f^2}{m_a^2}}. \tag{3.12}$$

with Γ_a the decay width of a. The sum over SM fermion f annihilation channels involves quarks ($N_C = 3$) and charged leptons ($N_C = 1$). Reproducing the observed DM relic density via thermal freeze-out requires $\langle\sigma{\rm v}\rangle \simeq 3 \times 10^{-26}{\rm cm}^3/{\rm s}$, which generically leads to $\mathcal{O}(1)$ values for y_χ. For $m_\chi < 2$ GeV the DM annihilation into SM fermions (b, c-quarks and/or τ-leptons, depending on m_χ) ceases to be the dominant DM annihilation process, and instead annihilation into QCD hadrons (via the 1-loop coupling of a to gluons) dominates. Due to its complexity, we do not explore that region of the 2HDM+a parameter space, which may also involve $y_\chi \gg 1$, in this thesis.

3.3 A Comment on Dark Photons

Dark photons (see *e.g.* Ref. [237] for a review) embody the idea of bridging SM and dark sector through the vector portal, with the interaction between them arising as a result of the kinetic mixing between a pair of dark and visible Abelian gauge bosons. The former is typically considered to be the SM photon, the gauge boson of the electromagnetic interaction $U(1)_{em}$, or, above the EWSB scale, the hypercharge boson of the $U(1)_Y$ group. While the first can be identified as the gauge boson of a dark $U(1)_D$ symmetry, and can also interact with other particles with dark charges within the dark sector. The Lagrangian of a dark photon interacting with the SM via hypercharge kinetic mixing reads [134, 238]

$$\mathcal{L} \supset -\frac{1}{4}B_{\mu\nu}B^{\mu\nu} - \frac{1}{4}X_{\mu\nu}X^{\mu\nu} + \frac{\epsilon}{2\cos\theta_W}B_{\mu\nu}X^{\mu\nu}. \tag{3.13}$$

The dark photon Z_D mixes with the SM Z boson, so that, after the diagonalization of the kinetic terms in Eq. (3.13) and rotation to the mass basis, there is an interaction term of the form $\propto \epsilon\, h Z_\mu Z_D^\mu$. For a light Z_D, the former gives rise to the exotic Higgs decay $h \to ZZ_D$. If coupled to the dark sector and invisibly-decaying, these dark photons would then constitute another new physics scenario that semi-dark Higgs decays could be sensitive to. However, current 95% C.L. bounds on the kinetic mixing parameter ϵ from EW precision observables set $\epsilon \lesssim 0.03$ for dark photon masses $m_{Z_D} < 30$ GeV [239]. The corresponding $h \to ZZ_D$ branching fraction

is then smaller than $< 10^{-3}$ (see *e.g.* Ref. [134]) and thus, below the *Higgs neutrino floor*.

Departing the canonical picture, other possibilities have been discussed in the literature involving extra sources of $Z - Z_D$ mass mixing [148, 240–243] beyond the kinetic term considered in Eq. (3.13). This mixing could, for instance, originate from extended scalar sectors (*e.g.* a 2HDM), loop effects or different mechanisms of dynamical symmetry breaking. These sources could provide an additional contribution decorrelated from ϵ to the $h \to ZZ_D$ decay, potentially enhancing it with respect to the initial expectation. This possibility is however left for future work.

4 Conclusion

Semi-invisible Higgs decays remain largely unexplored both theoretically and experimentally despite constituting a rather generic prediction of many well motivated BSM extensions, specifically those seeking to provide an explanation for the observed DM abundance in the form of dark sectors. In this Chapter we have explored the exotic Higgs decay $h \to ZX$, with X an invisible BSM particle resulting in a semi-dark final state. Such exotic Higgs decays may occur in theories of ALPs, dark photons or pseudoscalar mediators between the SM and dark matter. The SM process $h \to Z\nu\bar{\nu}$ represents an irreducible "neutrino floor" background to these new physics searches, but also provides a target experimental sensitivity for them.

In order to search for this decay we have targeted ZH associated production, leading to a $4\ell + \not{E}_{(T)}$ final state benefiting from both a clean missing energy reconstruction and reduced backgrounds. We implement a first multivariate neural network analysis to identify the Z boson produced by the Higgs decay, and a second to discriminate between the signal and the relevant SM backgrounds. We analyze $h \to Z + \textit{invisible}$ searches at the LHC (both at present and future luminosities) and an hypothetical ILC, and derive their projected sensitivities to $\mathrm{BR}(h \to ZX) \times \mathrm{BR}(X \to \not{E}_{(T)})$. Present luminosity constraints are well competitive, at the level of the branching ratio, with those resulting from the two other semi-invisible decays currently being searched for at the LHC: $h \to \gamma + \not{E}_T$ [151–155], and $h \to b\bar{b} + \not{E}_T$ [156]. Whereas the HL-LHC comes close to being able to probe the *Higgs neutrino floor* (for $m_X = 1$ GeV, it probes $\mathrm{BR}(h \to ZX) \times \mathrm{BR}(\mathrm{X} \to \not{E}_{\mathrm{T}}) = 2.8 \times \mathrm{BR}(\mathrm{h} \to \mathrm{Z}\nu\bar{\nu})_{\mathrm{SM}}$ at 2σ). The ILC, on the other hand, is well capable of sweeping the entire new physics parameter space of semi-dark Higgs decays down to the *Higgs neutrino floor*, and could potentially find the first evidence for this SM process.

Finally, we have translated the resulting constraints onto the parameter space of some well-motivated BSM extensions. While direct searches for this decay cannot compete with the most sensitive probes available in the case of a dark photon (at least considering its simplest realization through kinetic mixing), they prove competitive for the 2HDM+a, where there is a strong interplay between this search, Higgs signal strengths and the fully-invisible decay. This is also particularly true for the case of ALPs, given the assumptions discussed in the previous Section, semi-dark $h \to Za$

decays could probe a vast region of otherwise unexplored parameter space. The latter would include the thermal relic line, encompassing the tantalizing possibility that the ALP might be the mediator between the SM and the dark matter.

4

Higgs CP-Violating Portal: Assisting Baryogenesis from the Dark

1 Introduction

As discussed in Chapter 1, while the SM does in fact present all the necessary ingredients to fulfill the Sakharov conditions, and as such, could have conceivably accommodated the generation of the observed baryon asymmetry of the Universe (BAU), it ultimately fails on two fronts.

On the one hand, CP conjugation is an approximate symmetry of the SM, only broken as a consequence of the mismatch between weak and mass eigenstates of three families of quarks and leptons (*c.f.* Chapter 1). However, the presence of CP violation in the early Universe, together with baryon number violation (which occurs at high temperature in the SM via sphaleron processes [30]) and a departure from thermal equilibrium, is required to generate the BAU [29, 35, 36, 244, 245]. The amount of CP violation present in the SM is well-known to be insufficient for the generation of the BAU at the EW scale [31–34]. Nevertheless, new sources of CP violation beyond the SM are tightly constrained by experimental searches of electric dipole moments (EDM) of the electron [246], neutron [247] and atomic elements like mercury [248]. These constraints pose significant challenges to successful (EW) baryogenesis scenarios.

A possible way to alleviate EDM constraints is to seclude the CP violation, so that it is restricted to interactions between the visible and dark sectors. Consequently, new contributions to EDM necessarily involve hidden sector particles and are thus suppressed with respect to conventional scenarios. In this case, some dynamics is needed to enhance the CP violation in the early Universe such that baryogenesis is successful. This could be achieved by a period of transient CP breaking in the early Universe, which would act as a catalyzer for baryogenesis. Then, at

present-times, the EDM-limits would naturally be avoided.[1]

On the other hand, such a non-minimal Higgs sector could, at the same time, yield a strongly first-order EW phase transition (see *e.g.* [255–260]), thus addressing the second shortcoming standing between the SM and successful baryogenesis: a second-order EW transition unable to provide the necessary departure from thermal equilibrium. In the case of the first, this departure would be supplied by the nucleation of EW-vacuum bubbles expanding in the unbroken phase. Together with a period of transient CPV enhancement, they hint at the tantalizing possibility that the Universe might have undergone a two-step phase transition: by providing an additional source of spontaneous CPV, the first transition could have enabled successful EW baryogenesis during the second.

Nevertheless, it is important to note realizations which rely on spontaneous CPV to source EW baryogenesis often share a common pitfall. Generally a $\mathbb{Z}_2$-symmetric potential (*e.g.* invariant under a transformation $S \to -S$, where S is the field that will provide this breaking) is desirable, as it avoids phenomenologically dangerous features such as mixing between the singlet and Higgs states at the EW phase. Typically however, the net baryon number asymmetry is linearly tied to the VEV of this field (*e.g.* a higher-dimensional operator linear on S which provides a complex mass for a SM fermion [249, 252]), so that the degeneracy between the two $\mathbb{Z}_2$-symmetric vacua leads to the creation of cosmic domains where positive and negative numbers of baryons are created, ultimately washing the asymmetry on large scales. One possible solution is to consider realizations where the spontaneous CPV can only happen through quadratic terms S^2 instead. For renormalizable theories, these can only be a part of the scalar potential, so that we are naturally led to consider a $\mathbb{Z}_2$ symmetry for the latter. Successful baryogenesis then requires that S be protected by it, *i.e.* it naturally leads to a dark matter candidate. In this way, these scenarios could potentially address both, the observed DM abundance and the BAU.

In this Chapter, we show that this setup can be accommodated by a suitable extension of the SM Higgs sector (see also [261, 262] for related scenarios), specifically, we consider a 2HDM augmented by a real singlet scalar field. The singlet has CP violating interactions with the SM, and is protected by a $\mathbb{Z}_2$ symmetry, so that it also constitutes a viable DM candidate. We explore the regions of the parameter space where an early-Universe period of CPV enhancement occurs and the required thermal history takes place. We also discuss ongoing work studying the rich phenomenology of this scenario, including its testability through a combination of LHC searches and dark matter constraints.

2 The Model: 2HDM + S^2 with CP Violation

We consider a 2HDM with the addition of a real singlet scalar field S, which is odd under a *dark* $\mathbb{Z}_2$-symmetry. The tree-level scalar potential for the two Higgs doublets $H_{1,2}$ and S is:

[1] See Refs. [249–254] for other weak-scale baryogenesis setups which avoid current EDM experimental constraints via suppressed BSM contributions to EDM.

$$
\begin{aligned}
V(H_1,H_2,S) =& \mu_1^2 |H_1|^2 + \mu_2^2 |H_2|^2 - \left[\mu_{12}^2 H_1^\dagger H_2 + \text{H.c.}\right] + \frac{\lambda_1}{2} |H_1|^4 + \frac{\lambda_2}{2} |H_2|^4 \\
&+ \lambda_3 |H_1|^2 |H_2|^2 + \lambda_4 \left|H_1^\dagger H_2\right|^2 + \frac{1}{2}\left[\lambda_5 \left(H_1^\dagger H_2\right)^2 + \text{H.c.}\right] \\
&+ \frac{\mu_S^2}{2} S^2 + \frac{\lambda_S}{4} S^4 + \lambda_{S_1} S^2 |H_1|^2 + \lambda_{S_2} S^2 |H_2|^2 \\
&+ \frac{1}{2}\left[\lambda_{S_3} S^2 H_1^\dagger H_2 + \text{H.c.}\right]
\end{aligned}
\tag{4.1}
$$

The μ_{12}^2 term above yields a soft-breaking of the 2HDM $\mathbb{Z}_2$-symmetry which forbids tree-level-FCNCs. Note however that the last term in Eq. (4.1), proportional to λ_{S_3}, also induces a (hard) breaking of the 2HDM $\mathbb{Z}_2$-symmetry. This breaking is nevertheless tied to the connection between the dark and visible sectors, which inhibits the appearance of other $\mathbb{Z}_2$-symmetry breaking terms in the 2HDM scalar potential, *i.e.* $\lambda_6 |H_1|^2 H_1^\dagger H_2 + \lambda_7 |H_1|^2 H_1^\dagger H_2 + \text{H.c.}$, at tree-level. This is guaranteed because the singlet scalar S does not acquire a VEV and the dark $\mathbb{Z}_2$-symmetry is exact. The implications of this breaking will be further discussed in Section 4.

The parameters μ_{12}^2, λ_5 and λ_{S_3} in Eq. (4.1) can, in general, be complex, so that the resulting Lagrangian would no longer be invariant under CP conjugation. Nevertheless, identifying the physical CP-violating (CPV) phases which intervene in observable processes further requires finding invariant combinations of these parameters under a phase redefinition of the doublets, which should lead to no observable consequence. Under a rephasing of the form $H_j \to e^{-i\theta_j} H_j$, it is possible to redefine $\mu_{12}^2 \to e^{i(\theta_2-\theta_1)}\mu_{12}^2$, $\lambda_5 \to e^{2i(\theta_2-\theta_1)}\lambda_5$, $\lambda_{S_3} \to e^{i(\theta_2-\theta_1)}\lambda_{S_3}$, so that the form of the scalar potential is unchanged. It follows that there are only two independent rephasing-invariant CPV-phases. To build a basis, it is sufficient to pick any two of them, for instance

$$
\begin{aligned}
\delta_1 &\equiv \text{Arg}[\lambda_5^* (\mu_{12}^2)^2], \\
\delta_2 &\equiv \text{Arg}[\lambda_{S_3}^* \mu_{12}^2].
\end{aligned}
\tag{4.2}
$$

Other possible combinations can be expressed in terms of these two (*e.g.* $\delta_3 \equiv \text{Arg}[(\lambda_{S_3})^2 \lambda_5^*]$ can be written as $\delta_3 = \delta_1 - 2\delta_2$). If non-zero, these phases signal the presence of CP violation. Upon EW symmetry breaking, the two Higgs doublets read

$$
H_1 = \frac{1}{\sqrt{2}} \begin{pmatrix} \phi_1^+ \\ v_1 + h_1 + i\eta_1 \end{pmatrix}, \quad H_2 = \frac{1}{\sqrt{2}} \begin{pmatrix} \phi_2^+ \\ v_2 + h_2 + i\eta_2 \end{pmatrix}
\tag{4.3}
$$

with v_j the VEVs of the neutral components of the two Higgs doublets which are, in general, complex $v_j = |v_j| e^{\xi_j}$. For the purpose of this discussion, it is possible

to perform a $SU(2)_L \times U(1)_Y$ transformation so that the VEV of H_1 becomes real $v_1^* = v_1$. While that of H_2 remains, in general, complex $v_2 = |v_2| e^{i\xi}$, with $\xi = \xi_2 - \xi_1$ denoting the relative phase difference between them, which is preserved by this transformation. Under the same rephasing $H_j \to e^{-i\theta_j} H_j$, the VEVs can be trivially redefined as $v_j \to v_j e^{-i\theta_j}$ to absorb this transformation. We may then construct further rephasing invariants involving the VEVs, such as $\mathrm{Arg}[\lambda_5^* \mu_{12}^2 v_1 v_2^*]$. These, however, are not independent of those in Eq. (4.2), but related to them by the minimization conditions of the scalar potential [263]. In particular, for any given complex values of μ_{12}^2 and λ_5 the phase difference between the doublets ξ is set by

$$\mathrm{Im}\left(\mu_{12}^2 e^{i\xi}\right) = \frac{v_1 v_2}{2} \mathrm{Im}\left(\lambda_5 e^{2i\xi}\right) \tag{4.4}$$

For the rest of this work, we will restrict to the case where $\delta_1 = 0$ in Eq. (4.2). This choice guarantees no non-vanishing physical CPV phase can be built without λ_{S_3}, effectively secluding the CP violation to interactions mediated by the dark sector.[1] In the EW minimum, given by $\sqrt{v_1^2 + v_2^2} = v = 246$ GeV, the 2HDM minimization conditions on the real parameters are

$$\mu_1^2 = \mu_{12}^2 t_\beta - \frac{v^2}{2} \frac{\lambda_1 + t_\beta^2 \lambda_{345}}{t_\beta^2 + 1}, \tag{4.5}$$

$$\mu_2^2 = \frac{\mu_{12}^2}{t_\beta} - \frac{v^2}{2} \frac{\lambda_2 t_\beta^2 + \lambda_{345}}{t_\beta^2 + 1}, \tag{4.6}$$

with $t_\beta \equiv \tan\beta = v_2/v_1$ and $\lambda_{345} = \lambda_3 + \lambda_4 + \mathrm{Re}\,(\lambda_5)$. Under the assumption of CP conservation in the 2HDM scalar sector, the physical 2HDM states are two CP-even neutral scalars, h and H_0 with masses $m_{H_0} > m_h$ (we will identify h with the observed 125-GeV Higgs boson), plus a neutral CP-odd scalar A_0 and a charged scalar $H^\pm$. These mass eigenstates are related to the fields in Eq. (4.3) by two different rotations of mixing angles α and β:

$$\begin{aligned} H^\pm &= \cos\beta\, \phi_2^\pm - \sin\beta\, \phi_1^\pm, \qquad A_0 = \cos\beta\, \eta_2 - \sin\beta\, \eta_1, \\ h &= \cos\alpha\, h_2 - \sin\alpha\, h_1, \qquad H = -\sin\alpha\, h_2 - \cos\alpha\, h_1. \end{aligned} \tag{4.7}$$

As previously noted, the 2HDM $\mathbb{Z}_2$-symmetry of the scalar potential in Eq. (4.1) is typically extended to the Yukawa sector so that each fermion type couples exclusively to one of the doublets $H_{1,2}$ and not the other, avoiding tree-level FCNCs. Conventionally, and without the loss of generality, up-type quarks are always coupled to H_2, leading to four different possibilities (*Types*) to couple down-type quarks and leptons to each of the doublets, which are shown in Table 4.1. Explicitly, the

[1] For some regions of the parameter space, Eq. (4.4) can also yield additional solutions leading to spontaneous CPV within the 2HDM sector (see Refs. [263, 264]). Nevertheless, the regions of phenomenological interest for the work on this Chapter are free from this issue.

	Type-I	Type-II	Lepton-specific	Flipped
u_R^i	H_2	H_2	H_2	H_2
d_R^i	H_2	H_1	H_2	H_1
e_R^i	H_2	H_1	H_1	H_2

Table 4.1: The four 2HDM *Types* leading to tree-level flavor conservation. Each SM fermion couples exclusively to one of the doublets. The index $i = 1, 2, 3$ runs over generation space.

Yukawa Lagrangian including the couplings of the fermions to the four scalars of the 2HDM reads (see *e.g.* Ref. [48])

$$\mathcal{L} \supset -\sum_{f=u,d,l} \frac{m_f}{v}\left(y_h^f h\overline{f}f + y_H^f H\overline{f}f + +iy_A^f A\overline{f}\gamma_5 f\right)\Bigg(- \frac{\sqrt{2}}{v}\Big[V_{ud}H^+\overline{u}(y_A^u m_u P_L + y_A^d m_d P_R)d + y_A^\ell m_\ell H^+\overline{\nu_L}\ell_R + H.c.\Big]\Bigg(\tag{4.8}$$

where $P_{R,L}$ are the right/left projection operators for fermions and the couplings y_X^f are presented in Table 4.2 for the Type I and II 2HDM.[1] In terms of the physical masses $m_h, m_{H_0}, m_{H^\pm}, m_{A_0}$, and the parameters $M^2 \equiv \mu_{12}^2(t_\beta + t_\beta^{-1})$, $c_{\beta-\alpha} \equiv \cos(\beta-\alpha)$ and t_β, the 2HDM scalar potential parameters in Eq. (4.1) read (see *e.g.* Ref. [265])

$$\begin{aligned}
\mu_1^2 &= M^2 s_\beta^2 - \frac{1}{2}\left(m_h^2 + (m_{H_0}^2 - m_h^2)c_{\beta-\alpha}\left(c_{\beta-\alpha} + s_{\beta-\alpha}t_\beta\right)\right),\\
\mu_2^2 &= M^2 c_\beta^2 - \frac{1}{2}\left(m_h^2 + (m_{H_0}^2 - m_h^2)c_{\beta-\alpha}\left(c_{\beta-\alpha} - s_{\beta-\alpha}t_\beta^{-1}\right)\right),\\
\lambda_1 v^2 &= m_h^2 - t_\beta^2(M^2 - m_{H_0}^2) + (m_h^2 - m_{H_0}^2)\left[c_{\beta-\alpha}^2(t_\beta^2 - 1) - 2t_\beta s_{\beta-\alpha}c_{\beta-\alpha}\right],\\
\lambda_2 v^2 &= m_h^2 - t_\beta^{-2}(M^2 - m_{H_0}^2) + (m_h^2 - m_{H_0}^2)\left[c_{\beta-\alpha}^2(t_\beta^{-2} - 1) - 2t_\beta^{-1}s_{\beta-\alpha}c_{\beta-\alpha}\right],\\
\lambda_3 v^2 &= m_h^2 + 2m_{H^\pm}^2 - m_{H_0}^2 - M^2 - (m_h^2 - m_{H_0}^2)\left[2c_{\beta-\alpha}^2 + s_{\beta-\alpha}c_{\beta-\alpha}(t_\beta - t_\beta^{-1})\right],\\
\lambda_4 v^2 &= m_{A_0}^2 - 2m_{H^\pm}^2 + M^2,\\
\lambda_5 v^2 &= M^2 - m_{A_0}^2.
\end{aligned} \tag{4.9}$$

Regarding the scalar potential parameters involving the singlet field S, the coupling $\lambda_\beta S^2|\tilde{H}_1|^2$ between S and the linear combination of Higgs doublets $\tilde{H}_1 = c_\beta H_1 + s_\beta H_2$ that develops the EW breaking VEV — *i.e.* working in the *Higgs basis* of the 2HDM [218] — is given by

[1] Our results can be generalized between Types I and II, and Lepton-specific and Flipped respectively, as couplings to leptons will not play a significant role in the phenomenology discussed in this Chapter.

	y_h^u	y_h^d	y_h^ℓ	y_H^u	y_H^d	y_H^ℓ	y_A^u	y_A^d	y_A^ℓ
Type-I	c_α/s_β	c_α/s_β	c_α/s_β	s_α/s_β	s_α/s_β	s_α/s_β	$\cot\beta$	$-\cot\beta$	$-\cot\beta$
Type-II	c_α/s_β	$-s_\alpha/c_\beta$	$-s_\alpha/c_\beta$	s_α/s_β	c_α/c_β	c_α/c_β	$\cot\beta$	$\tan\beta$	$\tan\beta$

Table 4.2: Fermion Yukawa couplings for the Type I and II 2HDM as defined in Eq.(4.8), where c and s have been used as short-hand notation for sin and cos respectively.

$$\lambda_\beta = \lambda_{S_1} c_\beta^2 + \lambda_{S_2} s_\beta^2 + \lambda_{S_3}^R s_\beta c_\beta = \frac{\lambda_{S_1} + \lambda_{S_3}^R t_\beta + \lambda_{S_2} t_\beta^2}{1 + t_\beta^2}, \tag{4.10}$$

with $\lambda_{S_3}^R \equiv \mathrm{Re}(\lambda_{S_3})$. In terms of λ_β and the singlet scalar mass m_s, the singlet squared-mass parameter in Eq.(4.1) reads

$$\mu_S^2 = m_s^2 - \lambda_\beta v^2. \tag{4.11}$$

The couplings between the singlet scalar S and the neutral 2HDM state h, H_0 and A_0 are respectively given by

$$\begin{aligned} \lambda_{S^2 h}/v &= s_{\beta-\alpha}\lambda_\beta + c_{\beta-\alpha}\left[t_\beta(\lambda_{S_2} - \lambda_\beta) + \lambda_{S_3}^R/2\right] \\ \lambda_{S^2 H_0}/v &= c_{\beta-\alpha}\lambda_\beta - s_{\beta-\alpha}\left[t_\beta(\lambda_{S_2} - \lambda_\beta) + \lambda_{S_3}^R/2\right] \\ \lambda_{S^2 A_0}/v &= \lambda_{S_3}^I/2, \end{aligned} \tag{4.12}$$

with $\lambda_{S_3}^I \equiv \mathrm{Im}(\lambda_{S_3})$. The existence of non-vanishing couplings of the dark scalar S with both A_0 and h, H_0 is a sign of CP violation in the interactions between the dark sector and the 2HDM states, corresponding to $\delta_2 \neq 0$ in Eq.(4.2). Yet, for $\delta_1 = 0$, it can be seen that the pure 2HDM sector of the theory is CP-conserving at tree-level, as the only source of bosonic CP violation involves the interactions with the dark sector. It is nevertheless expected that these very interactions source CP violation among the 2HDM states at 1-loop order. These 1-loop corrections would yield a small misalignment between the neutral states h, H_0 and A_0, with definite CP properties, and the mass eigenstates (physical spectrum) of the theory. A proper discussion of these effects would require the 1-loop renormalization of the scalar sector of the theory, which we will pursue in the future. In the rest of this Chapter, we consider the CP eigenstates h, H_0 and A_0 to be physical states and perform our analysis at tree-level. Nevertheless, we will comment briefly on the phenomenological impact of such loop-suppressed effects in Section 4.

3 Transient Enhancement of CP Violation in the Early Universe

In the present scenario, the CP violating phenomenology has been effectively secluded at tree-level to the interactions between the dark and visible sectors, only manifesting itself at 1-loop in the scalar spectrum and other CPV phenomena such as EDM. Nevertheless, as briefly discussed in the introduction, it is possible to enhance the presence of CP violation in the early Universe by sourcing additional spontaneous CP breaking through a non-vanishing VEV for the singlet field S, enabling successful baryogenesis (see Ref. [266] for related work). Such a transient enhancement of CP violation would end after the EW phase transition, so that expected signatures in low energy probes (such as EDM experiments) could be well-below current experimental sensitivities. In this Section we explore the viable regions of the parameter space leading to this transient CP violation enhancement.

3.1 Tree-Level Requirements

First, in order to guarantee a realistic scenario, we need to consider the theoretical constraints stemming from unitarity, perturbativity and stability of the scalar potential in Eq. (4.1) (see *e.g.* Ref. [260] for an analogous analysis of the 2HDM). Tree-level boundedness from below of a potential of the form $\Lambda_{ab}\phi_a^2\phi_b^2$ requires the matrix of quartic couplings λ_{ab} to be *copositive*, that is, positive semidefinite when acting on non-negative vectors [267]. To this end, we can parametrize the field bilinears appearing in Eq. (4.1) as

$$|H_1|^2 = h_1^2, \qquad |H_2|^2 = h_2^2, \qquad H_1^\dagger H_2 = \rho h_1 h_2 e^{i\xi}, \qquad S^2 = s^2, \tag{4.13}$$

where ξ represents again the relative phase between the doublets and the parameter ρ is bounded by $|\rho| \leq 1$ as implied by the Cauchy-inequality $0 \leq |H_1^\dagger H_2| \leq |H_1||H_2|$. With this parametrization, the scalar potential in Eq. (4.1) is cast into the form

$$\begin{aligned} V_\lambda = &\frac{\lambda_1}{2}h_1^4 + \frac{\lambda_2}{2}h_2^4 + \frac{\lambda_S}{4}s^4 + \lambda_{S1}h_1^2 s^2 + \lambda_{S2}h_2^2 s^2 \\ &+ \lambda_3 h_1^2 h_2^2 + \lambda_4 h_1^2 h_2^2 \rho^2 + |\lambda_5| h_1^2 h_2^2 \rho^2 \cos(2\xi + \mathrm{Arg}[\lambda_5]). \end{aligned} \tag{4.14}$$

Where quadratic terms have been omitted, as their contribution is subleading in the large field limit (which is the only relevant region to the boundedness of a polynomial potential).[1] Additionally, we have neglected terms involving λ_{S3}, which is considered in the following to be hierarchically smaller than the rest of the quartic

[1] Quadratic terms could be important if $V_\lambda \to 0$ for a given direction in field space. We will thus demand that the matrix of quartic couplings be *strictly* coposite (*i.e.* positive definite rather than semidefinite over non-negative vectors), which forbids this possibility.

couplings. The motivation for this choice is two-fold: on the one hand previous work has shown baryogenesis requires only a small amount of CPV (linked to the imaginary part of λ_{S3}, see Eq. (4.2)) in similar setups [266]; on the other, a small λ_{S3} will further suppress potentially dangerous CP and $\mathbb{Z}_2$ breaking effects in the 2HDM sector of the theory.[1]

To find the set of necessary conditions for the boundedness of this potential, we must minimize with respect to the free parameters ρ and ξ in the large field limit. The minimization with respect to ξ trivially leads to $\cos(2\xi + \text{Arg}[\lambda_5]) = -1$. Along this direction, the matrix of quartic couplings in the (h_1^2, h_1^2, s^2) basis reads

$$\Lambda = \frac{1}{2}\begin{pmatrix} \lambda_1 & \lambda_3 + \rho^2(\lambda_4 - |\lambda_5|) & \lambda_{S1} \\ \lambda_3 + \rho^2(\lambda_4 - |\lambda_5|) & \lambda_2 & \lambda_{S2} \\ \lambda_{S1} & \lambda_{S2} & \lambda_S \end{pmatrix}. \tag{4.15}$$

The minimization of ρ depends on whether the combination $\lambda_4 - |\lambda_5|$ is positive or negative, resulting in $\rho^2 = 0$ or 1 respectively. Applying the strict copositivity criteria [267] to both cases yields

$$\begin{aligned} &\lambda_1 > 0, \quad \lambda_2 > 0, \quad \lambda_S > 0, \quad \sqrt{\lambda_1\lambda_2} + \lambda_3 > 0, \quad \sqrt{\lambda_1\lambda_2} + \lambda_3 + \lambda_4 - |\lambda_5| > 0, \\ &2\lambda_{S1} + \sqrt{2\lambda_1\lambda_S} > 0, \quad 2\lambda_{S2} + \sqrt{2\lambda_2\lambda_S} > 0, \\ &\lambda_{S1}\sqrt{2\lambda_2} + \lambda_{S2}\sqrt{2\lambda_1} + \lambda_3\sqrt{\lambda_S} + \sqrt{\lambda_1\lambda_2\lambda_S} + \\ &\quad + \sqrt{\left(\sqrt{\lambda_1\lambda_2} + \lambda_3\right)\left(2\lambda_{S1} + \sqrt{2\lambda_1\lambda_S}\right)\left(2\lambda_{S2} + \sqrt{2\lambda_2\lambda_S}\right)} > 0, \\ &\lambda_{S1}\sqrt{2\lambda_2} + \lambda_{S2}\sqrt{2\lambda_1} + (\lambda_3 + \lambda_4 - |\lambda_5|)\sqrt{\lambda_S} + \sqrt{\lambda_1\lambda_2\lambda_S} + \\ &\quad + \sqrt{\left(\sqrt{\lambda_1\lambda_2} + \lambda_3 + \lambda_4 - |\lambda_5|\right)\left(2\lambda_{S1} + \sqrt{2\lambda_1\lambda_S}\right)\left(2\lambda_{S2} + \sqrt{2\lambda_2\lambda_S}\right)} > 0. \end{aligned} \tag{4.16}$$

The first set are the well known 2HDM vacuum stability conditions [48], but the existence of the singlet yields further non-trivial constraints. Additionally, in order to ensure the absolute tree-level stability of the EW minimum, preventing the existence of a "panic vacuum" [268, 269] (*i.e.* a second deeper minimum beyond the one which we currently inhabit), the parameters of the 2HDM must satisfy the condition

$$\left[\left(\frac{m_{H^\pm}^2}{v^2} + \frac{\lambda_4}{2}\right)^2 - \frac{|\lambda_5|^2}{4}\right]\left[\frac{m_{H^\pm}^2}{v^2} + \frac{\sqrt{\lambda_1\lambda_2} - \lambda_3}{2}\right] > 0, \tag{4.17}$$

[1] Additionally, λ_{S3} would obscure the analytical computation of the boundedness conditions, as it would both require an enlargement of the monomial basis and complicate the minimization over the spare degrees of freedom in the large field limit (see discussion below).

which directly translates into [260]

$$\Omega \equiv \text{Sign}\left(\Omega^2\right)\sqrt{|\Omega^2|} \leq m_{H_0}, \tag{4.18}$$

with $\Omega^2 \equiv m_{H_0}^2 - \mu_{12}^2(t_\beta + t_\beta^{-1})$. Finally, the unitarity of the scattering matrix also imposes upper bounds on various combinations of the quartic couplings λ_i (see Refs. [270, 271] for a tree-level study of the 2HDM and Ref. [272] for a more recent one-loop analysis leading to slightly stronger bounds). Similar (although generically less stringent) bounds on λ_i may be obtained from perturbativity arguments. We take here a conservative approach and demand that every quartic coupling is smaller than $|\lambda_i| \leq 2\pi$, ensuing both unitarity and perturbativity. The different constraints are presented in Figure 4.1, which shows the resulting bounds on the $(c_{\beta-\alpha}, \Omega)$ plane for a set of (m_{A_0}, t_β) parameter choices and a benchmark point

$$m_{H_0} = m_{H^\pm} = 400\,\text{GeV}, \quad \lambda_\beta = 1, \quad \lambda_{S2} = 1.5\lambda_\beta, \quad \lambda_{S3} \simeq 0, \quad \lambda_S = 1. \tag{4.19}$$

A transient period of CPV enhancement further requires a negative quadratic term for the singlet at tree-level $\mu_S^2 < 0$, so that S can develop a non-vanishing VEV in the early Universe.[1] By virtue of Eq. (4.11), this requirement translates into

$$m_s^2 < \lambda_\beta v^2. \tag{4.20}$$

Further requiring that the tree-level EW minimum be the global minimum of the scalar potential leads to

$$V_{EW} = -\frac{v^2}{8}\left[m_h^2 + c_{\beta-\alpha}^2\left(m_{H_0}^2 - m_h^2\right)\right] < -\frac{1}{4\lambda_S}\left(\lambda_\beta v^2 - m_s^2\right)^2 < 0, \tag{4.21}$$

with V_{EW} the energy of the EW vacuum. Combining Eq. (4.20) and Eq. (4.21) we get an allowed range for the DM mass m_s

$$\lambda_\beta v^2 - 2\sqrt{\lambda_S\,|V_{EW}|} < m_s^2 < \lambda_\beta v^2. \tag{4.22}$$

We note that while the minimum and maximum allowed values for m_s^2 depend on λ_β, the range itself $\delta m_s^2 \equiv m_{s,\max}^2 - m_{s,\min}^2 = 2\sqrt{\lambda_S\,|V_{EW}|}$ does not. Increasing λ_S widens the viable range for m_s.

3.2 Finite-Temperature Effective Potential

Our demands include a non-trivial thermal history, where the Universe would have started from a phase of restored EW symmetry at high temperatures $T \gg v$ to

[1] The leading thermal corrections to this quantity will be positive as we shall discuss below, so that a singlet phase could not exist otherwise.

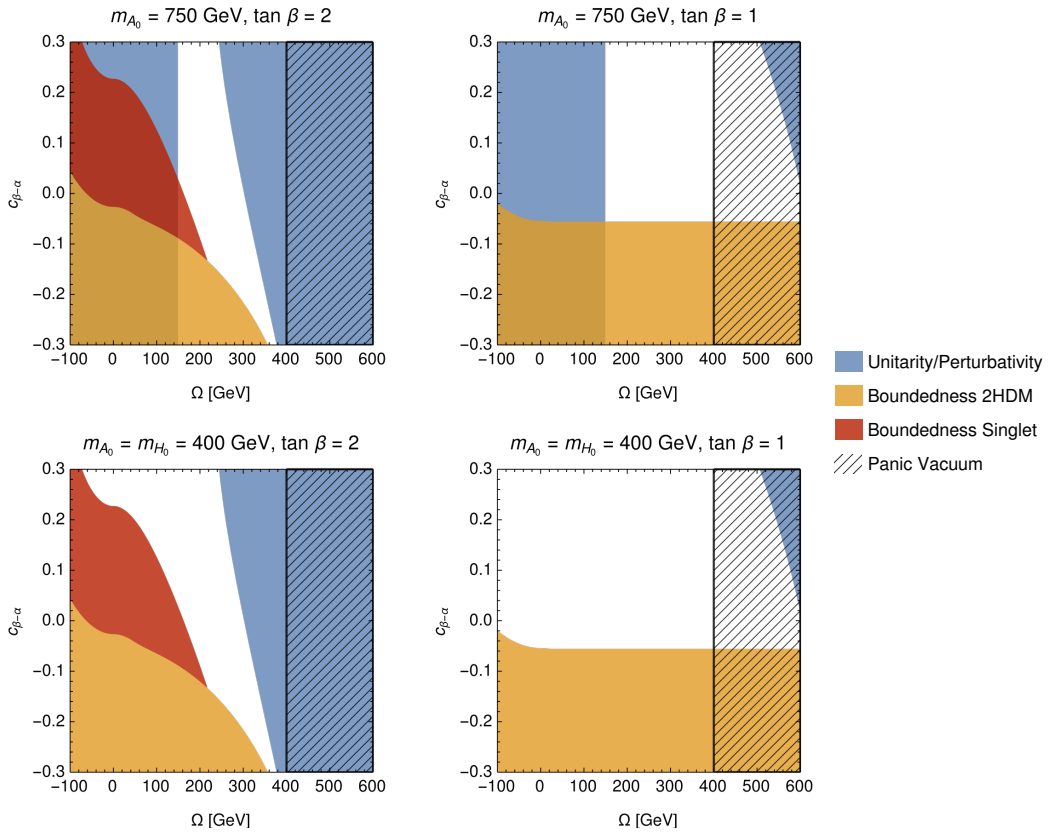

Figure 4.1: $(c_{\beta-\alpha}, \Omega)$-plane for $t_\beta = 2, 1$ (left-to-right) and $m_A = 750, 400$ GeV (top-to-bottom) for the benchmark point shown in Eq. (4.19). Colored and hatched regions show the areas excluded by each of the constraints discussed in the main text. Boundedness constraints have been split for illustrative purposes: **Boundedness 2HDM** labels the region excluded by the 2HDM vacuum stability conditions — first line of Eq. (3.1), whereas **Boundedness Singlet** shows the impact of considering the full set of inequalities resulting from the addition of the singlet — the whole Eq. (3.1).

subsequently generate a VEV for the singlet S via a second order phase transition, before finally tunneling into the EW vacuum through a (strong) first-order phase transition (FOPT). The following Sections aim to explore the regions of the parameter space leading to this two-step phase transition.

To study the evolution of vacua in the early Universe, we have to make use of field theory at finite temperature. Conventional QFT methods such as those employed so far on this thesis, while suitable to describe observables measured in approximately empty-space (*e.g.* particle interactions at colliders), are based on hypotheses which cannot be easily formulated on the highly dense matter and radiation environments characteristic of the early stages of our Universe. Instead, it is convenient to replace them by other approaches, which, building on thermodynamics, treat this background state as a thermal bath. This is the basis of field theory at finite temperature, and through its methods, it is possible to compute the finite-temperature effective potential. A complete derivation of the latter is beyond the scope of this thesis (see *e.g.* Ref. [273] for a review). Instead, we will be focusing on the impact of the leading thermal corrections to the tree-level potential of Eq. (4.1), which will nevertheless showcase all of the relevant phenomenology to our discussion. These one-loop thermal corrections to the scalar potential are found to be

$$V_T = \frac{T^4}{2\pi^2}\sum_i n_i \int_0^\infty x^2 \log\left(1 \mp e^{-\sqrt{x^2+m_i^2(\varphi)/T^2}}\right) dx, \tag{4.23}$$

where the sum is carried over bosonic ($i = B$) and fermionic ($i = F$) degrees of freedom (d.o.f.) with field-dependent masses $m_i^2(\varphi)$ in the background field φ. The sign of the exponential is negative (positive) for bosons (fermions), and n_i denotes the number of d.o.f. of a given field: 1 for each neutral scalar, 2 for each charged scalar, 3 for the Z boson, 6 for the W boson and -12 for the top quark (the contribution from the rest of the fields is subleading and can be safely neglected). In the limit where $m_i^2(\varphi)/T^2 \ll 1$, Eq. (4.23) admits the following high-temperature expansion

$$\begin{aligned} V_T^{\rm HT} \simeq & T^4 \sum_B n_B \left[-\frac{\pi^2}{90} + \frac{1}{24}\frac{m_B^2}{T^2} - \frac{1}{12\pi}\left(\frac{m_B^2}{T^2}\right)^{\frac{3}{2}} - \frac{1}{64\pi^2}\frac{m_B^4}{T^4}\log\left(\frac{m_B^2}{c_B T^2}\right)\right] \\ & + T^4 \sum_F n_F \left[\left(\frac{7\pi^2}{720} + \frac{1}{48}\frac{m_F^2}{T^2} + \frac{1}{64\pi^2}\frac{m_F^4}{T^4}\log\left(\frac{m_F^2}{c_F T^2}\right)\right] \right. \end{aligned} \tag{4.24}$$

with $c_F = \pi^2 \exp(\frac{3}{2} - 2\gamma)$ and $c_B = 16 c_F$. In the so-called *Hartree approximation* [274], only the leading, $\mathcal{O}(T^2)$ pieces of $V_T^{\rm HT}$ are retained, such that the finite-temperature corrections to the tree-level scalar potential amount to modifications of the bare mass terms in the potential. This approach is particularly convenient to study the vacuum evolution of multi-scalar models, as it allows to gain an analytical understanding of the symmetry-breaking patterns throughout their thermal history

(see *e.g.* Refs.[257,275]). For this reason, we will restrict to this approximation for the rest of this Chapter.

For a transient period of CPV enhancement to occur in the early Universe, we demand that the VEVs of both Higgs doublets $H_{1,2}$ and the singlet field S vanish at very high temperatures. Then, as temperature decreases during the radiation-dominated era, the S-field direction should be destabilized from the origin of field-space before that of the Higgs doublets. This will lead to a two-step phase transition, proceeding first by spontaneous CP-violation via $\langle S^2\rangle \neq 0$ and a subsequent breaking of the EW symmetry by the VEVs of the Higgs doublets (with $\langle S^2\rangle \to 0$ in this second step). We then have to consider contributions to V_T from all relevant d.o.f. in the singlet scalar background field s and in the background fields of the four neutral components of the Higgs doublets, which we denote h_1, h_2 (real parts, with some abuse of notation), and a_1, a_2 (imaginary parts). The contributions to V_T stemming from SM fermions (the top quark) and EW gauge bosons read

$$\begin{aligned}\sum_F n_F m_F^2 &= \frac{12m_t^2}{v^2}(1+t_\beta^{-2})(h_2^2+a_2^2)\\ \sum_{\text{gauge}} n_B m_B^2 &= \frac{6m_W^2+3m_Z^2}{v^2}(h_1^2+a_1^2+h_2^2+a_2^2).\end{aligned} \tag{4.25}$$

where the overall factors $T^2/48$ for fermions and $T^2/24$ for bosons have been omitted. The contributions to V_T from the scalars in the *Hartree approximation* can be obtained from the trace of the field-dependent scalar mass matrix. Working on a basis where both λ_5 and μ_{12}^2 are real,[1] the diagonal entries of the scalar mass matrix read

$$\begin{aligned}M_{h_1h_1} &= \mu_1^2+\frac{\lambda_1}{2}(3h_1^2+a_1^2)+\frac{\lambda_3+\lambda_4}{2}(h_2^2+a_2^2)+\frac{\lambda_5}{2}(h_2^2-a_2^2)+\lambda_{S_1}s^2,\\ M_{h_2h_2} &= \mu_2^2+\frac{\lambda_2}{2}(3h_2^2+a_2^2)+\frac{\lambda_3+\lambda_4}{2}(h_1^2+a_1^2)+\frac{\lambda_5}{2}(h_1^2-a_1^2)+\lambda_{S_2}s^2,\\ M_{\eta_1\eta_1} &= \mu_1^2+\frac{\lambda_1}{2}(h_1^2+3a_1^2)+\frac{\lambda_3+\lambda_4}{2}(h_2^2+a_2^2)-\frac{\lambda_5}{2}(h_2^2-a_2^2)+\lambda_{S_1}s^2,\\ M_{\eta_2\eta_2} &= \mu_2^2+\frac{\lambda_2}{2}(h_2^2+3a_2^2)+\frac{\lambda_3+\lambda_4}{2}(h_1^2+a_1^2)-\frac{\lambda_5}{2}(h_1^2-a_1^2)+\lambda_{S_2}s^2,\\ M_{SS} &= \mu_S^2+3\lambda_S s^2+\lambda_{S_1}(h_1^2+a_1^2)+\lambda_{S_2}(h_2^2+a_2^2)+\lambda_{S_3}^R(h_1h_2+a_1a_2)\\ &\quad +\lambda_{S_3}^I(h_2a_1-h_1a_2),\\ M_{\phi_1^+\phi_1^-} &= 2\mu_1^2+\lambda_1(h_1^2+a_1^2)+\lambda_3(h_2^2+a_2^2)+2\lambda_{S_1}s^2,\\ M_{\phi_2^+\phi_2^-} &= 2\mu_2^2+\lambda_2(h_2^2+a_2^2)+\lambda_3(h_1^2+a_1^2)+2\lambda_{S_2}s^2.\end{aligned} \tag{4.26}$$

Dropping field-independent terms, which only provide an overall energy shift to

[1] The existence of such basis is guaranteed by $\delta_1 = 0$, *c.f.* Eq. (4.2).

the potential, and omitting again a $T^2/24$ factor, the contribution to V_T can be evaluated as

$$\sum_{\text{scalar}} n_B m_B^2 = (3\lambda_1 + 2\lambda_3 + \lambda_4 + \lambda_{S_1})(h_1^2 + a_1^2) + (3\lambda_2 + 2\lambda_3 + \lambda_4 + \lambda_{S_2})(h_2^2 + a_2^2) + (3\lambda_S + 4\lambda_{S_1} + 4\lambda_{S_2})s^2 + \lambda_{S_3}^R(h_1 h_2 + a_1 a_2) + \lambda_{S_3}^I(h_2 a_1 - h_1 a_2). \tag{4.27}$$

Altogether, the finite-T effective potential in this approximation, corresponding to the tree-level scalar potential from Eq. (4.1) together with the $\mathcal{O}(T^2)$ terms from V_T, reads

$$\begin{aligned} V_T^{\text{eff}} &= \bar{\mu}_1^2(T)(h_1^2 + a_1^2) + \bar{\mu}_2^2(T)(h_2^2 + a_2^2) + \bar{\mu}_S^2(T)s^2 - \bar{\mu}_{12}^2(T)(h_1 h_2 + a_1 a_2) \\ &+ \bar{\mu}_{\text{CP}}^2(T)(h_2 a_1 - h_1 a_2) + \frac{\lambda_1}{8}(h_1^2 + a_1^2)^2 + \frac{\lambda_2}{8}(h_2^2 + a_2^2)^2 + \frac{\lambda_S}{4}s^4 \\ &+ \frac{\lambda_3 + \lambda_4}{4}(h_1^2 + a_1^2)(h_2^2 + a_2^2) + \frac{\lambda_{S_1}}{2}s^2(h_1^2 + a_1^2) + \frac{\lambda_{S_2}}{2}s^2(h_2^2 + a_2^2) \\ &+ \frac{\lambda_5}{4}\left[h_1(h_2 - a_2) + a_1(h_2 + a_2)\right]\left[h_1(h_2 a_2) + a_1(a_2 - h_2)\right] \\ &+ \frac{\lambda_{S_3}^R}{2}s^2(h_1 h_2 + a_1 a_2) + \frac{\lambda_{S_3}^I}{2}s^2(h_2 a_1 - h_1 a_2), \end{aligned} \tag{4.28}$$

with

$$\begin{aligned} \bar{\mu}_1^2(T) &= \frac{\mu_1^2}{2} + \frac{T^2}{24}\left(3\lambda_1 + 2\lambda_3 + \lambda_4 + \lambda_{S_1} + \frac{6m_W^2 + 3m_Z^2}{v^2}\right), \\ \bar{\mu}_2^2(T) &= \frac{\mu_2^2}{2} + \frac{T^2}{24}\left(3\lambda_2 + 2\lambda_3 + \lambda_4 + \lambda_{S_2} + \frac{6m_W^2 + 3m_Z^2}{v^2} + \frac{6m_t^2}{v^2}(1 + t_\beta^{-2})\right), \\ \bar{\mu}_S^2(T) &= \frac{\mu_S^2}{2} + \frac{T^2}{24}\left(3\lambda_S + 4\lambda_{S_1} + 4\lambda_{S_2}\right), \\ \bar{\mu}_{12}^2(T) &= \mu_{12}^2 - \frac{T^2}{24}\lambda_{S_3}^R \\ \bar{\mu}_{\text{CP}}^2(T) &= \frac{T^2}{24}\lambda_{S_3}^I. \end{aligned} \tag{4.29}$$

At this point it is worth stressing that a combination of the background fields a_1 and a_2 can be rotated away in the tree-level potential of Eq. (4.1) by an equal-phase redefinition of both Higgs doublets $H_{1,2}$ (leaving all of its parameters unchanged). This is precisely the combination that corresponds to the neutral Goldstone boson of the SM. It is also possible to reduce the number of dynamical background fields from 5 to 4 in the *Hartree approximation* for V_T, since the finite-temperature contributions do not break the symmetry that allows to perform the corresponding

field redefinition in Eq. (4.1) (*i.e.* the SM photon remains massless at finite-T in this approximation).[1] Then, without the loss of generality we can set $a_1 = 0$ in Eq. (4.28).

3.3 Thermal History Requirements

Having computed the effective thermal potential (in the *Hartree approximation*), we are finally in position to discuss the constraints imposed by the prescribed thermal history. The requirement that both, the EW symmetry is restored at high temperatures and the CPV enhancement is transient, demands that the origin in field-space be a minimum for $T \to \infty$. The 5×5 Hessian of this potential is block diagonal at the origin, with a diagonal entry for the singlet and a 4×4 block for the neutral Higgs field directions. This requirement can then be cast into two separate constraints: the diagonal entry for the singlet (its quadratic term) must be positive $\bar{\mu}_S^2(T) = \mu_S^2/2 + C_S T^2 > 0$ for $T \to \infty$, whereas the thermal mass matrix for the neutral Higgs field directions

$$
\begin{aligned}
M_H(T) &= \begin{pmatrix} 2\bar{\mu}_1^2(T) & -\bar{\mu}_{12}^2(T) & 0 & -\bar{\mu}_{\rm CP}^2(T) \\ -\bar{\mu}_{12}^2(T) & 2\bar{\mu}_2^2(T) & \bar{\mu}_{\rm CP}^2(T) & 0 \\ 0 & \bar{\mu}_{\rm CP}^2(T) & 2\bar{\mu}_1^2(T) & -\bar{\mu}_{12}^2(T) \\ \bar{\mu}_{\rm CP}^2(T) & 0 & -\bar{\mu}_{12}^2(T) & 2\bar{\mu}_2^2(T) \end{pmatrix} \\
&= \begin{pmatrix} \mu_1^2 + C_1 T^2 & -\mu_{12}^2 + \frac{T^2}{24}\lambda_{S_3}^R & 0 & -\frac{T^2}{24}\lambda_{S_3}^I \\ -\mu_{12}^2 + \frac{T^2}{24}\lambda_{S_3}^R & \mu_2^2 + C_2 T^2 & \frac{T^2}{24}\lambda_{S_3}^I & 0 \\ 0 & \frac{T^2}{24}\lambda_{S_3}^I & \mu_1^2 + C_1 T^2 & -\mu_{12}^2 + \frac{T^2}{24}\lambda_{S_3}^R \\ -\frac{T^2}{24}\lambda_{S_3}^I & 0 & -\mu_{12}^2 + \frac{T^2}{24}\lambda_{S_3}^R & \mu_2^2 + C_2 T^2 \end{pmatrix},
\end{aligned}
\tag{4.30}
$$

should have only positive eigenvalues in this limit. The coefficients C_1, C_2 and C_S, which can be read directly from Eq. (4.29), need then to be positive.

In addition, destabilizing the origin of field-space along the singlet field direction prior to EW symmetry breaking requires that $\bar{\mu}_S^2(T)$ becomes negative at a temperature T_S higher than the temperature T_H at which the Higgs-field-directions are destabilized, which happens when $M_H(T)$ develops its first negative eigenvalue, or equivalently, when its determinant first goes negative $\mathrm{Det}[M_H(T)] < 0$. These temperatures read

[1] Going beyond this approximation for the finite-temperature potential V_T, the longitudinal component of the photon can develop a thermal mass, and thus it is no longer possible to reduce the number of dynamical background fields from 5 to 4.

$$T_S^2 = \frac{-12\mu_S^2}{3\lambda_S + 4(\lambda_{S_1} + \lambda_{S_2})},$$
$$T_H^2 = -\frac{\mu_1^2 C_2 + \mu_2^2 C_1 + \lambda_{S_3}^R \mu_{12}^2/12}{2C_1C_2 - |\lambda_{S_3}|^2/288} + \frac{\sqrt{[\mu_1^2 C_2 + \mu_2^2 C_1 + \lambda_{S_3}^R \mu_{12}^2/12]^2 - 2(\mu_1^2\mu_2^2 - \mu_{12}^4)(2C_1C_2 - |\lambda_{S_3}|^2/288)}}{2C_1C_2 - |\lambda_{S_3}|^2/288}, \tag{4.31}$$

with $|\lambda_{S_3}|^2 = (\lambda_{S_3}^R)^2 + (\lambda_{S_3}^I)^2$. Our requirement can then be stated as $T_H < T_S$, ensuing that the singlet phase is born earlier than the EW phase.

3.4 Regions of Transient CP Violation Enhancement

We now show the regions of parameter space where the transient CPV enhancement occurs. The constraints discussed in the previous Sections are presented in Figures 4.2 and 4.3, which show the resulting bounds on the (m_s, λ_β) plane along the regions where the two-step phase transition is possible. They showcase the effect of varying (λ_S, t_β) and $(\lambda_S, \lambda_{S2})$ respectively. For definiteness, we also set

$$m_{H_0} = m_{H^\pm} = 400\,\text{GeV}, \quad \Omega = 200\,\text{GeV}, \quad c_{\beta-\alpha} = 0, \tag{4.32}$$

so that these figures are compatible with the tree-level constraints discussed in Figure 4.1, with the red hatching showing the regions where the potential becomes unbounded.

4 Outlook

To conclude this Chapter, we discuss the outlook of the results presented on the previous Sections, including preliminary work and ongoing efforts to study the phenomenology of this realization. While Figures 4.2 and 4.3 show the regions of the parameter space with a thermal history leading to the EW vacuum after a period of transient CPV enhancement (*i.e.* after the singlet phase), it is important to note they do not guarantee the absence of more phases in between them (*e.g.* a mixed one) nor the strong first-order EW phase transition required for successful baryogenesis. Nevertheless, it is still possible to derive semi-analytical constraints resulting from demanding both a two-step phase transition (as opposed to more complicated thermal histories) and a barrier between the singlet and EW minima. The analysis follows that shown in the previous Section, only that now, instead of evaluating the Hessian at the origin (*c.f.* Eq. (4.30)), it is evaluated at both the singlet and EW phases. Just as before, the zeros of its determinant indicate the change of character of its extrema and thus provide information on the evolution of its phases. If the

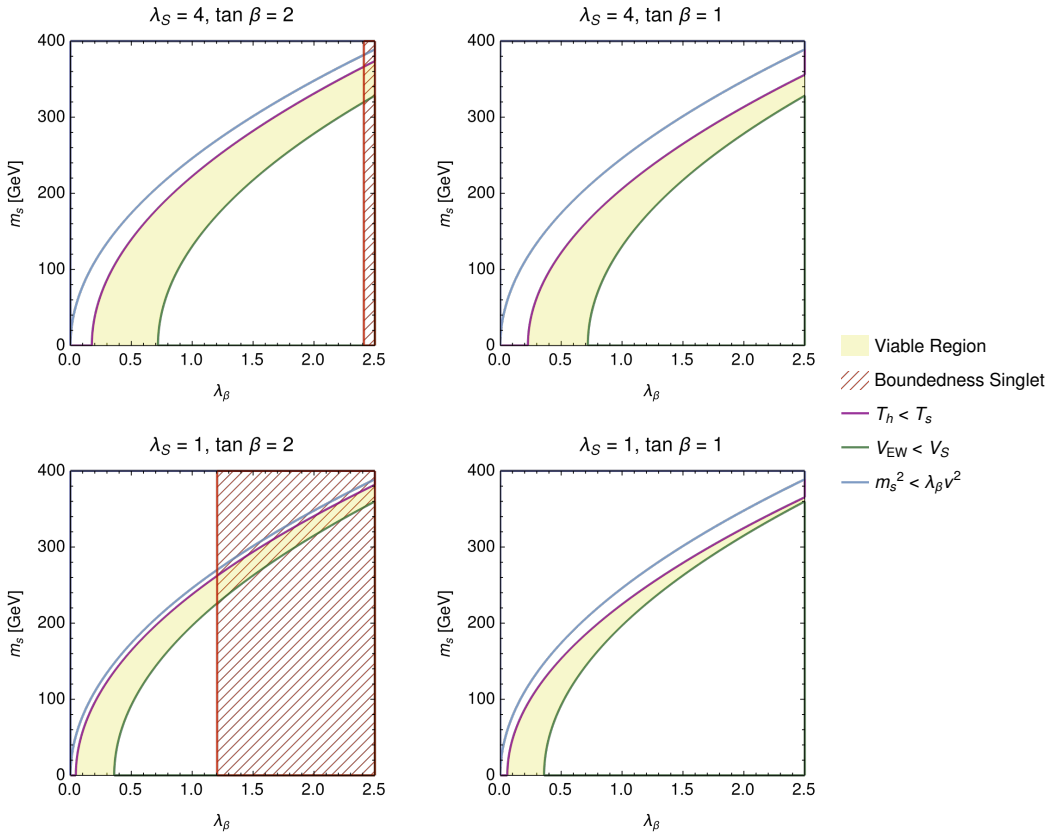

Figure 4.2: (m_s, λ_β)-plane for $t_\beta = 2, 1$ (left-to-right) and $\lambda_S = 4, 1$ (top-to-bottom) for the benchmark point shown in Eq. (4.32) with $\lambda_{S2} = 1.5\,\lambda_\beta$. Colored lines and hatched regions delimit the areas excluded by each of the constraints discussed in the main text.

singlet and EW phases coexist for a given range of temperatures, a potential barrier between them is guaranteed. Of course, if the singlet minimum persists all the way down to zero temperature, the existence of a barrier is not enough to guarantee a FOPT. In that case, one should also check that the Universe is not trapped on the singlet phase and can actually tunnel in cosmic timescales from the singlet to the EW vacuum. The results of this analysis are preliminary and have thus been omitted from this thesis, but they suggest the existence of large regions of parameter space that can successfully accommodate this thermal history. Finally, a realistic assessment of baryogenesis should also include the computation of the resulting baryon abundance, which will be tied to the size of δ_2.

As previously noted, the singlet scalar S is also a viable DM candidate due to the exact dark $\mathbb{Z}_2$-symmetry. Nevertheless, it is important to check whether the model can accommodate the production of the observed DM relic abundance in the early Universe and the desired thermal history simultaneously. Given the regions of the parameter space being considered for the latter, this production would

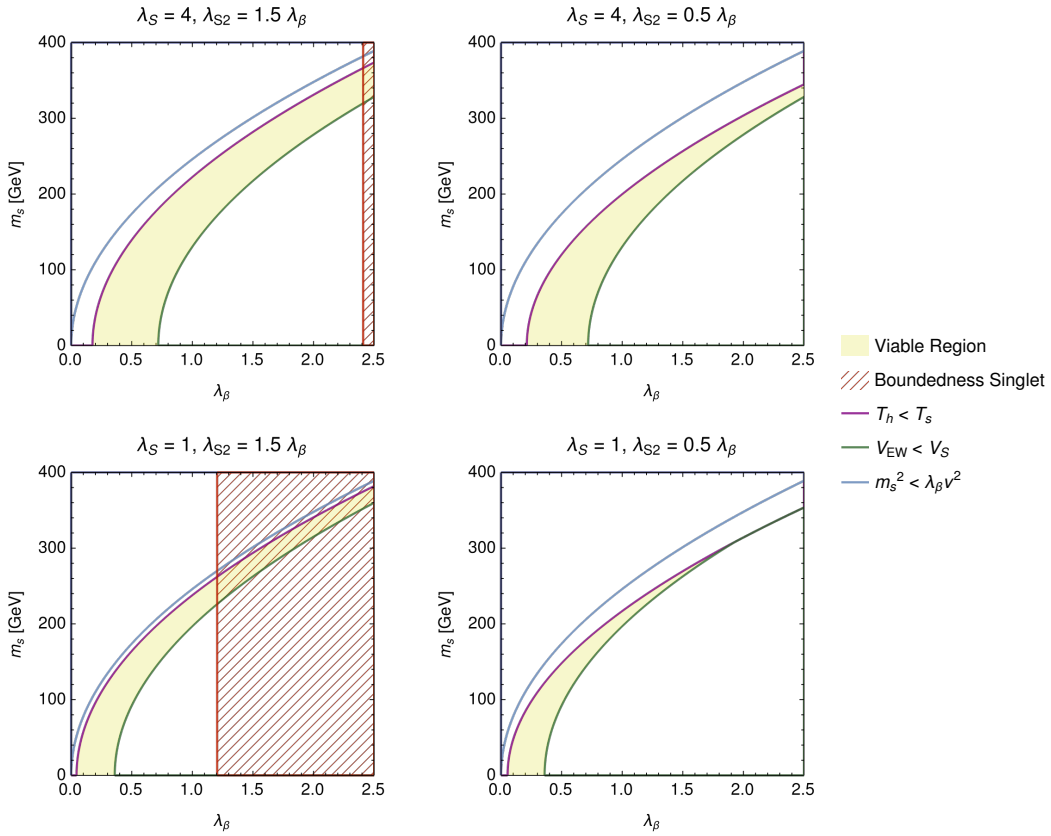

Figure 4.3: (m_s, λ_β)-plane for $\lambda_{S2} = 1.5\lambda_\beta, 0.5\lambda_\beta$ (left-to-right) and $\lambda_S = 4, 1$ (top-to-bottom) for the benchmark point shown in Eq. (4.32) with $t_\beta = 2$. Colored lines and hatched regions delimit the areas excluded by each of the constraints discussed in the main text (note the left column of each Figure is the same).

be mediated by thermal freeze-out. On the other hand, if S is the DM, we must also require agreement with the bounds on the DM-nucleon scattering cross section from DM direct detection experiments. At tree-level, DM-nucleon scattering processes occur via h, H_0, A_0 single exchange, with the size of the corresponding cross section controlled by the couplings in Eq. (4.12). Both the λ_{S^2h} and $\lambda_{S^2H_0}$ couplings contribute to the spin-independent DM-nucleon scattering cross section $\sigma^N_{\rm SI}$ (via h and H_0 exchange, respectively), whereas $\lambda_{S^2A_0}$ only contributes at tree-level to the spin-dependent [276] cross section $\sigma^N_{\rm SD}$, for which DM direct detection experimental bounds are much weaker [277]. At 1-loop, $\lambda_{S^2A_0}$ will contribute to the spin-independent cross section via double A_0 exchange (see *e.g.* Ref. [278]), yet this loop-suppressed contribution may be safely neglected for our analysis. Preliminary results show that XENONnT bounds [279] place relatively stringent constraints on the parameter space of the 2HDM+S^2 discussed in this work, however, it is still possible to find regions that yield the correct thermal history.

On the other hand, the LHC also probes viable regions of the parameter space.

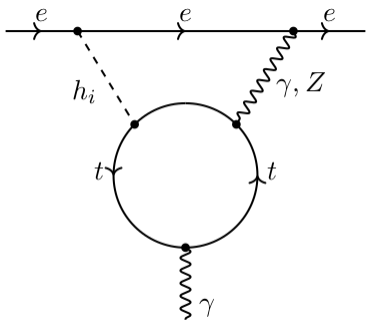

Figure 4.4: 2-loop "Barr-Zee" contribution to the electron EDM.

In particular, Higgs signal strengths constrain the couplings of the 125 GeV Higgs boson, which, in the context of the 2HDM, translates on Type dependent bounds on the $(c_{\beta-\alpha}, t_\beta)$ plane. Furthermore, direct searches for the heavy states H_0, A_0 and $H^\pm$ also yield sensitivity to viable regions of the parameter space, and could potentially feature striking signatures such as decay chains, *e.g.* $H_0 \to Z A_0$, with $A_0 \to SS$.

Finally, while both the CPV and explicit 2HDM $\mathbb{Z}_2$ breaking are secluded and thus suppressed at tree-level, the model will also be subject to constraints coming from both EDMs and FCNCs. In the 2HDM, the electron EDM receives contributions from two-loop diagrams, the dominant of which are the so-called "Barr-Zee" diagrams (see Figure 4.4). For the 2HDM+S^2 model discussed in this work, the fact that the CP violating interactions necessarily involve the dark matter particle S, would result in contributions to the electron EDM with a further loop suppression, *i.e.* 3-loop diagrams, rendering the CP violation significantly below current and foreseeable future electron EDM measurements. Still, computing explicitly these 3-loop contributions to EDMs is a priory a daunting task. This computation might however be feasible in a certain limit of the 2HDM+S^2, corresponding to the scenario where the singlet S is the heaviest particle in the spectrum and can thus be integrated out, leading to an effective theory for the two doublets. The matching at 1-loop would result in contributions to $|H_1|^2 H_1^\dagger H_2$ and $|H_2|^2 H_1^\dagger H_2$ (traditionally parametrized as λ_6 and λ_7) proportional to λ_{S3}, and suppressed by a loop factor $(4\pi)^{-2}$. The CP violation could then be understood from the perspective of the general 2HDM. The same procedure could also provide an expectation for the size of FCNCs.

Lastly, it is important to note the CP eigenstates h, H_0 and A_0 can no longer be considered mass eigenstates beyond tree-level, as the CP breaking tied to the dark sector bleeds to the 2HDM spectrum. The impact of this CPV in the 2HDM sector at 1-loop could be assessed by a perturbative expansion [280] for the mass eigenstates in terms of the small CP violating phase tied to δ_2.

Summary and Conclusion

This thesis covers several aspects of Higgs phenomenology in connection with flavor, DM, CP violation and baryogenesis, putting emphasis on their testability at present experiments, and particularly, on their exploration at the LHC.

In Chapter 2, we studied $h + \gamma$ production at the LHC. While interesting in its own right, as this process remains yet to be observed, we demonstrated its role as a sensitive probe of the Higgs boson couplings to the light quarks of the first two generations of matter, still largely unconstrained by present measurements. The associated production with a photon is quadratically sensitive to a combination of these couplings, each weighted by the respective quark electric charges. The contribution of up-type quarks is thus enhanced with respect to that of their down-type counterparts, providing an unique way to disentangle deviations among them. This makes $h+\gamma$ highly complementary to other existing light quark Yukawa probes, which are often flavor-blind or sensitive to their masses instead.

Focusing on the $h \to \ell^+\nu\ell^-\bar{\nu}$ decay channel of the Higgs boson, we performed a multivariate neural network analysis to fully exploit the kinematics of this final state, and derived HL-LHC projected sensitivities to the Higgs Yukawa couplings to charm and up quarks. Our results were summarized and compared to other representative probes in Tables 2.1 and 2.2, including the experimental limits that have resulted from a preliminary CMS $h + \gamma$ analysis [45]. While our projected bounds for κ_c are complementary to existing methods, they are probably not competitive with the most sensitive direct probes of the charm Yukawa coupling in the literature. The latter benefits the most from flavor-specific approaches, as it is the heaviest of the remaining quarks. In contrast, the achievable $h + \gamma$ sensitivity to κ_u does lie in the same ballpark of other currently proposed probes. Particularly in the latter case, $h + \gamma$ may help to gain further insight on Higgs flavor at the LHC.

In Chapter 3, we turned our attention to the search for semi-invisible exotic decay modes of the Higgs boson. These decays remain largely unexplored both theoretically and experimentally despite constituting a rather generic prediction of many well motivated BSM extensions, specifically those seeking to provide an explanation for the observed DM abundance in the form of dark sectors. We focused on the exotic Higgs decay $h \to ZX$, with X an invisible BSM particle resulting in a semi-dark final state. Such exotic Higgs decays may occur in theories of ALPs, dark photons or pseudoscalar mediators between the SM and dark matter. The SM process $h \to Z\nu\bar{\nu}$ represents an irreducible "*neutrino floor*" background to these

new physics searches, but also provides a target experimental sensitivity for them.

In order to search for this decay we targeted ZH associated production, leading to a $4\ell + \not{E}_{(T)}$ final state benefiting from both a clean missing energy reconstruction and reduced backgrounds. We implemented a first multivariate neural network analysis to identify the Z boson produced by the Higgs decay, and a second to discriminate between the signal and the relevant SM backgrounds. We analyzed $h \to Z +$*invisible* searches at the LHC (both at present and future luminosities) and an hypothetical ILC, and derived their projected sensitivities to $\text{BR}(h \to ZX) \times \text{BR}(X \to \not{E}_{(T)})$ in Figure 3.3. Present luminosity constraints are well-competitive, at the level of the branching ratio, with those resulting from the two other semi-invisible decays currently being searched for at the LHC: $h \to \gamma + \not{E}_T$ [151–155], and $h \to b\bar{b} + \not{E}_T$ [156]. Whereas the HL-LHC comes close to being able to probe the *Higgs neutrino floor* (for $m_X = 1$ GeV, it probes $\text{BR}(h \to ZX) \times \text{BR}(\text{X} \to \not{E}_{\text{T}}) = 2.8 \times \text{BR}(\text{h} \to \text{Z}\nu\bar{\nu})_{\text{SM}}$ at 2σ). The ILC, on the other hand, is well capable of sweeping the entire new physics parameter space of semi-dark Higgs decays down to the *Higgs neutrino floor*, and could potentially find the first evidence for this SM process.

Finally, we translated the resulting constraints onto the parameter space of some well-motivated BSM extensions. While direct searches for this decay cannot compete with the most sensitive probes available in the case of a dark photon (at least considering its simplest realization through kinetic mixing), they prove competitive for the 2HDM+a, where there is a strong interplay between this search, Higgs signal strengths and the fully-invisible decay (see Figures 3.6 and 3.7). This is also particularly true for the case of ALPs, given the assumptions discussed in the text, semi-dark $h \to Za$ decays could probe a vast region of otherwise unexplored parameter space (see Figure 3.5). The latter would include the thermal relic line, encompassing the tantalizing possibility that the ALP might be the mediator between the dark and visible sectors.

Lastly, in Chapter 4, we explored the possibility that the CP violation (CPV) required for baryogenesis is active in the early Universe but is now suppressed. A scenario well-motivated by the strong constraints placed by EDMs on the existence of BSM sources of CPV that could catalyze the latter. By considering CP-violating interactions between a dark and the Higgs sectors, the multi-scalar dynamics in the early Universe is able to yield a transient period of CPV enhancement. This CPV then leaks to the visible sector, enabling a first-order EW phase transition to generate the observed baryon asymmetry. We argued that the requirement to generate a net baryon asymmetry avoiding cosmic domains naturally leads to a viable DM candidate. Through this two-step phase transition, the latter becomes the catalyzer for baryogenesis via its CP-violating interactions.

We showed that this setup can be easily accommodated by a suitable extension of the SM Higgs sector, specifically, a 2HDM augmented by a real singlet scalar field. We found the regions of parameter space that are consistent with perturbativity, unitarity and boundedness from below constraints (see Figure 4.1) and lead to such an early Universe period of CPV enhancement (see Figures 4.2 and 4.2), showing

that the required thermal history leads to a predictive scenario. Finally, we discussed preliminary results indicating that this model can successfully accommodate both baryogenesis and the observed DM abundance. Along with the possibility to test this scenario at the LHC through a combination of Higgs signal strengths and direct searches, the latter would make it also subject to DM direct detection constraints, both restricting the available parameter space.

Sumario y Conclusión

Esta tesis abarca varios aspectos de la fenomenología del Higgs en relación con el sabor, la materia oscura, la violación de CP y la bariogénesis, poniendo énfasis en su testabilidad en experimentos actuales y, en particular, en su exploración en el LHC.

En el Capítulo 2, estudiamos la producción $h+\gamma$ en el LHC. Si bien este proceso es interesante por sí mismo, ya que todavía no ha sido observado, mostramos que también es sensible a los acoplamientos del bosón de Higgs a los quarks ligeros de las dos primeras generaciones de la materia, aún poco constreñidos por las mediciones actuales. La producción asociada con un fotón es cuadráticamente sensible a una combinación de estos acoplamientos, cada uno pesado por la carga eléctrica respectiva de cada quark. La contribución de los quarks de tipo *up* se ve así potenciada en comparación con la de sus contrapartes de tipo *down*, proporcionando una forma única de distinguir las desviaciones entre ellos. Esto hace que $h+\gamma$ sea altamente complementario a otros métodos existentes para medir los acoplos de Yukawa de los quarks ligeros, que a menudo son ciegos al sabor o sensibles a sus masas en su lugar.

Centrándonos en el canal de decaimiento $h \to \ell^+\nu\ell^-\bar{\nu}$ del bosón de Higgs, realizamos un análisis multivariable de redes neuronales para aprovechar al máximo la cinemática de este estado final, y derivamos las sensibilidades proyectadas del HL-LHC a los acoplamientos de Yukawa de los quarks charm y up. Resumimos y comparamos nuestros resultados con otros métodos representativos en las Tablas 2.1 y 2.2, incluyendo los límites experimentales que han resultado de un análisis preliminar de $h+\gamma$ por parte de CMS [45]. Mientras que los límites proyectados para κ_c son complementarios a los de métodos existentes, probablemente no sean competitivos con los más sensibles en la literatura para el acoplamiento de Yukawa del charm. Este último se beneficia más de enfoques específicos al sabor, ya que es el más pesado de los quarks restantes. En cambio, la sensibilidad alcanzable para κ_u vía $h+\gamma$ se encuentra en el mismo orden de magnitud que otros métodos propuestos actualmente. Particularmente en este último caso, $h+\gamma$ podría ayudar a seguir explorando la fenomenología del sabor en el LHC.

En el Capítulo 3, dirigimos nuestra atención a la búsqueda de modos de decaimiento exóticos semi-invisibles del bosón de Higgs. Estos decaimientos siguen estando inexplorados en gran medida tanto desde un punto de vista teórico como experimental, a pesar de constituir una predicción bastante genérica de muchas extensiones BSM bien motivadas, específicamente aquellas que buscan proporcionar una explicación para la abundancia observada de materia oscura en forma de sec-

tores oscuros. Concretamente, nos centramos en el decaimiento exótico del Higgs $h \to ZX$, siendo X una partícula BSM invisible que resulta en un estado final semi-oscuro. Tales decaimientos exóticos del Higgs pueden ocurrir en teorías de ALPs, fotones oscuros o mediadores pseudoscalares entre el SM y la materia oscura. El proceso del SM $h \to Z\nu\bar{\nu}$ representa un fondo de "*suelo de neutrinos*" irreducible para estas búsquedas de nueva física, pero también proporciona una sensibilidad experimental objetivo para ellas.

Para buscar este decaimiento, nos enfocamos en la producción asociada de ZH, lo que conduce a un estado final $4\ell + \not{E}_{(T)}$ que se beneficia de una reconstrucción de energía pérdida limpia y de fondos reducidos. Implementamos un primer análisis multivariable de redes neuronales para identificar el bosón Z producido por el decaimiento del Higgs, y un segundo para discriminar entre la señal y los fondos relevantes del SM. Analizamos las búsquedas de $h \to Z +$*invisible* en el LHC (tanto a luminosidades actuales como futuras) y en un hipotético ILC, y derivamos las correspondientes sensibilidades proyectadas para $\mathrm{BR}(h \to ZX) \times \mathrm{BR}(X \to \not{E}_{(T)})$ en la Figura 3.3. A luminosidades actuales, estos límites son competitivos, a nivel de *branching ratio*, con los que resultan de los otros dos decaimientos semi-invisibles actualmente buscados en el LHC: $h \to \gamma + \not{E}_T$ [151–155], y $h \to b\bar{b} + \not{E}_T$ [156]. Mientras que el HL-LHC se acerca a poder sondear el *suelo de neutrinos del Higgs* (para $m_X =$ 1 GeV, sondea $\mathrm{BR}(h \to ZX) \times \mathrm{BR}(\mathrm{X} \to \not{E}_{\mathrm{T}}) = 2.8 \times \mathrm{BR}(\mathrm{h\,to Z}\nu\bar{\nu})_{\mathrm{SM}}$ a 2σ). Por otro lado, el ILC es capaz de barrer todo el espacio de parámetros de nueva física en los decaimientos semi-oscuros del bosón de Higgs hasta el *suelo de neutrinos*, y sería capaz de encontrar los primeros signos de la evidencia de este proceso del SM.

Finalmente, trasladamos las restricciones resultantes al espacio de parámetros de algunas extensiones bien motivadas mas allá del SM. Si bien las búsquedas directas de este decaimiento no pueden competir con los métodos más sensibles disponibles en el caso de un fotón oscuro (al menos considerando su realización más simple a través de mezcla cinética), sí son competitivas para el 2HDM+a, donde existe una fuerte interacción entre esta búsqueda, *Higgs signal strengths* y el decaimiento completamente invisible del Higgs (ver Figuras 3.6 y 3.7). Esto es especialmente cierto en el caso de las ALPs, dadas las suposiciones discutidas en el texto, los decaimientos semi-oscuros $h \to Za$ podrían sondear una vasta región de espacio de parámetros hasta ahora inexplorada (ver Figura 3.5). Esta incluiría la línea favorecida por la *relic density*, comprendiendo la intrigante posibilidad de que el ALP pudiera ser el mediador entre los sectores oscuro y visible.

Por último, en el Capítulo 4, exploramos la posibilidad de que la violación de CP (CPV) requerida para la bariogénesis se encontrase activa en el Universo primitivo pero esté suprimida ahora. Este escenario estaría motivado por las fuertes restricciones impuestas por la ausencia de momentos dipolares eléctricos a la existencia de fuentes más allá del SM de CPV, que podrían ser las encargadas de catalizar dicha bariogénesis. Al considerar interacciones que violan CP entre un sector oscuro y el sector del Higgs, la dinámica multi-escalar en el Universo temprano es capaz de producir un período transitorio de aumento de CPV. Esta CPV se filtraría luego hacia

el sector visible, permitiendo que una transición de fase electrodébil de primer orden generase la asimetría bariónica observada. La necesidad de generar una asimetría bariónica neta evitando dominios cósmicos conduce naturalmente a un candidato viable de materia oscura. A través de esta transición de fase de dos etapas, esta última se convierte en el catalizador de la bariogénesis mediante sus interacciones que violan CP.

Mostramos que esta estructura se puede acomodar fácilmente mediante una extensión del sector de Higgs en el SM, específicamente, un 2HDM aumentado por un campo singlete escalar real. Encontramos las regiones del espacio de parámetros que son consistentes con las restricciones de perturbatividad, unitariedad y potencial acotado (ver Figura 4.1) y que conducen a un período en el Universo primitivo de aumento de la CPV (ver Figuras 4.2 y 4.2), mostrando que la historia térmica requerida conduce a un escenario predictivo. Finalmente, discutimos resultados preliminares que indican que este modelo podría acomodar con éxito tanto la bariogénesis como la abundancia de materia oscura observada. Junto con la posibilidad de probar este escenario en el LHC a través de *Higgs signal strengths* y búsquedas directas, este último requisito lo sometería también a los constreñimientos derivados de los experimentos de detección directa de materia oscura, de forma que ambos restringirían espacio de parámetros disponible.

Acknowledgements

The work of the author was supported by the Spanish MICIU and the EU Fondo Social Europeo (FSE) through the grant PRE2018-083563. The author also acknowledges support from the IFT Centro de Excelencia Severo Ochoa program SEV-2016-0597, the grant PGC2018-096646-A-I00 from the Spanish Proyectos de I+D de Generación de Conocimiento, and the European Union's Horizon Europe research and innovation programme under the Marie Skłodowska-Curie Staff Exchange grant agreement No 101086085 — ASYMMETRY. The author is also grateful to the University of California Santa Cruz, the University of Tokyo and the Kavli IPMU for their hospitality during the development of this thesis.

References

[1] J.A. Aguilar-Saavedra, J.M. Cano and J.M. No, *More light on Higgs flavor at the LHC: Higgs boson couplings to light quarks through $h+\gamma$ production*, *Phys. Rev. D* **103** (2021) 095023 [2008.12538]. III, 30, 31

[2] J.A. Aguilar-Saavedra, J.M. Cano, J.M. No and D.G. Cerdeño, *Semidark Higgs boson decays: Sweeping the Higgs neutrino floor*, *Phys. Rev. D* **106** (2022) 115023 [2206.01214]. III

[3] S.L. Glashow, *Partial Symmetries of Weak Interactions*, *Nucl. Phys.* **22** (1961) 579. 3

[4] S. Weinberg, *A Model of Leptons*, *Phys. Rev. Lett.* **19** (1967) 1264.

[5] A. Salam, *Weak and electromagnetic interactions.*, *pp 367-77 of Elementary Particle Theory. Svartholm, Nils (ed.). New York, John Wiley and Sons, Inc., 1968.* (1969).

[6] S.L. Glashow, J. Iliopoulos and L. Maiani, *Weak interactions with lepton-hadron symmetry*, *Phys. Rev. D* **2** (1970) 1285. 3

[7] F. Englert and R. Brout, *Broken Symmetry and the Mass of Gauge Vector Mesons*, *Phys. Rev. Lett.* **13** (1964) 321. 4

[8] P.W. Higgs, *Spontaneous Symmetry Breakdown without Massless Bosons*, *Phys. Rev.* **145** (1966) 1156.

[9] G.S. Guralnik, C.R. Hagen and T.W.B. Kibble, *Global Conservation Laws and Massless Particles*, *Phys. Rev. Lett.* **13** (1964) 585. 4

[10] Particle Data Group collaboration, *Review of Particle Physics*, *PTEP* **2022** (2022) 083C01. 5, 9, 10

[11] N. Cabibbo, *Unitary Symmetry and Leptonic Decays*, *Phys. Rev. Lett.* **10** (1963) 531. 8

[12] M. Kobayashi and T. Maskawa, *CP Violation in the Renormalizable Theory of Weak Interaction*, *Prog. Theor. Phys.* **49** (1973) 652. 8

[13] Z. Maki, M. Nakagawa and S. Sakata, *Remarks on the unified model of elementary particles*, *Prog. Theor. Phys.* **28** (1962) 870. 9

[14] B. Pontecorvo, *Neutrino Experiments and the Problem of Conservation of Leptonic Charge*, *Zh. Eksp. Teor. Fiz.* **53** (1967) 1717. 9

[15] ATLAS collaboration, *Observation of a new particle in the search for the Standard Model Higgs boson with the ATLAS detector at the LHC*, *Phys. Lett. B* **716** (2012) 1 [1207.7214]. 9

[16] CMS collaboration, *Observation of a New Boson at a Mass of 125 GeV with the CMS Experiment at the LHC*, *Phys. Lett. B* **716** (2012) 30 [1207.7235]. 9

[17] ATLAS collaboration, *A detailed map of Higgs boson interactions by the ATLAS experiment ten years after the discovery*, *Nature* **607** (2022) 52 [2207.00092]. 10, 15, 16, 17

[18] CMS collaboration, *A portrait of the Higgs boson by the CMS experiment ten years after the discovery*, *Nature* **607** (2022) 60 [2207.00043]. 10, 16

[19] ATLAS collaboration, *A search for the dimuon decay of the Standard Model Higgs boson with the ATLAS detector*, *Phys. Lett. B* **812** (2021) 135980 [2007.07830]. 10, 17

[20] CMS collaboration, *Evidence for Higgs boson decay to a pair of muons*, *JHEP* **01** (2021) 148 [2009.04363]. 10, 17

[21] H. G., *Naturalness, Chiral Symmetry, and Spontaneous Chiral Symmetry Breaking*, *Series B. Physics* **59** (1980) . 12

[22] G.F. Giudice, *Naturally Speaking: The Naturalness Criterion and Physics at the LHC*, 0801.2562. 12

[23] Planck collaboration, *Planck 2018 results. VI. Cosmological parameters*, *Astron. Astrophys.* **641** (2020) A6 [1807.06209]. 12

[24] B. Holdom, *Two U(1)'s and Epsilon Charge Shifts*, *Phys. Lett. B* **166** (1986) 196. 13

[25] A. Falkowski, J. Juknevich and J. Shelton, *Dark Matter Through the Neutrino Portal*, 0908.1790. 13

[26] V. Silveira and A. Zee, *SCALAR PHANTOMS*, *Phys. Lett. B* **161** (1985) 136. 13

[27] R.M. Schabinger and J.D. Wells, *A Minimal spontaneously broken hidden sector and its impact on Higgs boson physics at the large hadron collider*, *Phys. Rev. D* **72** (2005) 093007 [hep-ph/0509209].

[28] B. Patt and F. Wilczek, *Higgs-field portal into hidden sectors*, hep-ph/0605188. 13

[29] A.D. Sakharov, *Violation of CP Invariance, C asymmetry, and baryon asymmetry of the universe*, *Pisma Zh. Eksp. Teor. Fiz.* **5** (1967) 32. 13, 53

[30] V.A. Kuzmin, V.A. Rubakov and M.E. Shaposhnikov, *On the Anomalous Electroweak Baryon Number Nonconservation in the Early Universe*, *Phys. Lett. B* **155** (1985) 36. 14, 53

[31] M.B. Gavela, P. Hernandez, J. Orloff and O. Pene, *Standard model CP violation and baryon asymmetry*, *Mod. Phys. Lett. A* **9** (1994) 795 [hep-ph/9312215]. 14, 53

[32] M.B. Gavela, M. Lozano, J. Orloff and O. Pene, *Standard model CP violation and baryon asymmetry. Part 1: Zero temperature*, *Nucl. Phys. B* **430** (1994) 345 [hep-ph/9406288].

[33] M.B. Gavela, P. Hernandez, J. Orloff, O. Pene and C. Quimbay, *Standard model CP violation and baryon asymmetry. Part 2: Finite temperature*, *Nucl. Phys. B* **430** (1994) 382 [hep-ph/9406289].

[34] P. Huet and E. Sather, *Electroweak baryogenesis and standard model CP violation*, *Phys. Rev. D* **51** (1995) 379 [hep-ph/9404302]. 14, 53

[35] A.G. Cohen, D.B. Kaplan and A.E. Nelson, *Progress in electroweak baryogenesis*, *Ann. Rev. Nucl. Part. Sci.* **43** (1993) 27 [hep-ph/9302210]. 14, 53

[36] D.E. Morrissey and M.J. Ramsey-Musolf, *Electroweak baryogenesis*, *New J. Phys.* **14** (2012) 125003 [1206.2942]. 14, 53

[37] LHC Higgs Cross Section Working Group collaboration, *LHC HXSWG interim recommendations to explore the coupling structure of a Higgs-like particle*, 1209.0040. 15

[38] G.F. Giudice, C. Grojean, A. Pomarol and R. Rattazzi, *The Strongly-Interacting Light Higgs*, *JHEP* **06** (2007) 045 [hep-ph/0703164]. 15

[39] S. Willenbrock and C. Zhang, *Effective Field Theory Beyond the Standard Model*, *Ann. Rev. Nucl. Part. Sci.* **64** (2014) 83 [1401.0470].

[40] I. Brivio and M. Trott, *The Standard Model as an Effective Field Theory*, *Phys. Rept.* **793** (2019) 1 [1706.08945].

[41] S. Dawson, C. Englert and T. Plehn, *Higgs Physics: It ain't over till it's over*, *Phys. Rept.* **816** (2019) 1 [1808.01324].

[42] T. Cohen, *As Scales Become Separated: Lectures on Effective Field Theory*, *PoS* **TASI2018** (2019) 011 [1903.03622]. 15

[43] CMS collaboration, *Search for Higgs boson decay to a charm quark-antiquark pair in proton-proton collisions at $\sqrt{s}$ = 13 TeV*, 2205.05550. 17, 28, 30

[44] ATLAS collaboration, *Measurement of the total and differential Higgs boson production cross-sections at $\sqrt{s}$ = 13 TeV with the ATLAS detector by combining the $H \to ZZ^* \to 4\ell$ and $H \to \gamma\gamma$ decay channels*, *JHEP* **05** (2023) 028 [2207.08615]. 17, 28, 30

[45] CMS collaboration, *Observation of $WW\gamma$ production and constraints on Higgs couplings to light quarks in proton-proton collisions at $\sqrt{s}$* =13 TeV, *CMS-PAS-SMP-22-006* (2023). 17, 29, 30, 31, 71, 75

[46] R.A. Porto and A. Zee, *The Private Higgs*, *Phys. Lett. B* **666** (2008) 491 [0712.0448]. 18

[47] G.F. Giudice and O. Lebedev, *Higgs-dependent Yukawa couplings*, *Phys. Lett. B* **665** (2008) 79 [0804.1753]. 18

[48] G. Branco, P. Ferreira, L. Lavoura, M. Rebelo, M. Sher and J.P. Silva, *Theory and phenomenology of two-Higgs-doublet models*, *Phys. Rept.* **516** (2012) 1 [1106.0034]. 18, 45, 46, 47, 57, 60

[49] M. Bauer, M. Carena and K. Gemmler, *Flavor from the Electroweak Scale*, *JHEP* **11** (2015) 016 [1506.01719]. 18

[50] M. Bauer, M. Carena and K. Gemmler, *Creating the fermion mass hierarchies with multiple Higgs bosons*, *Phys. Rev. D* **94** (2016) 115030 [1512.03458]. 18

[51] W. Altmannshofer, J. Eby, S. Gori, M. Lotito, M. Martone and D. Tuckler, *Collider Signatures of Flavorful Higgs Bosons*, *Phys. Rev. D* **94** (2016) 115032 [1610.02398]. 18

[52] W. Altmannshofer, S. Gori, D.J. Robinson and D. Tuckler, *The Flavor-locked Flavorful Two Higgs Doublet Model*, *JHEP* **03** (2018) 129 [1712.01847]. 18

[53] S. Bar-Shalom and A. Soni, *Universally enhanced light-quarks Yukawa couplings paradigm*, *Phys. Rev. D* **98** (2018) 055001 [1804.02400]. 18

[54] G. D'Ambrosio, G.F. Giudice, G. Isidori and A. Strumia, *Minimal flavor violation: An Effective field theory approach*, *Nucl. Phys. B* **645** (2002) 155 [hep-ph/0207036]. 18

[55] D. Egana-Ugrinovic, S. Homiller and P. Meade, *Aligned and Spontaneous Flavor Violation*, *Phys. Rev. Lett.* **123** (2019) 031802 [1811.00017]. 18

[56] D. Egana-Ugrinovic, S. Homiller and P.R. Meade, *Higgs bosons with large couplings to light quarks*, *Phys. Rev. D* **100** (2019) 115041 [1908.11376]. 18

[57] A. Abbasabadi, D. Bowser-Chao, D.A. Dicus and W.W. Repko, *Higgs - photon associated production at hadron colliders*, *Phys. Rev. D* **58** (1998) 057301 [hep-ph/9706335]. 19

[58] E. Gabrielli, B. Mele and J. Rathsman, *Higgs boson plus photon production at the LHC: a clean probe of the b-quark parton densities*, *Phys. Rev. D* **77** (2008) 015007 [0707.0797].

[59] P. Agrawal and A. Shivaji, *Gluon Fusion Contribution to VHj Production at Hadron Colliders*, *Phys. Lett. B* **741** (2015) 111 [1409.8059].

[60] E. Gabrielli, B. Mele, F. Piccinini and R. Pittau, *Asking for an extra photon in Higgs production at the LHC and beyond*, *JHEP* **07** (2016) 003 [1601.03635]. 19, 21

[61] K. Arnold, T. Figy, B. Jager and D. Zeppenfeld, *Next-to-leading order QCD corrections to Higgs boson production in association with a photon via weak-boson fusion at the LHC*, *JHEP* **08** (2010) 088 [1006.4237]. 21

[62] H. Khanpour, S. Khatibi and M. Mohammadi Najafabadi, *Probing Higgs boson couplings in $H+\gamma$ production at the LHC*, *Phys. Lett. B* **773** (2017) 462 [1702.05753].

[63] B.A. Dobrescu, P.J. Fox and J. Kearney, *Higgs–photon resonances*, *Eur. Phys. J. C* **77** (2017) 704 [1705.08433]. 19

[64] W.H. Furry, *A Symmetry Theorem in the Positron Theory*, *Phys. Rev.* **51** (1939) 125. 19

[65] M. Peskin and D. Schroeder, *An Introduction to quantum field theory*, *An introduction to Quantum Field Theory, (1995), 318* (1995). 19

[66] J. Ellis, *TikZ-Feynman: Feynman diagrams with TikZ*, *Comput. Phys. Commun.* **210** (2017) 103 [1601.05437]. 20

[67] S.P. Martin and D.G. Robertson, *Standard model parameters in the tadpole-free pure ms¯ scheme*, *Physical Review D* **100** (2019). 20

[68] J. Alwall, R. Frederix, S. Frixione, V. Hirschi, F. Maltoni, O. Mattelaer et al., *The automated computation of tree-level and next-to-leading order differential cross sections, and their matching to parton shower simulations*, *Journal of High Energy Physics* **2014** (2014). 20, 22, 35

[69] NNPDF collaboration, *Illuminating the photon content of the proton within a global PDF analysis*, *SciPost Phys.* **5** (2018) 008 [1712.07053]. 20, 35

[70] ATLAS Collaboration collaboration, *Trigger Menu in 2017*, Tech. Rep. ATL-DAQ-PUB-2018-002, CERN, Geneva (Jun, 2018). 21

[71] M. Ishino, *Atlas trigger and daq upgrades for high-luminosity lhc*, *EPJ Web of Conferences* **164** (2017) 07003. 21

[72] ATLAS collaboration, *Measurements of the production cross section of a Z boson in association with jets in pp collisions at $\sqrt{s}$ = 13 TeV with the ATLAS detector*, *Eur. Phys. J. C* **77** (2017) 361 [1702.05725]. 22

[73] CMS collaboration, *Measurement of differential cross sections for Z boson production in association with jets in proton-proton collisions at $\sqrt{s}$ = 13 TeV*, *Eur. Phys. J. C* **78** (2018) 965 [1804.05252].

[74] ATLAS collaboration, *Measurement of the $Z(\to \ell^+\ell^-)\gamma$ production cross-section in pp collisions at $\sqrt{s}$ = 13 TeV with the ATLAS detector*, *JHEP* **03** (2020) 054 [1911.04813]. 22

[75] T. Sjöstrand, S. Ask, J.R. Christiansen, R. Corke, N. Desai, P. Ilten et al., *An introduction to PYTHIA 8.2*, *Comput. Phys. Commun.* **191** (2015) 159 [1410.3012]. 22, 35

[76] DELPHES 3 collaboration, *DELPHES 3, A modular framework for fast simulation of a generic collider experiment*, *JHEP* **02** (2014) 057 [1307.6346]. 22, 35, 40

[77] M. Cacciari, G.P. Salam and G. Soyez, *The anti-k_t jet clustering algorithm*, *JHEP* **04** (2008) 063 [0802.1189]. 22

[78] M. Cacciari, G.P. Salam and G. Soyez, *FastJet User Manual*, *Eur. Phys. J. C* **72** (2012) 1896 [1111.6097]. 22

[79] D. Bertolini, P. Harris, M. Low and N. Tran, *Pileup Per Particle Identification*, *JHEP* **10** (2014) 059 [1407.6013]. 22, 35

[80] M. Cacciari, G.P. Salam and G. Soyez, *SoftKiller, a particle-level pileup removal method*, *Eur. Phys. J. C* **75** (2015) 59 [1407.0408]. 22, 35

[81] P. Berta, M. Spousta, D.W. Miller and R. Leitner, *Particle-level pileup subtraction for jets and jet shapes*, *JHEP* **06** (2014) 092 [1403.3108]. 22, 35

[82] D.P. Kingma and J. Ba, *Adam: A method for stochastic optimization*, 2014. 23

[83] C.W. Murphy, *Class Imbalance Techniques for High Energy Physics*, *SciPost Phys.* **7** (2019) 076 [1905.00339]. 23

[84] D. Zeppenfeld, R. Kinnunen, A. Nikitenko and E. Richter-Was, *Measuring Higgs boson couplings at the CERN LHC*, *Phys. Rev. D* **62** (2000) 013009 [hep-ph/0002036]. 26

[85] M. Duhrssen, S. Heinemeyer, H. Logan, D. Rainwater, G. Weiglein and D. Zeppenfeld, *Extracting Higgs boson couplings from CERN LHC data*, *Phys. Rev. D* **70** (2004) 113009 [hep-ph/0406323].

[86] G. Belanger, B. Dumont, U. Ellwanger, J. Gunion and S. Kraml, *Global fit to Higgs signal strengths and couplings and implications for extended Higgs sectors*, *Phys. Rev. D* **88** (2013) 075008 [1306.2941]. 26

[87] N.M. Coyle, C.E.M. Wagner and V. Wei, *Bounding the charm Yukawa coupling*, *Phys. Rev.* **D100** (2019) 073013 [1905.09360]. 26, 27, 28, 29, 30

[88] CMS collaboration, *Combined Higgs boson production and decay measurements with up to 137 fb-1 of proton-proton collision data at sqrts = 13 TeV*, *CMS-PAS-HIG-19-005* (2020). 26, 47

[89] ATLAS collaboration, *Combined measurements of Higgs boson production and decay using up to* 139 fb^{-1} *of proton-proton collision data at* $\sqrt{s}$ = 13 *TeV collected with the ATLAS experiment*, *ATLAS-CONF-2021-053* (2021).

[90] ATLAS collaboration, *Measurements of the Higgs boson inclusive and differential fiducial cross sections in the* 4ℓ *decay channel at* $\sqrt{s}$ = 13 *TeV*, *Eur. Phys. J. C* **80** (2020) 942 [2004.03969]. 26, 28

[91] C. Englert and M. Spannowsky, *Limitations and Opportunities of Off-Shell Coupling Measurements*, *Phys. Rev. D* **90** (2014) 053003 [1405.0285]. 26

[92] I. Brivio, F. Goertz and G. Isidori, *Probing the Charm Quark Yukawa Coupling in Higgs+Charm Production*, *Phys. Rev. Lett.* **115** (2015) 211801 [1507.02916]. 27, 30

[93] J. Cohen, S. Bar-Shalom, G. Eilam and A. Soni, *Light-quarks Yukawa couplings and new physics in exclusive high-* p_T *Higgs boson+jet and Higgs boson +* b *-jet events*, *Phys. Rev. D* **97** (2018) 055014 [1705.09295]. 27

[94] F. Bishara, U. Haisch, P.F. Monni and E. Re, *Constraining Light-Quark Yukawa Couplings from Higgs Distributions*, *Phys. Rev. Lett.* **118** (2017) 121801 [1606.09253]. 27, 30

[95] Y. Soreq, H.X. Zhu and J. Zupan, *Light quark Yukawa couplings from Higgs kinematics*, *JHEP* **12** (2016) 045 [1606.09621]. 31

[96] G. Bonner and H.E. Logan, *Constraining the Higgs couplings to up and down quarks using production kinematics at the CERN Large Hadron Collider*, 1608.04376. 27, 31

[97] L. Alasfar, R. Corral Lopez and R. Gröber, *Probing Higgs couplings to light quarks via Higgs pair production*, *JHEP* **11** (2019) 088 [1909.05279]. 27, 30, 31

[98] L. Alasfar, R. Gröber, C. Grojean, A. Paul and Z. Qian, *Machine learning the trilinear and light-quark Yukawa couplings from Higgs pair kinematic shapes*, *JHEP* **11** (2022) 045 [2207.04157]. 27, 31

[99] F. Yu, *Phenomenology of Enhanced Light Quark Yukawa Couplings and the $W^{\pm}h$ Charge Asymmetry*, *JHEP* **02** (2017) 083 [1609.06592]. 27, 30

[100] B. Henning, D. Lombardo, M. Riembau and F. Riva, *Measuring Higgs Couplings without Higgs Bosons*, *Phys. Rev. Lett.* **123** (2019) 181801 [1812.09299]. 27

[101] A. Falkowski, S. Ganguly, P. Gras, J.M. No, K. Tobioka, N. Vignaroli et al., *Light quark Yukawas in triboson final states*, *JHEP* **04** (2021) 023 [2011.09551]. 28, 31

[102] N. Vignaroli, *Off-Shell Probes of the Higgs Yukawa Couplings: Light Quarks and Charm*, *Symmetry* **14** (2022) 1183 [2205.09449]. 28

[103] E. Balzani, R. Gröber and M. Vitti, *Light-quark Yukawa couplings from off-shell Higgs production*, 2304.09772. 28, 31

[104] G.T. Bodwin, F. Petriello, S. Stoynev and M. Velasco, *Higgs boson decays to quarkonia and the $H\bar{c}c$ coupling*, *Phys. Rev. D* **88** (2013) 053003 [1306.5770]. 28

[105] A.L. Kagan, G. Perez, F. Petriello, Y. Soreq, S. Stoynev and J. Zupan, *Exclusive Window onto Higgs Yukawa Couplings*, *Phys. Rev. Lett.* **114** (2015) 101802 [1406.1722].

[106] G. Perez, Y. Soreq, E. Stamou and K. Tobioka, *Constraining the charm Yukawa and Higgs-quark coupling universality*, *Phys. Rev. D* **92** (2015) 033016 [1503.00290]. 28, 29

[107] G. Perez, Y. Soreq, E. Stamou and K. Tobioka, *Prospects for measuring the Higgs boson coupling to light quarks*, *Phys. Rev. D* **93** (2016) 013001 [1505.06689]. 28

[108] M. König and M. Neubert, *Exclusive Radiative Higgs Decays as Probes of Light-Quark Yukawa Couplings*, *JHEP* **08** (2015) 012 [1505.03870].

[109] S. Mao, Y. Guo-He, L. Gang, Z. Yu and G. Jian-You, *Probing the charm-Higgs Yukawa coupling via Higgs boson decay to h_c plus a photon*, *J. Phys. G* **46** (2019) 105008 [1905.01589]. 28

[110] J. Walker and F. Krauss, *Constraining the Charm-Yukawa coupling at the Large Hadron Collider*, *Phys. Lett. B* **832** (2022) 137255 [2202.13937]. 28, 30

[111] B. Carlson, T. Han and S.C.I. Leung, *Higgs boson to charm quark decay in vector boson fusion plus a photon*, *Phys. Rev. D* **104** (2021) 073006 [2105.08738]. 28, 30

[112] C. Delaunay, R. Ozeri, G. Perez and Y. Soreq, *Probing Atomic Higgs-like Forces at the Precision Frontier*, *Phys. Rev. D* **96** (2017) 093001 [1601.05087]. 28

[113] F. Goertz, *Indirect Handle on the Down-Quark Yukawa Coupling*, *Phys. Rev. Lett.* **113** (2014) 261803 [1406.0102]. 28

[114] F. Bishara, J. Brod, P. Uttayarat and J. Zupan, *Nonstandard Yukawa Couplings and Higgs Portal Dark Matter*, *JHEP* **01** (2016) 010 [1504.04022]. 28

[115] ATLAS collaboration, *Search for Higgs and Z Boson Decays to $J/\psi\gamma$ and $\Upsilon(nS)\gamma$ with the ATLAS Detector*, *Phys. Rev. Lett.* **114** (2015) 121801 [1501.03276]. 28

[116] ATLAS collaboration, *Search for Higgs and Z Boson Decays to $\phi\gamma$ with the ATLAS Detector*, *Phys. Rev. Lett.* **117** (2016) 111802 [1607.03400].

[117] ATLAS collaboration, *Search for exclusive Higgs and Z boson decays to $\phi\gamma$ and $\rho\gamma$ with the ATLAS detector*, *JHEP* **07** (2018) 127 [1712.02758].

[118] CMS collaboration, *Search for decays of the 125 GeV Higgs boson into a Z boson and a ρ or ϕ meson*, 2007.05122.

[119] CMS collaboration, *Search for Higgs boson decays into Z and J/ψ and for Higgs and Z boson decays into J/ψ or Υ pairs in pp collisions at s=13 TeV*, *Phys. Lett. B* **842** (2023) 137534 [2206.03525].

[120] ATLAS collaboration, *Searches for exclusive Higgs and Z boson decays into a vector quarkonium state and a photon using 139 fb^{-1} of ATLAS $\sqrt{s}$ = 13 TeV proton−proton collision data*, 2208.03122. 30

[121] ATLAS collaboration, *Search for exclusive Higgs and Z boson decays to $\omega\gamma$ and Higgs boson decays to $K^*\gamma$ with the ATLAS detector*, 2301.09938. 28

[122] LHCb collaboration, *Search for $H^0 \to b\bar{b}$ or $c\bar{c}$ in association with a W or Z boson in the forward region of pp collisions*, *LHCb-CONF-2016-006, CERN-LHCb-CONF-2016-006* (2016). 28

[123] ATLAS collaboration, *Search for the Decay of the Higgs Boson to Charm Quarks with the ATLAS Experiment*, *Phys. Rev. Lett.* **120** (2018) 211802 [1802.04329].

[124] ATLAS collaboration, *Direct constraint on the Higgs-charm coupling from a search for Higgs boson decays into charm quarks with the ATLAS detector*, *Eur. Phys. J. C* **82** (2022) 717 [2201.11428]. 28

[125] CMS collaboration, *Search for Higgs Boson and Observation of Z Boson through their Decay into a Charm Quark-Antiquark Pair in Boosted Topologies in Proton-Proton Collisions at s=13 TeV*, *Phys. Rev. Lett.* **131** (2023) 041801 [2211.14181]. 28

[126] CMS collaboration, *Measurements of inclusive and differential cross sections for the Higgs boson production and decay to four-leptons in proton-proton collisions at $\sqrt{s}$ = 13 TeV*, 2305.07532. 28, 30

[127] J. de Blas et al., *Higgs Boson Studies at Future Particle Colliders*, *JHEP* **01** (2020) 139 [1905.03764]. 29, 30, 31

[128] A. Falkowski, S. Rychkov and A. Urbano, *What if the Higgs couplings to W and Z bosons are larger than in the Standard Model?*, *JHEP* **04** (2012) 073 [1202.1532]. 29

[129] LHC Higgs Cross Section Working Group collaboration, *Handbook of LHC Higgs Cross Sections: 3. Higgs Properties*, 1307.1347. 29

[130] CMS collaboration, *Measurement of the Higgs boson width and evidence of its off-shell contributions to ZZ production*, *Nature Phys.* **18** (2022) 1329 [2202.06923]. 29

[131] ATLAS collaboration, *Evidence of off-shell Higgs boson production from ZZ leptonic decay channels and constraints on its total width with the ATLAS detector*, 2304.01532. 29

[132] A. Falkowski, F. Riva and A. Urbano, *Higgs at last*, *JHEP* **11** (2013) 111 [1303.1812]. 29

[133] ATLAS collaboration, *Prospects for $H \to c\bar{c}$ using Charm Tagging with the ATLAS Experiment at the HL-LHC*, . 30

[134] D. Curtin et al., *Exotic decays of the 125 GeV Higgs boson*, *Phys. Rev. D* **90** (2014) 075004 [1312.4992]. 33, 50, 51

[135] CMS collaboration, *Search for low-mass dilepton resonances in Higgs boson decays to four-lepton final states in proton–proton collisions at $\sqrt{s}$ = 13 TeV*, *Eur. Phys. J. C* **82** (2022) 290 [2111.01299]. 33

[136] ATLAS collaboration, *Search for Higgs bosons decaying into new spin-0 or spin-1 particles in four-lepton final states with the ATLAS detector with 139 fb^{-1} of pp collision data at $\sqrt{s}$ = 13 TeV*, 2110.13673.

[137] CMS collaboration, *Search for a light pseudoscalar Higgs boson in the boosted $\mu\mu\tau\tau$ final state in proton-proton collisions at $\sqrt{s}$ = 13 TeV*, *JHEP* **08** (2020) 139 [2005.08694]. 48

[138] CMS collaboration, *Search for an exotic decay of the Higgs boson to a pair of light pseudoscalars in the final state of two muons and two τ leptons in proton-proton collisions at $\sqrt{s}$ = 13 TeV*, *JHEP* **11** (2018) 018 [1805.04865]. 48

[139] CMS collaboration, *Search for light pseudoscalar boson pairs produced from decays of the 125 GeV Higgs boson in final states with two muons and two nearby tracks in pp collisions at $\sqrt{s}$ = 13 TeV*, *Phys. Lett. B* **800** (2020) 135087 [1907.07235]. 48

[140] ATLAS collaboration, *Search for Higgs boson decays into two new low-mass spin-0 particles in the 4b channel with the ATLAS detector using pp collisions at $\sqrt{s}$ = 13 TeV*, *Phys. Rev. D* **102** (2020) 112006 [2005.12236].

[141] ATLAS collaboration, *Search for Higgs boson decays into a pair of pseudoscalar particles in the bb$\mu\mu$ final state with the ATLAS detector in pp collisions at $\sqrt{s}$ = 13 TeV*, 2110.00313. 48

[142] CMS collaboration, *Search for an exotic decay of the Higgs boson to a pair of light pseudoscalars in the final state with two muons and two b quarks in pp collisions at 13 TeV*, *Phys. Lett. B* **795** (2019) 398 [1812.06359].

[143] CMS collaboration, *Search for an exotic decay of the Higgs boson to a pair of light pseudoscalars in the final state with two b quarks and two τ leptons in proton-proton collisions at $\sqrt{s}$ = 13 TeV*, *Phys. Lett. B* **785** (2018) 462 [1805.10191]. 48

[144] ATLAS collaboration, *Search for the Higgs boson produced in association with a vector boson and decaying into two spin-zero particles in the $H \to aa \to 4b$ channel in pp collisions at $\sqrt{s}$ = 13 TeV with the ATLAS detector*, *JHEP* **10** (2018) 031 [1806.07355].

[145] ATLAS collaboration, *Search for Higgs boson decays into pairs of light (pseudo)scalar particles in the $\gamma\gamma jj$ final state in pp collisions at $\sqrt{s}$ = 13 TeV with the ATLAS detector*, *Phys. Lett. B* **782** (2018) 750 [1803.11145].

[146] ATLAS collaboration, *Search for Higgs Boson Decays into a Z Boson and a Light Hadronically Decaying Resonance Using 13 TeV pp Collision Data from the ATLAS Detector*, *Phys. Rev. Lett.* **125** (2020) 221802 [2004.01678]. 33

[147] M. Cepeda, S. Gori, V.M. Outschoorn and J. Shelton, *Exotic Higgs Decays*, 2111.12751. 33, 48

[148] H. Davoudiasl, H.-S. Lee and W.J. Marciano, *'Dark' Z implications for Parity Violation, Rare Meson Decays, and Higgs Physics*, *Phys. Rev. D* **85** (2012) 115019 [1203.2947]. 33, 34, 51

[149] C. Petersson, A. Romagnoni and R. Torre, *Higgs Decay with Monophoton + MET Signature from Low Scale Supersymmetry Breaking*, *JHEP* **10** (2012) 016 [1203.4563].

[150] C. Englert, M. Spannowsky and C. Wymant, *Partially (in)visible Higgs decays at the LHC*, *Phys. Lett. B* **718** (2012) 538 [1209.0494]. 33

[151] CMS collaboration, *Search for exotic decays of a Higgs boson into undetectable particles and one or more photons*, *Phys. Lett. B* **753** (2016) 363 [1507.00359]. 33, 51, 72, 76

[152] CMS collaboration, *Search for dark photons in decays of Higgs bosons produced in association with Z bosons in proton-proton collisions at $\sqrt{s}$ = 13 TeV*, *JHEP* **10** (2019) 139 [1908.02699].

[153] CMS collaboration, *Search for dark photons in Higgs boson production via vector boson fusion in proton-proton collisions at $\sqrt{s}$ = 13 TeV*, *JHEP* **03** (2021) 011 [2009.14009].

[154] ATLAS collaboration, *Observation of electroweak production of two jets in association with an isolated photon and missing transverse momentum, and search for a Higgs boson decaying into invisible particles at 13 TeV with the ATLAS detector*, 2109.00925.

[155] ATLAS collaboration, *Search for dark photons from Higgs boson decays via ZH production with a photon plus missing transverse momentum signature from pp collisions at $\sqrt{s}$ = 13 TeV with the ATLAS detector*, *JHEP* **07** (2023) 133 [2212.09649]. 33, 51, 72, 76

[156] ATLAS collaboration, *Search for exotic decays of the Higgs boson into $b\bar{b}$ and missing transverse momentum in pp collisions at $\sqrt{s}$ = 13 TeV with the ATLAS detector*, 2109.02447. 33, 51, 72, 76

[157] J. Monroe and P. Fisher, *Neutrino Backgrounds to Dark Matter Searches*, *Phys. Rev. D* **76** (2007) 033007 [0706.3019]. 34

[158] LHC Higgs Cross Section Working Group collaboration, *Handbook of LHC Higgs Cross Sections: 4. Deciphering the Nature of the Higgs Sector*, 1610.07922. 34, 35

[159] A. Alloul, N.D. Christensen, C. Degrande, C. Duhr and B. Fuks, *FeynRules 2.0 - A complete toolbox for tree-level phenomenology*, *Comput. Phys. Commun.* **185** (2014) 2250 [1310.1921]. 35

[160] J.M. No, *Looking through the pseudoscalar portal into dark matter: Novel mono-Higgs and mono-Z signatures at the LHC*, *Phys. Rev. D* **93** (2016) 031701 [1509.01110]. 35, 44, 47, 49

[161] D. Goncalves, P.A.N. Machado and J.M. No, *Simplified Models for Dark Matter Face their Consistent Completions*, *Phys. Rev. D* **95** (2017) 055027 [1611.04593]. 47

[162] M. Bauer, U. Haisch and F. Kahlhoefer, *Simplified dark matter models with two Higgs doublets: I. Pseudoscalar mediators*, *JHEP* **05** (2017) 138 [1701.07427]. 35, 44, 46, 47, 49

[163] T. Binoth, G. Ossola, C. Papadopoulos and R. Pittau, *Nlo qcd corrections to tri-boson production*, *Journal of High Energy Physics* **2008** (2008) 082–082. 35

[164] A. Kulesza, L. Motyka, D. Schwartländer, T. Stebel and V. Theeuwes, *Associated production of a top quark pair with a heavy electroweak gauge boson at nlo+nnll accuracy*, *The European Physical Journal C* **79** (2019) . 35

[165] F. Cascioli, T. Gehrmann, M. Grazzini, S. Kallweit, P. Maierhöfer, A. von Manteuffel et al., *Zz production at hadron colliders in nnlo qcd*, *Physics Letters B* **735** (2014) 311–313. 35

[166] S. Frixione, E. Laenen, P. Motylinski, B.R. Webber and C.D. White, *Single-top hadroproduction in association with a W boson*, *JHEP* **07** (2008) 029 [0805.3067]. 35

[167] H.E. Faham, F. Maltoni, K. Mimasu and M. Zaro, *Single top production in association with a WZ pair at the LHC in the SMEFT*, *JHEP* **01** (2022) 100 [2111.03080]. 35

[168] ATLAS collaboration, *Trigger menu in 2018*, *ATL-DAQ-PUB-2019-001* (2019) . 35

[169] G. Cowan, K. Cranmer, E. Gross and O. Vitells, *Asymptotic formulae for likelihood-based tests of new physics*, *The European Physical Journal C* **71** (2011) . 37

[170] ATLAS collaboration, *Search for associated production of a Z boson with an invisibly decaying Higgs boson or dark matter candidates at s=13 TeV with the ATLAS detector*, *Phys. Lett. B* **829** (2022) 137066 [2111.08372]. 38, 49

[171] CMS collaboration, *Search for dark matter produced in association with a leptonically decaying Z boson in proton-proton collisions at* $\sqrt{s} =$ *13 TeV*, *Eur. Phys. J. C* **81** (2021) 13 [2008.04735]. 38, 49

[172] T. Behnke, J.E. Brau, B. Foster, J. Fuster, M. Harrison, J.M. Paterson et al., *The International Linear Collider Technical Design Report - Volume 1: Executive Summary*, 1306.6327. 39

[173] P. Bambade, T. Barklow, T. Behnke, M. Berggren, J. Brau, P. Burrows et al., *The international linear collider: A global project*, 1903.01629. 39

[174] C.T. Potter, *DSiD: a Delphes Detector for ILC Physics Studies*, in *International Workshop on Future Linear Colliders*, 2, 2016 [1602.07748]. 40

[175] R.D. Peccei and H.R. Quinn, *CP Conservation in the Presence of Instantons*, *Phys. Rev. Lett.* **38** (1977) 1440. 41

[176] S. Weinberg, *A New Light Boson?*, *Phys. Rev. Lett.* **40** (1978) 223.

[177] F. Wilczek, *Problem of Strong P and T Invariance in the Presence of Instantons*, *Phys. Rev. Lett.* **40** (1978) 279. 41

[178] A.R. Zhitnitsky, *On Possible Suppression of the Axion Hadron Interactions. (In Russian)*, *Sov. J. Nucl. Phys.* **31** (1980) 260. 41

[179] M. Dine, W. Fischler and M. Srednicki, *A Simple Solution to the Strong CP Problem with a Harmless Axion*, *Phys. Lett. B* **104** (1981) 199. 41

[180] J.E. Kim, *Weak Interaction Singlet and Strong CP Invariance*, *Phys. Rev. Lett.* **43** (1979) 103. 41

[181] M.A. Shifman, A.I. Vainshtein and V.I. Zakharov, *Can Confinement Ensure Natural CP Invariance of Strong Interactions?*, *Nucl. Phys. B* **166** (1980) 493. 41

[182] I. Brivio, M.B. Gavela, L. Merlo, K. Mimasu, J.M. No, R. del Rey et al., *ALPs Effective Field Theory and Collider Signatures*, *Eur. Phys. J. C* **77** (2017) 572 [1701.05379]. 41, 42

[183] M. Bauer, M. Neubert and A. Thamm, *Collider Probes of Axion-Like Particles*, *JHEP* **12** (2017) 044 [1708.00443]. 41, 42, 44

[184] M.J. Dolan, T. Ferber, C. Hearty, F. Kahlhoefer and K. Schmidt-Hoberg, *Revised constraints and Belle II sensitivity for visible and invisible axion-like particles*, *JHEP* **12** (2017) 094 [1709.00009]. 42, 43

[185] A. Alves, A.G. Dias and D.D. Lopes, *Probing ALP-Sterile Neutrino Couplings at the LHC*, *JHEP* **08** (2020) 074 [1911.12394]. 42

[186] N. Craig, A. Hook and S. Kasko, *The Photophobic ALP*, *JHEP* **09** (2018) 028 [1805.06538]. 42

[187] K. Mimasu and V. Sanz, *ALPs at Colliders*, *JHEP* **06** (2015) 173 [1409.4792]. 42, 44

[188] G. Alonso-Álvarez, M.B. Gavela and P. Quilez, *Axion couplings to electroweak gauge bosons*, *Eur. Phys. J. C* **79** (2019) 223 [1811.05466]. 42

[189] Planck collaboration, *Planck 2015 results. XIII. Cosmological parameters*, *Astron. Astrophys.* **594** (2016) A13 [1502.01589]. 42, 50

[190] P.J. Fox, R. Harnik, J. Kopp and Y. Tsai, *LEP Shines Light on Dark Matter*, *Phys. Rev. D* **84** (2011) 014028 [1103.0240]. 43

[191] DELPHI collaboration, *Search for one large extra dimension with the DELPHI detector at LEP*, *Eur. Phys. J. C* **60** (2009) 17 [0901.4486]. 43

[192] BaBar collaboration, *Search for Production of Invisible Final States in Single-Photon Decays of $\Upsilon(1S)$*, *Phys. Rev. Lett.* **107** (2011) 021804 [1007.4646]. 43

[193] BaBar collaboration, *Search for Invisible Decays of a Light Scalar in Radiative Transitions $\upsilon_{3S} \to \gamma$ A0*, in *34th International Conference on High Energy Physics*, 7, 2008 [0808.0017]. 43

[194] Crystal Ball collaboration, *Limits on axion and light Higgs boson production in Upsilon (1s) decays*, *Phys. Lett. B* **251** (1990) 204. 43

[195] S. Knapen, T. Lin, H.K. Lou and T. Melia, *Searching for Axionlike Particles with Ultraperipheral Heavy-Ion Collisions*, *Phys. Rev. Lett.* **118** (2017) 171801 [1607.06083]. 43

[196] ATLAS collaboration, *Measurement of light-by-light scattering and search for axion-like particles with 2.2 nb^{-1} of Pb+Pb data with the ATLAS detector*, *JHEP* **11** (2021) 050 [2008.05355]. 43

[197] CMS collaboration, *Evidence for light-by-light scattering and searches for axion-like particles in ultraperipheral PbPb collisions at $\sqrt{s_{\mathrm{NN}}} = 5.02$ TeV*, *Phys. Lett. B* **797** (2019) 134826 [1810.04602]. 43

[198] J. Bonilla, I. Brivio, J. Machado-Rodríguez and J.F. de Trocóniz, *Nonresonant Searches for Axion-Like Particles in Vector Boson Scattering Processes at the LHC*, 2202.03450. 43

[199] G.G. Raffelt, *Astrophysical axion bounds*, *Lect. Notes Phys.* **741** (2008) 51 [hep-ph/0611350]. 43

[200] J. Jaeckel and M. Spannowsky, *Probing MeV to 90 GeV axion-like particles with LEP and LHC*, *Phys. Lett. B* **753** (2016) 482 [1509.00476]. 44

[201] B. Döbrich, J. Jaeckel, F. Kahlhoefer, A. Ringwald and K. Schmidt-Hoberg, *ALPtraum: ALP production in proton beam dump experiments*, *JHEP* **02** (2016) 018 [1512.03069]. 44

[202] L3 collaboration, *Search for new physics in energetic single photon production in e^+e^- annihilation at the Z resonance*, *Phys. Lett. B* **412** (1997) 201. 44

[203] G. Brooijmans et al., *Les Houches 2019 Physics at TeV Colliders: New Physics Working Group Report*, in *11th Les Houches Workshop on Physics at TeV Colliders: PhysTeV Les Houches*, 2, 2020 [2002.12220]. 44

[204] S. Ipek, D. McKeen and A.E. Nelson, *A Renormalizable Model for the Galactic Center Gamma Ray Excess from Dark Matter Annihilation*, *Phys. Rev. D* **90** (2014) 055021 [1404.3716]. 44, 45

[205] T. Robens, *The THDMa Revisited*, *Symmetry* **13** (2021) 2341 [2106.02962]. 44

[206] XENON collaboration, *Dark Matter Search Results from a One Ton-Year Exposure of XENON1T*, *Phys. Rev. Lett.* **121** (2018) 111302 [1805.12562]. 45

[207] F. Ertas and F. Kahlhoefer, *Loop-induced direct detection signatures from CP-violating scalar mediators*, *JHEP* **06** (2019) 052 [1902.11070]. 45

[208] T. Abe, M. Fujiwara, J. Hisano and Y. Shoji, *Maximum value of the spin-independent cross section in the 2HDM+a*, *JHEP* **01** (2020) 114 [1910.09771]. 45

[209] C. Boehm, M.J. Dolan, C. McCabe, M. Spannowsky and C.J. Wallace, *Extended gamma-ray emission from Coy Dark Matter*, *JCAP* **05** (2014) 009 [1401.6458]. 45

[210] E. Izaguirre, G. Krnjaic and B. Shuve, *The Galactic Center Excess from the Bottom Up*, *Phys. Rev. D* **90** (2014) 055002 [1404.2018].

[211] P. Tunney, J.M. No and M. Fairbairn, *Probing the pseudoscalar portal to dark matter via $\bar{b}bZ(\to \ell\ell)+\not{E}_T$: From the LHC to the Galactic Center excess*, *Phys. Rev. D* **96** (2017) 095020 [1705.09670]. 45, 47

[212] L. Goodenough and D. Hooper, *Possible Evidence For Dark Matter Annihilation In The Inner Milky Way From The Fermi Gamma Ray Space Telescope*, 0910.2998. 45

[213] D. Hooper and L. Goodenough, *Dark Matter Annihilation in The Galactic Center As Seen by the Fermi Gamma Ray Space Telescope*, *Phys. Lett. B* **697** (2011) 412 [1010.2752].

[214] D. Hooper, *The status of the galactic center gamma-ray excess*, *SciPost Phys. Proc.* **12** (2023) 006 [2209.14370]. 45

[215] Fermi-LAT collaboration, *Fermi-LAT Observations of High-Energy γ-Ray Emission Toward the Galactic Center*, *Astrophys. J.* **819** (2016) 44 [1511.02938]. 45

[216] LHC Dark Matter Working Group collaboration, *LHC Dark Matter Working Group: Next-generation spin-0 dark matter models*, *Phys. Dark Univ.* **27** (2020) 100351 [1810.09420]. 45

[217] J.F. Gunion, H.E. Haber, G.L. Kane and S. Dawson, *The Higgs Hunter's Guide*, vol. 80, Front. Phys. (2000). 45

[218] J.F. Gunion and H.E. Haber, *The CP conserving two Higgs doublet model: The Approach to the decoupling limit*, *Phys. Rev. D* **67** (2003) 075019 [hep-ph/0207010]. 45, 46, 57

[219] ATLAS collaboration, *A combination of measurements of Higgs boson production and decay using up to* 139 fb^{-1} *of proton–proton collision data at* $\sqrt{s}$ = *13 TeV collected with the ATLAS experiment*, *ATLAS-CONF-2020-027* (2020). 47

[220] ATLAS collaboration, *Combination of searches for invisible Higgs boson decays with the ATLAS experiment*, *ATLAS-CONF-2020-052* (2020). 47

[221] CMS collaboration, *Search for invisible decays of a Higgs boson produced through vector boson fusion at the High-Luminosity LHC*, *CMS-PAS-FTR-18-016* (2018). 47

[222] ATLAS collaboration, *Prospects for New Physics in Higgs Couplings Studies with the ATLAS Detector at the HL-LHC*, *ATL-PHYS-PUB-2014-017* (2014). 47

[223] P. Bechtle, S. Heinemeyer, O. Stål, T. Stefaniak and G. Weiglein, *HiggsSignals: Confronting arbitrary Higgs sectors with measurements at the Tevatron and the LHC*, *Eur. Phys. J. C* **74** (2014) 2711 [1305.1933]. 48

[224] P. Bechtle, S. Heinemeyer, T. Klingl, T. Stefaniak, G. Weiglein and J. Wittbrodt, *HiggsSignals-2: Probing new physics with precision Higgs measurements in the LHC 13 TeV era*, *Eur. Phys. J. C* **81** (2021) 145 [2012.09197]. 48

[225] M. Mühlleitner, M.O.P. Sampaio, R. Santos and J. Wittbrodt, *ScannerS: parameter scans in extended scalar sectors*, *Eur. Phys. J. C* **82** (2022) 198 [2007.02985]. 48

[226] CMS collaboration, *Search for new particles in events with energetic jets and large missing transverse momentum in proton-proton collisions at* $\sqrt{s}$ = 13 TeV, *CMS-PAS-EXO-20-004* (2021). 48

[227] OPAL collaboration, *Search for the standard model Higgs boson with the OPAL detector at LEP*, *Eur. Phys. J. C* **26** (2003) 479 [hep-ex/0209078]. 49

[228] L3 collaboration, *Standard model Higgs boson with the L3 experiment at LEP*, *Phys. Lett. B* **517** (2001) 319 [hep-ex/0107054]. 49

[229] ALEPH collaboration, *Final results of the searches for neutral Higgs bosons in e+ e- collisions at s**(1/2) up to 209-GeV*, *Phys. Lett. B* **526** (2002) 191 [hep-ex/0201014]. 49

[230] ALEPH collaboration, *Observation of an excess in the search for the standard model Higgs boson at ALEPH*, *Phys. Lett. B* **495** (2000) 1 [hep-ex/0011045]. 49

[231] DELPHI collaboration, *Final results from DELPHI on the searches for SM and MSSM neutral Higgs bosons*, *Eur. Phys. J. C* **32** (2004) 145 [hep-ex/0303013]. 49

[232] T. Hermann, M. Misiak and M. Steinhauser, $\bar{B} \to X_s\gamma$ *in the Two Higgs Doublet Model up to Next-to-Next-to-Leading Order in QCD*, *JHEP* **11** (2012) 036 [1208.2788]. 49

[233] M. Misiak, A. Rehman and M. Steinhauser, *Towards* $\overline{B} \to X_s\gamma$ *at the NNLO in QCD without interpolation in* m_c, *JHEP* **06** (2020) 175 [2002.01548]. 49

[234] W. Skiba and J. Kalinowski, $B_s \to \tau^+\tau^-$ *decay in a two Higgs doublet model*, *Nucl. Phys. B* **404** (1993) 3. 49

[235] H.E. Logan and U. Nierste, $B_{s,d} \to \ell^+\ell^-$ *in a two Higgs doublet model*, *Nucl. Phys. B* **586** (2000) 39 [hep-ph/0004139]. 49

[236] ATLAS collaboration, *Search for heavy resonances decaying into a pair of* Z *bosons in the* $\ell^+\ell^-\ell'^+\ell'^-$ *and* $\ell^+\ell^-\nu\bar{\nu}$ *final states using 139* fb^{-1} *of proton–proton collisions at* $\sqrt{s} = 13$ *TeV with the ATLAS detector*, *Eur. Phys. J. C* **81** (2021) 332 [2009.14791]. 49

[237] M. Fabbrichesi, E. Gabrielli and G. Lanfranchi, *The Dark Photon*, 2005.01515. 50

[238] J. Jaeckel, M. Jankowiak and M. Spannowsky, *LHC probes the hidden sector*, *Phys. Dark Univ.* **2** (2013) 111 [1212.3620]. 50

[239] A. Hook, E. Izaguirre and J.G. Wacker, *Model Independent Bounds on Kinetic Mixing*, *Adv. High Energy Phys.* **2011** (2011) 859762 [1006.0973]. 50

[240] P. Galison and A. Manohar, *TWO Z's OR NOT TWO Z's?*, *Phys. Lett. B* **136** (1984) 279. 51

[241] X.-G. He, G.C. Joshi, H. Lew and R.R. Volkas, *Simplest* Z' *model*, *Phys. Rev. D* **44** (1991) 2118.

[242] K.S. Babu, C.F. Kolda and J. March-Russell, *Implications of generalized Z - Z-prime mixing*, *Phys. Rev. D* **57** (1998) 6788 [hep-ph/9710441].

[243] T. Appelquist, B.A. Dobrescu and A.R. Hopper, *Nonexotic Neutral Gauge Bosons*, *Phys. Rev. D* **68** (2003) 035012 [hep-ph/0212073]. 51

[244] M. Trodden, *Electroweak baryogenesis*, *Rev. Mod. Phys.* **71** (1999) 1463 [hep-ph/9803479]. 53

[245] T. Konstandin, *Quantum Transport and Electroweak Baryogenesis*, *Phys. Usp.* **56** (2013) 747 [1302.6713]. 53

[246] ACME collaboration, *Improved limit on the electric dipole moment of the electron*, *Nature* **562** (2018) 355. 53

[247] nEDM collaboration, *Measurement of the permanent electric dipole moment of the neutron*, *Phys. Rev. Lett.* **124** (2020) 081803 [2001.11966]. 53

[248] W.C. Griffith, M.D. Swallows, T.H. Loftus, M.V. Romalis, B.R. Heckel and E.N. Fortson, *Improved Limit on the Permanent Electric Dipole Moment of Hg-199*, *Phys. Rev. Lett.* **102** (2009) 101601 [0901.2328]. 53

[249] J.R. Espinosa, B. Gripaios, T. Konstandin and F. Riva, *Electroweak Baryogenesis in Non-minimal Composite Higgs Models*, *JCAP* **01** (2012) 012 [1110.2876]. 54

[250] J.M. Cline and K. Kainulainen, *Electroweak baryogenesis and dark matter from a singlet Higgs*, *JCAP* **01** (2013) 012 [1210.4196].

[251] I. Baldes, T. Konstandin and G. Servant, *A first-order electroweak phase transition from varying Yukawas*, *Phys. Lett. B* **786** (2018) 373 [1604.04526].

[252] J.M. Cline, K. Kainulainen and D. Tucker-Smith, *Electroweak baryogenesis from a dark sector*, *Phys. Rev. D* **95** (2017) 115006 [1702.08909]. 54

[253] M. Carena, M. Quirós and Y. Zhang, *Electroweak Baryogenesis from Dark-Sector CP Violation*, *Phys. Rev. Lett.* **122** (2019) 201802 [1811.09719].

[254] E. Hall, T. Konstandin, R. McGehee, H. Murayama and G. Servant, *Baryogenesis From a Dark First-Order Phase Transition*, *JHEP* **04** (2020) 042 [1910.08068]. 54

[255] J.M. Cline and P.-A. Lemieux, *Electroweak phase transition in two Higgs doublet models*, *Phys. Rev. D* **55** (1997) 3873 [hep-ph/9609240]. 54

[256] S. Profumo, M.J. Ramsey-Musolf and G. Shaughnessy, *Singlet Higgs phenomenology and the electroweak phase transition*, *JHEP* **08** (2007) 010 [0705.2425].

[257] J.R. Espinosa, T. Konstandin and F. Riva, *Strong Electroweak Phase Transitions in the Standard Model with a Singlet*, *Nucl. Phys. B* **854** (2012) 592 [1107.5441]. 64

[258] G.C. Dorsch, S.J. Huber and J.M. No, *A strong electroweak phase transition in the 2HDM after LHC8*, *JHEP* **10** (2013) 029 [1305.6610].

[259] P. Basler, M. Krause, M. Muhlleitner, J. Wittbrodt and A. Wlotzka, *Strong First Order Electroweak Phase Transition in the CP-Conserving 2HDM Revisited*, *JHEP* **02** (2017) 121 [1612.04086]. 54, 59, 61

[260] G. Dorsch, S. Huber, K. Mimasu and J. No, *The Higgs Vacuum Uplifted: Revisiting the Electroweak Phase Transition with a Second Higgs Doublet*, *JHEP* **12** (2017) 086 [1705.09186]. 54, 59, 61

[261] W. Chao, *CP Violation at the Finite Temperature*, *Phys. Lett. B* **796** (2019) 102 [1706.01041]. 54

[262] L. Biermann, M. Mühlleitner and J. Müller, *Electroweak Phase Transition in a Dark Sector with CP Violation*, 2204.13425. 54

[263] S. Inoue, M.J. Ramsey-Musolf and Y. Zhang, *CP-violating phenomenology of flavor conserving two Higgs doublet models*, *Phys. Rev. D* **89** (2014) 115023 [1403.4257]. 56

[264] B. Grzadkowski, O.M. Ogreid and P. Osland, *Diagnosing CP properties of the 2HDM*, *JHEP* **01** (2014) 105 [1309.6229]. 56

[265] F. Kling, J.M. No and S. Su, *Anatomy of Exotic Higgs Decays in 2HDM*, *JHEP* **09** (2016) 093 [1604.01406]. 57

[266] S.J. Huber, K. Mimasu and J.M. No, *Baryogenesis from transitional CP violation in the early Universe*, *Phys. Rev. D* **107** (2023) 075042 [2208.10512]. 59, 60

[267] K. Kannike, *Vacuum Stability Conditions From Copositivity Criteria*, *Eur. Phys. J. C* **72** (2012) 2093 [1205.3781]. 59, 60

[268] A. Barroso, P.M. Ferreira, I.P. Ivanov and R. Santos, *Metastability bounds on the two Higgs doublet model*, *JHEP* **06** (2013) 045 [1303.5098]. 60

[269] I.P. Ivanov and J.P. Silva, *Tree-level metastability bounds for the most general two Higgs doublet model*, *Phys. Rev. D* **92** (2015) 055017 [1507.05100]. 60

[270] A.G. Akeroyd, A. Arhrib and E.-M. Naimi, *Note on tree level unitarity in the general two Higgs doublet model*, *Phys. Lett. B* **490** (2000) 119 [hep-ph/0006035]. 61

[271] I.F. Ginzburg and I.P. Ivanov, *Tree-level unitarity constraints in the most general 2HDM*, *Phys. Rev. D* **72** (2005) 115010 [hep-ph/0508020]. 61

[272] B. Grinstein, C.W. Murphy and P. Uttayarat, *One-loop corrections to the perturbative unitarity bounds in the CP-conserving two-Higgs doublet model with a softly broken $\mathbb{Z}_2$ symmetry*, *JHEP* **06** (2016) 070 [1512.04567]. 61

[273] M. Quiros, *Finite temperature field theory and phase transitions*, in *ICTP Summer School in High-Energy Physics and Cosmology*, 1, 1999 [hep-ph/9901312]. 63

[274] H.J. Schnitzer, *The Hartree Approximation in Relativistic Field Theory*, *Phys. Rev. D* **10** (1974) 2042. 63

[275] E. Fernández-Martínez, J. López-Pavón, J.M. No, T. Ota and S. Rosauro-Alcaraz, *ν Electroweak Baryogenesis: The Scalar Singlet Strikes Back*, 2210.16279. 64

[276] J. Fan, M. Reece and L.-T. Wang, *Non-relativistic effective theory of dark matter direct detection*, *JCAP* **11** (2010) 042 [1008.1591]. 69

[277] M. Schumann, *Direct Detection of WIMP Dark Matter: Concepts and Status*, *J. Phys. G* **46** (2019) 103003 [1903.03026]. 69

[278] G. Arcadi, M. Lindner, F.S. Queiroz, W. Rodejohann and S. Vogl, *Pseudoscalar Mediators: A WIMP model at the Neutrino Floor*, *JCAP* **03** (2018) 042 [1711.02110]. 69

[279] XENON collaboration, *First Dark Matter Search with Nuclear Recoils from the XENONnT Experiment*, 2303.14729. 69

[280] S. Ipek, *Perturbative analysis of the electron electric dipole moment and CP violation in two-Higgs-doublet models*, *Phys. Rev. D* **89** (2014) 073012 [1310.6790]. 70